
# PREDICTING THE WEAR OF HIGH SPEED ROCKET SLEDS

THESIS

Lauren B. Wuertemberger, USAF

AFIT-ENY-12-D-02

**DEPARTMENT OF THE AIR FORCE**
**AIR UNIVERSITY**

***AIR FORCE INSTITUTE OF TECHNOLOGY***

**Wright-Patterson Air Force Base, Ohio**

AFIT-ENY-12-D-02

# PREDICTING THE WEAR OF HIGH SPEED ROCKET SLEDS

THESIS

Presented to the Faculty

Department of Aeronautical and Astronautical Engineering

Graduate School of Engineering and Management

Air Force Institute of Technology

Air University

Air Education and Training Command

In Partial Fulfillment of the Requirements for the

Degree of Master of Science in Aeronautical Engineering

Lauren B. Wuertemberger, BS

December 2012

AFIT-ENY-12-D-02

# PREDICTING THE WEAR OF HIGH SPEED ROCKET SLEDS

Lauren B. Wuertemberger, BS

Approved:

| | |
|---|---|
| _____ | _____ |
| Dr. Anthony N. Palazotto, USAF (Chairman) | Date |
| _____ | _____ |
| Dr. William P. Baker, USAF (Member) | Date |
| _____ | _____ |
| Dr. Donald L. Kunz, USAF (Member) | Date |

## Abstract

Holloman Air Force Base houses the 10 mile long Holloman High Speed Test Track in Alamogordo, New Mexico and can run hypersonic experiments at speeds up to 10,000m/s. Test objects are loaded onto sleds, which are connected to the track by "slippers" that slide along the rails. The payload sled is propelled down the track by a series of rocket sleds. The ability to predict the wear that will occur on the slippers during these experiments is important for slipper design and preventing catastrophic failure. However, high speeds complicate wear prediction since there are additional contributing factors, including inconsistent surface contact, fluctuating thermal and friction properties, and additional speed-induced melt wear. The goal of this project is to utilize a hydrocode program – CTH – to predict high speed wear results using a damage criterion that allows damage in cells to occur and have the cell removed. Results will be compared to the wear seen in other plane strain models which did not allow the damaged regions to be removed. Comparisons are made to a 3D ABAQUS simulation, and experimental data derived from a 2008 test run at the Holloman High Speed Test Track.

*To my amazing family*

**Acknowledgments**

This work could not have been completed without the help and support of many others. I would like to extend my sincere appreciation to my advisor Dr. Anthony Palazotto, who patiently worked with me as I grasped concepts, and was always enthusiastically willing to help me with concepts that eluded me. Many thanks to Dr. Baker for his contributions to the project – it was always entertaining to see him and Dr. P spar on some concept that was way over my head. Additionally, thanks to my parents and my family for their bottomless support while I embarked on this great endeavor. Many a time they were able to offer encouragement during frustrating stretches. Thanks to Rodolfo for mentoring me during this project. And finally many thanks to Major Geof Cox. His friendship and academic support have meant a great deal to me.

Lauren B. Wuertemberger

## Table of Contents

Page

## List of Figures

## List of Tables

Page

## List of Symbols

| Symbol | | Page |
|---|---|---|
| v | velocity. | 14 |
| $\lambda$ | wave length. | 14 |
| f | frequency. | 14 |
| y | wave displacement | 14 |
| $y_0$ | wave amplitude. | 14 |
| t | time. | 14 |
| x | position. | 14 |
| $\rho$ ds | mass per unit length. | 14 |
| $\frac{\partial^2 y}{\partial t^2}$ | acceleration | 14 |
| T | tension in the string | 14 |
| $\sigma$ | stress | 15 |
| E | elastic modulus | 15 |
| $\varepsilon$ | strain. | 15 |
| u | displacement | 16 |
| $C_0$ | elastic wave velocity. | 16 |
| $\rho$ | density. | 17 |
| n | work hardening. | 18 |
| m | strain rate sensitivity. | 18 |
| $V_1$ | plastic wave velocity at x=0. | 20 |
| $\varepsilon_1$ | maximum plastic strain | 20 |

| | | |
|---|---|---|
| ρ | material density. | 22 |
| V | material volume. | 22 |
| F | force. | 22 |
| m | mass. | 22 |
| v | velocity. | 22 |
| t | time. | 22 |
| E | internal energy. | 22 |
| $\frac{1}{2}\rho v^2$ | kinetic energy. | 22 |
| W | work done on the system. | 22 |
| i | index | 22 |
| f | index. | 22 |
| $\rho_0$ | initial density. | 24 |
| $U_s$ | shock velocity. | 24 |
| $\rho$ | density. | 24 |
| $U_p$ | particle (impact) velocity | 24 |
| $P$ | pressure. | 24 |
| $P_0$ | initial pressure. | 24 |
| $E$ | internal energy. | 24 |
| $E_0$ | initial internal energy. | 24 |
| P | pressure. | 25 |
| $\rho$ | density. | 25 |
| E | internal energy | 25 |

| | |
|---|---|
| i | summation index . . . . . .42 |
| j | summation index. . . . . 42 |
| $t$ | time . . . . . .42 |
| E | internal energy. . . . . .42 |
| $s_{ij}$ | stress deviators . . . . . 42 |
| $\dot{\varepsilon}_{ij}$ | strain rates. . . . . 43 |
| P | hydrostatic pressure . . . . . 42 |
| $F_f$ | Friction force . . . . . 55 |
| μ | Friction coefficient. . . . . 55 |
| $F_n$ | Normal force . . . . . 55 |
| $V_d$ | Damage volume. . . . . 55 |
| $W_{uAn}$ | Wear per unit area. . . . . 55 |
| $A_c$ | Area of contact . . . . . 55 |
| $D_s$ | Sliding distance . . . . . .55 |
| %Cont | Percent of contact time the slipper had with the rail. . . . . 55 |
| $W_{wolfson}$ | measured wear rate . . . . . 58 |
| $A_n$ | Wolfson test area . . . . . 58 |
| $t_{sim}$ | simulation time . . . . . 60 |
| $r_a$ | asperity radius . . . . . 60 |
| $v_{slide}$ | sliding velocity. . . . . 60 |
| $W_{uw}$ | wear per unit width . . . . . .71 |
| $A_d$ | damage area . . . . . 71 |

PREDICTING THE WEAR OF HIGH SPEED ROCKET SLEDS

# I. Introduction

## 1.1 Problem Background

The Holloman High Speed Test Track (HHSTT) at Holloman Air Force Base (AFB) in New Mexico runs hypervelocity experiments up to Mach 10 over its 10 mile track. These experiments provide valuable information about payload performance inflight environments. However, these speeds introduce dynamic wear challenges that have not been thoroughly investigated. Figure 1 shows an example experiment on the track.

**Figure 1: Example Experiment Set-Up at the Holloman High Speed Test Track [1]**

The setup is composed of multiple sleds mounted on a steel track. The front sled has the experimental payload, and the trailing sleds have rockets loaded on them that propel the fore body sled down the track. A better view of the stages is seen in Figure 2.

**Figure 2: Stages of the 2008 HHSTT Experiment [2]**

The connecting piece between the sled and the track is the slipper and is shown below in Figure 3.

**Figure 3: VascoMax300 Slipper attached to the 1080 steel Rail [3]**

As the slipper slides along the rail during the experiment, the bottom surface progressively wears down as material is removed. A microscopic view of the slipper surface provides some more insight into this phenomenon in Figure 4.

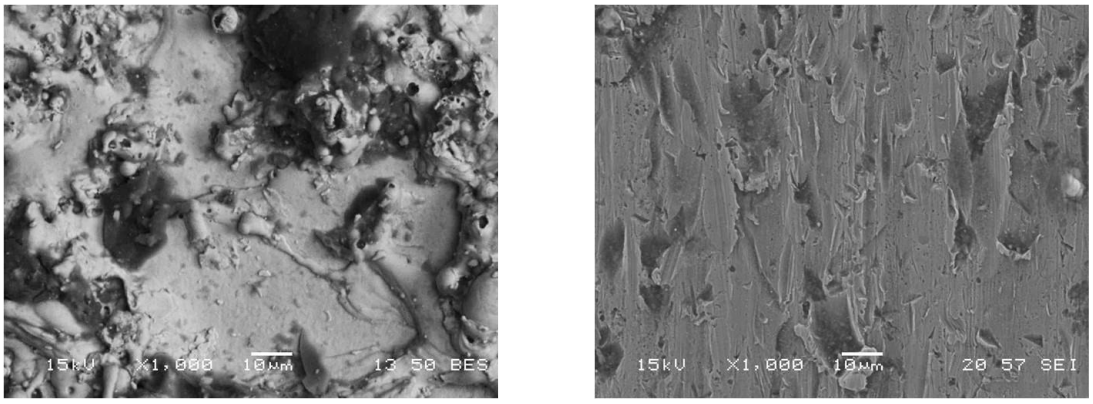


(a) (b)

**Figure 4: Scanning Electron Microscope photos of (a) an Unworn Slipper Sample and (b) a worn slipper sample [4]**

On the left is an unworn slipper sample, and on the right is a worn sample as seen under a scanning electron microscope. The worn surface looks fairly smooth except where there is teardrop-shaped plowing damage.

Wear at high speeds is a compilation of many different wear mechanisms. The sliding contact raises the temperature of the metal to the point where it will literally melt away. [5] Lift effects on the sled due to high speeds will cause the slipper to "bounce" along the rail, leading to inconsistent surface contact, further complicating the prediction of thermal and frictional properties of the interacting metal surfaces. Contact interactions such as adhesion and abrasion are also contributors to the overall wear. An example of Adhesion and abrasion can be seen in Figure 5.

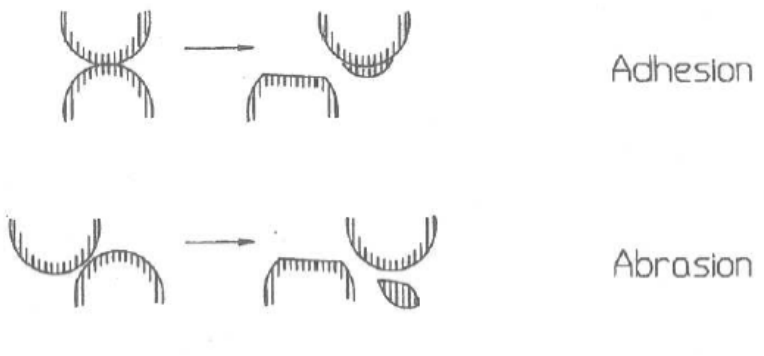


**Figure 5: Adhesion and Abrasion Wear [6]**

Adhesion occurs when two surfaces come into contact and stick together. If the adhesion is strong enough, the some of the softer material is removed and stays gripped to the harder material. Eventually the extra material falls off, causing additional wear damage in the process. Abrasion occurs when asperities collide with enough force to fracture the asperity and cause material to sheer off. Melt wear occurs when the sliding materials generate so much heat that the melting temperature of one or both of the metals is reached. Material drips off, alleviating some of the friction between the two metals, but as mentioned earlier, not decreasing the wear overall.

All of these factors and other tribological conditions make predicting the slipper wear difficult. For practical and financial reasons, it is desirous to be able to model the phenomenon. Major wear incidents can lead to heavy damage to both the slipper and the rail, potentially disrupting expensive experiments and requiring additional track repairs. Not being able to predict wear also makes design of similar high speed sliding components difficult, thus a way to determine the material interaction is valuable not only to those at HHSTT, but also anyone wanting to try similar high speed experiments.

## 1.2 Objective

The wear problem in question is a complicated one with many factors contributing to the overall loss of material. It is of interest to be able to simplify this problem and create a basic model that will predict wear accurately. This research focuses on developing a simple plane strain model using a hydrocode program called CTH to represent a 3D wear phenomenon. The results are carried out without the initial input of a temperature history, and will not be exact. The aim is see if a simple plane strain analysis has some merit for evaluating the wear effects at high velocity.

## 1.3 Prior Work

This is definitely not the first investigation into the wear of sliding materials. There have been many attempts at wear characterization for low speeds and high speed starting as early as the 1950s. [7] Research into the wear problem at HHSTT began around 1960, and AFIT has picked up the general problem around 1998. [8, 9] Much progress has been made in this area, and has been built into this project. The following is a brief review of the research and conclusions that have been made which provide the foundation for this work.

### *1.3.1 Wear Research*

There are many different aspects of wear to investigate. Concern about wear problems first arose in the US Army when wear from projectiles in cannons was taking a toll on weapons performance. Much progress was made when investigating the problem, though research on this subject was not released until 1975. [10] Early work proposed that wear was primarily a function of load and mostly independent of contact area. [7]

Investigation began in the 1950s into the effect of thermal environments in wearing materials and found that if the temperature of the material rose to the melting temperature, an interfluous layer forms between the sliding materials and is removed as the sliding progresses. [5, 11, 12, 13] This causes the coefficient of friction to lesson between the materials, but does not necessarily result in the reduction of the overall wear rate.

In 1979, Challen and Oxley introduced the idea that asperities (microscopic surface variations on material faces) can be used to create models for wear, noting that the contact area between surfaces is really just the area of asperities interfacing between the materials. [14]This is particularly of interest to this research since asperities are used in the developed model.

It was becoming apparent that there were different factors that caused different types of wear to dominate wear scenarios. In 1987, Lim and Ashby began developing "wear maps" that showed what kind of wear was dominating based on velocity and load. The maps predicted when particular types were occurring, such as delaminated wear (mild and severe), mild oxidation wear, severe oxidation wear, and melt wear. [15]

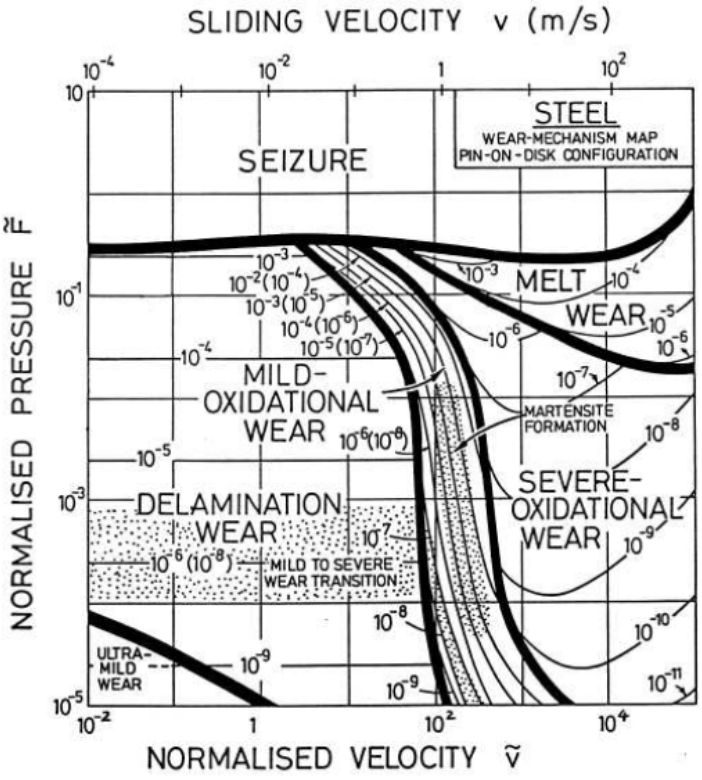


**Figure 6: Lim and Ashby's Wear Map for Steel [15]**

Further progress was made with asperities in 1982 with research done by Barber and Bauer, which showed that at certain velocities, asperity behavior changed from a quasi-steady mechanical behavior at low speeds, to higher speeds when inertia effects began to dominate. [16]

For as long as wear events had been studied, many analytical models for predicting wear have been produced. But as Meng and Ludema found in their study in 1995, most of those models were not practical for widespread use. [17] However, with the rise of numerical methods and computational modeling, the problem becomes much more approachable. Constitutive models that are able to track strain rate were introduced and Finite Element Analysis (FEA) models began to come onto the scene in the 1990s.

[18, 19] Additionally, new experimental methods have allowed for better characterization of materials at high speed impacts. [20]

### *1.3.2 Holloman Gouging Research*

The wear problem at Holloman AFB has its own history as well. In 1960, Wolfson began research into high speed wear utilizing a set up where a sled was accelerated down a track to a specific velocity. [21] Once the target velocity was reached, a pin was placed in contact with the rail for a specific distance. Wolfson was able to calculate wear rates by measuring and weighing the worn slider and comparing it to its initial state prior to the run. Some of his results are applicable to our studies, and are used as comparative data in this research.

The gouging phenomenon was first observed and recorded by Graff and Dettloff in 1969, when experiments progressed to speeds around 1800m/s. Teardrop-shaped gouges occurred randomly along the rail and on the rocket shoe.[8] The gouges were 2-4in. long, 1in. wide, and 1/16in. deep. Graff and Dettloff were able to successfully ballistically reproduce the phenomenon in the lab. Similar gouging wear occurred at Sandia National Labs in 1973 as observed by Gerstle, who was able to perform a metallurgical examination of the damaged metal and identified that there was melt wear, catastrophic thermoplastic shearing, and the damage affects which went deeper into the metal than just at the surface. [22]

In 2000, HHSTT began the development of a new track designed to handle experiments that would break land speed records. [23] With this goal in mind, minimizing wear and fully understanding the dynamic environment of the track became a

high priority. Software was developed called the Dynamic Analysis and Design System (DADS) which allowed dynamic time dependent characterization of the experimental results to be recorded. This data has been instrumental for the development and validation of models at the Air Force Institute of Technology (AFIT).

### *1.3.3 AFIT Research*

There has been an ongoing effort at AFIT to characterize high speed wear events, particularly focusing on those at HHSTT. Work began as early at 1998 with Schmitz, where the gouging problem was first investigated. [9] Since the phenomenon was a high energy impact problem, whose results had been reproduced with ballistics, it was determined that the hydrocode, CTH, developed by Sandia specifically for ballistic events, would be an appropriate program to model the high energy scenario. Laird in 2002 continued this research and developed a model in CTH that had a flyer (slipper) colliding with a target (rail). [24] He experimented with this model using various temperature profiles, horizontal and vertical velocities, collisions with asperities, collisions without asperities, and considered a gap between the rail and the slipper. Szmerekovsky in 2006 continued the investigation while adding coatings to the rail to see how they would affect the material surface temperatures. [25] Also in 2006, Cinnamon had a chance to do a metallographic analysis on materials from previous tests at the HHSTT, and developed improved material data for the model. [4] In 2007, Cameron attempted to separate the overall wear into two different categories- melt and mechanical. He used the CTH code to calculate each event separately and was able to compare his

results to a 2003 experiment data. His results were found to be reasonably equivalent. [26]

In 2008, Chmiel moved away from the CTH code and embarked on developing a finite element code in ABAQUS to model wear. [27] He attempted two different models: one macroscopic and one microscopic. The macroscopic code experienced technical difficulties, but the microscopic code, employing specific material characteristics and failure criteria, produced favorable results. This work was expanded on by Hale in 2009, which took the plane strain ABAQUS model and was able to use it to compare to a 2008 HHSTT experiment. [3]

The CTH model was not left behind with the rise of the FEA model as it was still computationally superior to FEA codes at higher speeds. Using Lim and Ashby's research, Meador continued using the CTH model and attempted to determine if the heat distribution coefficient between the slipper and the rail could be approximated at 50% (0.5). He found that since the slipper contact with the rail was not consistent, 0.5 was a poor assumption and more reasonable to assume a coefficient of 0.12-0.14. [28] In 2011, Huber continued development of the CTH code by experimenting with different failure criteria to see how they would affect the predicted wear results. [29] Work is currently ongoing with Buentello continuing the work on the ABAQUS FEA model.

### 1.4 Prior Work Summary

Research into wear has revealed that it is a complicated mechanism with several different types occurring simultaneously, and the wear behavior varies based on speed. At speeds over 1828.8 m/s, it has been found that teardrop gouging develops during testing

at HHSTT, and these same results have been reproduced in the lab using ballistic impacts. At AFIT, finite element models (both 2D and 3D) have been developed in ABAQUS. Additionally, a 2D CTH code using various failure criteria has been developed. The models are in the process of being refined, and are validated using experimental data from HHSTT experiments.

# II. Theory

## 2.1 Introduction

On a microscopic scale, surfaces are not smooth. They are actually composed of uneven jagged profiles, contact between the interfaces of the two surfaces only occurs at the tips of which touch the other surface. Figure 7 shows a representation of the uneven surface profile.

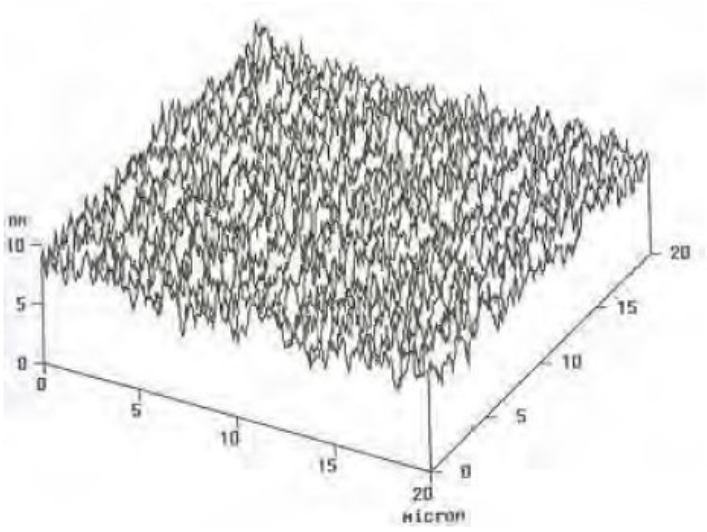


**Figure 7: Surface Profile of a Metal [30]**

These contact points can be modeled as small bumps, or "asperities." At high speeds, the collisions between asperities are actually impact phenomena, meaning that

there is the possibility of internal shock wave propagation. Inertia effects and stress wave propagation become significant factors at play. [31, 32], thus the employment of classic deformable body mechanics which use Hooke's Law to predict stress, strain, and deformation are not enough to explain what is happening with stress propagation inside the materials, since materials will behave differently at high speeds than at low speeds, and a different approach to modeling the event must be used.

## 2.2 Theory Overview

This problem's solution revolves around understanding how stress waves will travel through materials, along with trying to satisfy the three conservation equations: the conservation of mass, the conservation of momentum, and the conservation of energy. High speed impact complicated things, since materials will become more compressible and due to discontinuities in pressure in the wave profile, the thermodynamic behavior of the material is not standard. [33] Thus, more relations are needed to complete the solution set. An equation of state is introduced to take the unique density and thermodynamic behavior of the materials into account. A constitutive equation rounds out the solution and defines how the stress developed over time taking into account strain, energy, and other factors depending on the model that is used. Additionally, predicting dynamic failure is a challenge, so failure criteria are developed in an attempt to characterize it.

While the conservation equations are standard for all solutions, models can be varied based on the selection of the equations of state that represent the materials, the constitutive models that develop stress, and for numerical modeling, on how the program determines failure of a material during simulations. Thus, there numerous possible

models using various combinations of these components. These models can be validated by comparing them to experimental data, and it is attempted to do so in this research.

The conservation equations, an equation of state, and a constitutive equation, and a specific failure criterion are the basic tools that are used to solve this problem. First, the basics of wave propagation are explored to better understand why the thermal properties are discontinuous. Then the specifics of each of the relationships are further detailed in the following sections.

### 2.3 Wave Propagation

Meyer's *Dynamic Behavior of Materials* gives an excellent overview of wave propagation. Much of Section 2.3 is a summary of chapters 1-4 of his book. [34]

Technically speaking, everything is moving in waves. Atoms are constantly vibrating, but for most situations, the vibrations are too small to notice. They exist in a static or quasistatic equilibrium. Application of forces can be described as vibrations as well. Static deformation revolves around balancing forces in equilibrium without much thought to time and how stress moves through the material, because the application of force can be considered instantaneous. This is not true however in dynamic deformation where bodies are subjected to rapidly changing loads. In these cases, one must be able to track the velocity of a stress wave moving through a body.

To begin to understand how stress waves travels, it is helpful to understand how a simple uniaxial sinusoidal wave operates. A low, constant amplitude wave advances according to equation 2.1:

$$v = \lambda f \tag{2.1}$$

Where v is the velocity, $\lambda$ is the wave length, and f is the frequency.

The vertical position of the wave can be defined by equation:

$$y = y_0 \sin\left[2\pi f(t - \frac{x}{V})\right] \tag{2.2}$$

Where y is the displacement, $y_0$ is the wave amplitude, t is the time, and x is the position.

Now, assume that the wave can be represented by a string with a mass m and a line tension T. To get a wave equation in the differential form, one carries out an equilibrium analysis of the ends of a wave and applies Newton's Law (assuming all motion is in the Y direction):

$$\sum F_x = 0 \tag{2.3}$$

$$\sum F_y = ma_y = \rho\, ds \frac{\partial^2 y}{\partial t^2} \tag{2.4}$$

Where ($\rho$ ds) is the mass per unit length, $\frac{\partial^2 y}{\partial t^2}$ is the acceleration.

Summing the forces at the ends, accounting for the tension inside of the string, and assuming small oscillations (cosine theta = 1), brings us to the differential wave equation.

$$\rho \frac{\partial^2 y}{\partial t^2} = T^2 \frac{\partial^2 y}{\partial x^2} \tag{2.5}$$

Where T is the tension in the string.

Differentiate position equation twice and substitute it into the differential wave equation gives the traveling wave velocity relation:

$$v = \pm\left(\frac{T}{\rho}\right)^{\frac{1}{2}} \quad 2.6$$

In the next section, it will be shown that the tension is replaced by the modulus of elasticity for elastic waves. Substituting equation 2.6 into 2.5, the differential wave equation for a horizontal traveling wave with a horizontal displacement becomes:

$$\frac{\partial^2 y}{\partial t^2} = v^2 \frac{\partial^2 y}{\partial x^2} \quad 2.7$$

This equation applies when any shape of disturbance propagating at velocity v in a medium and remaining unchanged. It is an analogous representation to the development of traveling elastic waves. Each traveling wave in a body is going to do so at its own characteristic velocity. Velocities in traveling waves are a function of the stress response of the material to strain and density, and so will be different based on whether the wave is elastic, plastic, or includes shocks.

### *2.3.1 Elastic Waves*

For elastic waves, the stress-strain relations are based on elastic constants. When the dynamic process (application of force) is slow, a body can be considered in static equilibrium, however this is not technically the case. Internal stresses are not immediately transferred though materials, they travel atom-to-atom via waves. Essentially all atomic movement can be traced back to the conservation of momentum equation. The next section explains how elastic stress travels in a material.

For elastic waves in a bar, deformation is elastic and follows Hooke's Law:

$$\sigma = E\varepsilon \quad 2.8$$

Where $\sigma$ is the stress, E is the elastic modulus, and $\varepsilon$ is strain.

Horizontal strain can be defined in terms of displacement:

$$\varepsilon = \frac{\partial u}{\partial x} \tag{2.9}$$

Where u is displacement.

An elastic wave travels as

$$\frac{\partial^2 u}{\partial t^2} = \frac{E}{\rho}\frac{\partial^2 u}{\partial x^2} \tag{2.10}$$

Comparing this to equation 2.11, the velocity of wave is defined as:

$$C_0 = \sqrt{\frac{E}{\rho}} \tag{2.11}$$

There are several types of elastic waves that may occur. Longitudinal (or irrotational or dilatational) waves occur in infinite and semi-infinite media, and travel in the direction of the initial contact. Distortional (or shear or transverse or equivolumal) waves occur in solids perpendicular to the initial contact direction, and there is no change in density or longitudinal strains $\varepsilon_{11}$, $\varepsilon_{22}$, and $\varepsilon_{33}$. Surface (or Rayleigh) waves move up down back and forth along the surface. Interfacial (or Stonley) waves occur when two semi-infinite materials with different properties are in contact with each other. Finally bending waves, which occur in bars and plates, in 2D scenarios are the waves caused by bending stresses. Each kind of wave travels at a different velocity: surface waves are slow, while longitudinal waves are fast.

At boundaries, elastic waves divide into reflection and refraction when they come into contact with mediums with different sonic/sound impedances. The specific angles of the reflected and refracted waves can be found using Lenz's law. These waves are easiest

to deal with when the impact is normal to the surface in question. The total initial stress/particle velocity is equal to the sum of the transmitted and reflected velocities. The impedance of materials determines the amplitudes of the resulting transmitted and reflected waves. The impedance is based on the material properties of the material, and the relationship is seen in equation 2.12.

$$Impedance = \rho C_0 \qquad 2.12$$

Where $\rho$ is the density and $C_0$ is the elastic wave velocity.

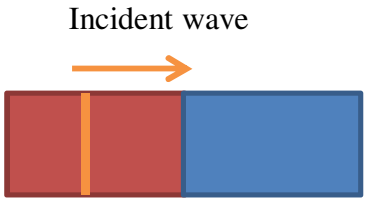


**Figure 8: Materials with Differing Impedances**

For example, consider two materials are subjected to an incident wave as shown in Figure 8. When impedance of blue material is greater than the red material, a pulse of the same sign is reflected. When impedance of the red material is greater than blue material , a pulse of the opposite sign is reflected.

On a free surface, the elastic modulus (E) is equal to 0. On a rigid body, E is equal to ∞.When a compressive wave encounters a free surface, it reflects back as a tensile wave. The stress sign changes but the velocity stays the same. When a compressive wave encounters a rigid body, a compressive wave is reflected back (the stress sign stays the same but the velocity changes). If the particle velocity and the wave direction have the

same direction, the stress is compressive. If they have opposite senses, the stress is tensile.

### *2.3.2 Plastic Waves*

For plastic waves, the stress-strain relations are based on work hardening and strain rate. Plastic waves occur when a stress in a material exceeds its elastic limit. This happens in both static and dynamic deformations. For elastic waves, the stress was entirely elastic and could be based on a linear equation. This is not necessarily the same for plastic stress. Figure 9 below shows 4 different stress-strain curves and how they change depending on how plastic flow stress develops.

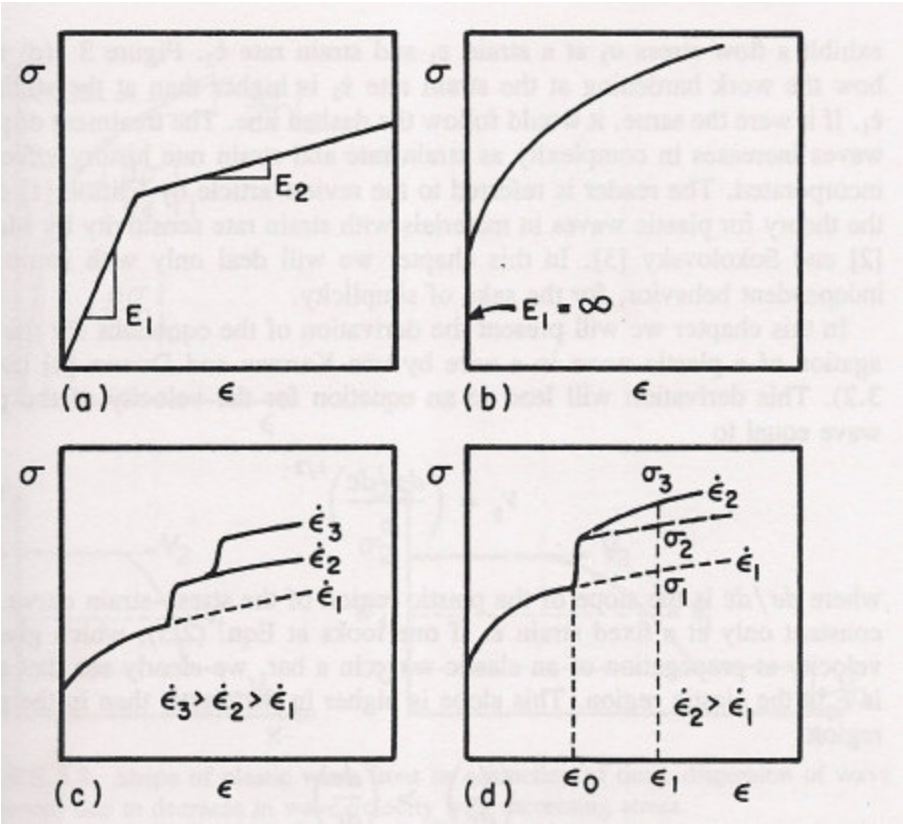


**Figure 9: Stress Strain curves for ductile materials with (a) bilinear elastoplastic; (b) power law work hardening; (c) strain rate dependent flow stress; (d) strain rate history dependent flow stress**

In Figure 9 (a), one assumes that both the plastic and the elastic portions of the stress-strain curve are assumed to be linear relations. In Figure 9 (b), the plastic portion is assumed to develop based on a power law, where the power exponent is the work hardening. In Figure 9 (c), the stress is increasing as the applied strain rate increases. Finally, in Figure 9 (d), the stress is increasing with the increasing strain rate, but is also dependent on when the strain rate is applied. One general stress-strain relation for a changing strain rate is represented as:

$$\sigma = \sigma_0 + k\varepsilon^n \dot{\varepsilon}^m \qquad 2.13$$

Where $\sigma_0$ is the material yield stress, n is work hardening, and m is the strain rate sensitivity.

Temperature, strain, and strain rate all affect mechanical material behavior and how the flow stress develops.

To get an idea of how the velocity of a plastic wave differs from that of an elastic wave, let's look at the development of stress in a plastic wave. For time independent waves, the speed that they travel at can be found to be:

$$V_p = \left( \frac{\frac{d\sigma}{d\varepsilon}}{\rho} \right)^{1/2} \qquad 2.14$$

The same velocity relation can be used as was previously used for elastic waves, but E must be replaced by the more specific $\frac{d\sigma}{d\varepsilon}$ term. Comparing this to the elastic wave velocity, the slope of E in the elastic region is greater than the slope in the plastic region, so it can be concluded that the elastic wave travels faster than the plastic wave.

Now that the behavior of elastic and plastic waves is known, a wave profile can be drawn, as seen in Figure 10.

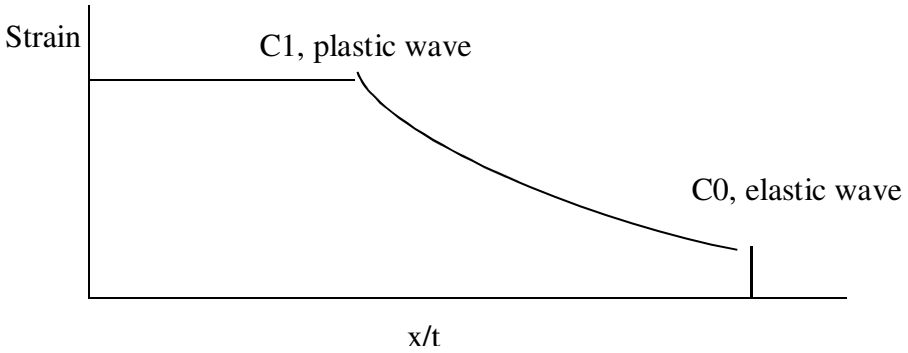


**Methodology Figure 10: Plastic-elastic wave profile**

There are three regions – where the plastic wave is dominating, where the elastic wave is dominating, and then when the wave comes to a complete stop. Note how C0 is faster than C1, but C1 incurs more strain.

To find the velocity at x = 0 (right when the plastic wave initiates), one arrives at this integral in equation 2.15:

$$V_1 = \int_0^{\varepsilon_1} \sqrt{\frac{\frac{d\sigma_0}{d\varepsilon}}{\rho_0}}\, d\varepsilon \qquad 2.15$$

Where $V_1$ is the velocity at x=0 and $\varepsilon_1$ is the maximum plastic strain.

This equation must be solved numerically, and it is impossible to know the velocity at this point without knowing the relationship between stress and strain. This relationship is known as a constitutive model. There have been many models developed and they have been divided into several different categories: linear viscoelastic, infinitesimal elastic-perfectly plastic, nonlinear viscoelastic, and thermoelastic.

### *2.3.3 Shock Waves*

Shock waves that occur in a material are largely due to adiabatic compressibility. Shear stresses are neglected since the event is at a high pressure. When the amplitude of the stress wave is greatly exceeding the flow strength of a material, a disturbance front will "steepen up" as it travels through the material. This is because as the strain increases, higher amplitude regions of the front travel faster than the lower regions. This leads to a shock wave – "a discontinuity in pressure, temperature (or internal energy), and density." [34] This is illustrated in Figure 11.

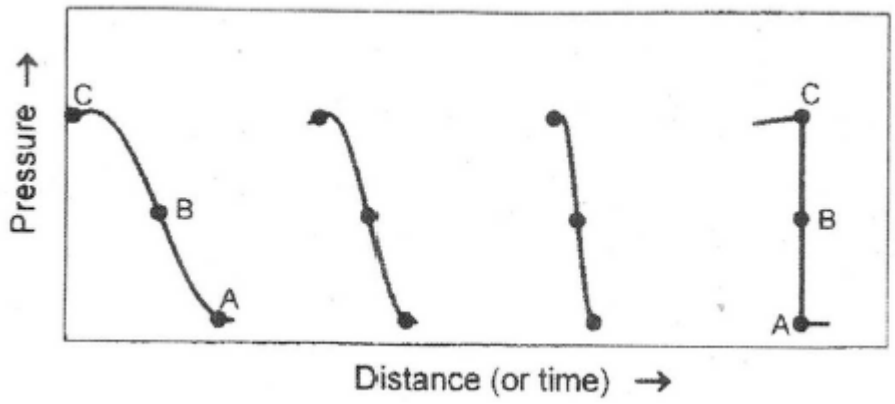


**Figure 11: Increasing Pressure with Time [32]**

The wave is shown traveling as one would expect, with the bottom part of the wave with lower pressure, representing where elastic stress would be occurring, is moving faster than the upper part of the wave where presumably plastic deformation would occur. As the wave progresses, the upper part of the wave speeds up and catches up with the lower part of the wave. Now the pressure wave no longer looks like a wave, but rather a straight vertical line causing a discontinuity in the pressure data, causing it to no longer be a continuous function. Because of this, additional shock relations must be employed to get us across the jump. This is possible by re-working the conservation equations to track the different particle velocities and employing an equation of state to create thermodynamic relationships of the materials at high speeds.

## 2.4 Conservation Equations

To solve this problem, one approaches wielding the basic conservation equations: conservation of mass, conservation of momentum, and conservation of energy, as shown below:

Conservation of mass shows that material is neither created nor destroyed.

$$\int_V \rho dV = const \tag{2.16}$$

Where ρ is the material density and V is the material volume.

The conservation of momentum equation shows that the net force in a system is equal to the rate of change of momentum.

$$F = m\frac{dv}{dt} \tag{2.17}$$

Where F is force, m is mass, v is velocity, and t is time

Conservation of Energy states that the total overall energy in a system is conserved.

$$\sum E_i = \sum \frac{1}{2}\rho v_i^2 = \sum E_f + \sum \frac{1}{2}\rho v_f^2 + W \tag{2.18}$$

Where E is the internal energy, $\frac{1}{2}\rho v^2$ is the kinetic energy, W is the work done on the system, and i and f are indices.

These equations track energy, pressure, density, and velocity inside of the materials. Due to the compressibility caused at high speeds, the density may not remain constant throughout the event. Additionally, there are the discontinuities caused by possible shocks to take into account. Consider the one-dimensional case illustrated below in figure 12:

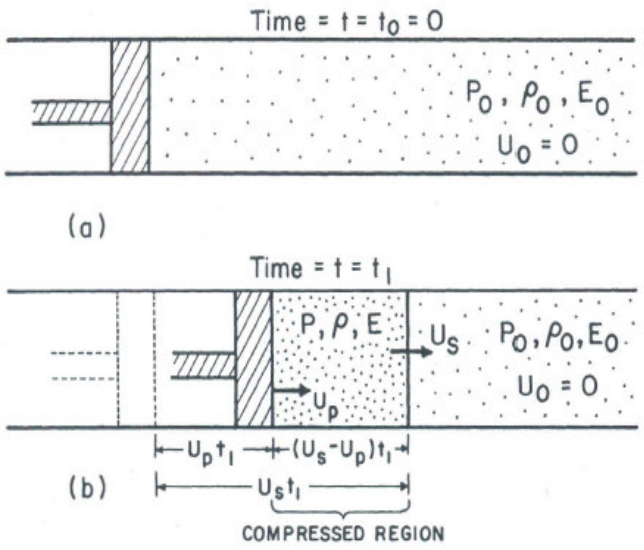


**Figure 12: Compression of a Medium with a Generated Shock Wave [34]**

Figure 12 (a) shows the initial state of shock impact at time (t) = 0, where the material in question is at rest. In figure 12 (b), the plunger moves forward, compresses the material, and sends a shockwave forward ahead of the initial impact site.

Rankine and Hugoniot went about rearranging the conservation equations for a 1D case, and are as displayed below:

$$\rho_0 U_s = \rho(U_s - U_p) \tag{2.19}$$

$$P - P_0 = \rho_0(U_s U_p) \tag{2.20}$$

$$(E - E_0) = \frac{1}{2}(P + P_0)\left(\frac{1}{\rho_0} - \frac{1}{\rho}\right) \tag{2.21}$$

Where: $\rho_0$ is the initial density, $U_s$ is the shock velocity, $\rho$ is the density, $U_p$ is the particle (impact) velocity, $P$ is the pressure, $P_0$ is the initial pressure, $E$ is the internal energy, $and\ E_0$ is the initial internal energy.

The three-dimensional equations are more complicated, but based on the same principles.

Note from equations 2.19-2.21 that there are five variables of interest: density, shock velocity, particle velocity, pressure, and energy. Since there are more unknowns than equations to solve them, additional relationships are needed. The first three relationships are provided by the conservation equations, and the fourth relationship is provided by an equation of state. With the addition of an equation of state, the ability is gained through experimentation to relate four of the unknowns in terms of one unknown.

## 2.5 Equation of State

The equation of state helps relate the thermodynamic properties of a material to its density and pressure. [31] They help deal with pressures that are higher than material strength, compressibility effects, and shock heating. Equations of state are dealing with the hydrodynamic (volumetric) portion of stress, while constitutive equations deal with the deviatoric portion of stress. They are of the general form:

$$P = P(\rho, E) \qquad 2.22$$

Where P is the pressure, $\rho$ is the density and E is the internal energy.

Equation of states can be either tabular or analytic.

### *2.5.1 SESAME tables*

The equation of state used in this study is a set of tables called the SESAME tables. It consists of thermodynamic properties such as pressure, density, and energy experimentally determined by Los Alamos National Laboratory. [35] Additionally,

vaporization, melt, and shear data is available, as well as shock data. This is notable because it is inclusive of any phase changes that are occurring.

### *2.5.2 Mie-Grüneisen*

The Mie-Grüneisen Equation of state is an example of an analytic EOS. It relates the materials pressure and internal energy to its pressure and temperature with the following equation:

$$p = \frac{\rho_0 c_0^2 \eta}{(1 - s\eta)^2}\left(1 - \frac{\Gamma_0 \eta}{2}\right) + \Gamma_0 \rho_0 E \qquad 2.23$$

Where:

$$\eta = 1 - \frac{\rho_0}{\rho} \qquad 2.23$$

$$U_s = c_0 + sU_o \qquad 2.24$$

Γ is the Grüneisen parameter, $c_0$ is the reference speed of sound, E is the internal energy, s is the parameter that relates shock and particle velocity, ρ is the density, and p is the pressure.

It allows for a finer control of temperature inputs, but isn't set up to handle phase changes.

## 2.6 Constitutive Equation

Stress can be divided into two components – a volumetric portion generating stresses from volumetric changes and a deviatoric portion generating stresses from changes in shape of the body. [36]

$$\sigma_{ij} = -P\delta_{ij} + s_{ij} \qquad 2.25$$

Where $\sigma_{ij}$ is he total stress, $-P\delta_{ij}$ is the volumetric stress, and $s_{ij}$ is the deviatoric stress component.

The volumetric stresses can be found using data from the equation of state and hydrostatic stress (the sum of the principal stresses), but an additional relation is needed to find the deviatoric stress. This relation comes from a constitutive equation, which calculates the dynamic yield stress (or flow stress) in terms of strain rates and temperature. [37]. Note that the dynamic yield strength is not the same as the static yield strength. Additionally, the dynamic flow stress is not representative of the entire stress-strain curve, but only the portion where plastic deformation has been initiated.

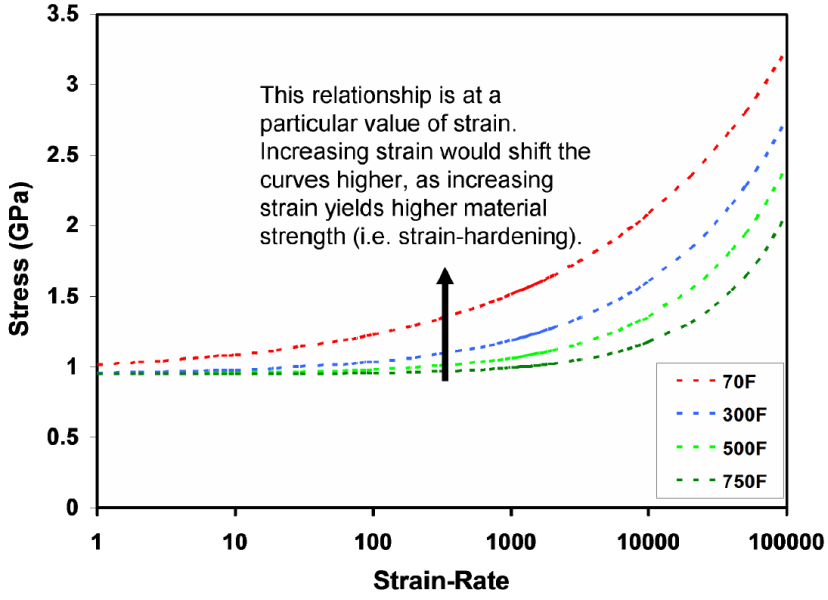


**Figure 13: General Constitutive Model Behavior [37]**

Figure 13 shows the general behavior of constitutive models and how they change based on increasing strain rate and temperature. Only strain rate and temperature changes are accounted for in this example, but models can take into account other factors, such as

material properties and work hardening. In addition to modeling the deviatoric stress, constitutive models help determine when a material is behaving elastically or plastically. An equivalent stress is calculated using the second invariant of the deviatoric stress tensor:

$$\sigma_{EQ} = \sqrt{3(s_{ij}s_{ij})} \qquad 2.26$$

When the equivalent stress is less than the flow stress, the material is assumed to be in its elastic deformation stage. When the equivalent stress is greater than the flow stress, the material is assumed to be in a state of plastic deformation. [36]

The constitutive model used in this research is the Johnson and Cook Viscoplastic Flow equation. "Viscoplastic" indicates that the material behavior is rate dependent [38]. The equation is shown below as: [39]

$$\sigma = (A + B\varepsilon^n)(1 + C \ln \dot{\varepsilon}^*)\,(1 - T^{*m}) \qquad 2.27$$

Where:

A = initial yield strength
B = hardening modulus
C = strain rate dependent coefficient
m = thermal softening coefficient
n = strain hardening coefficient
$\varepsilon$ = equivalent plastic strain
$\dot{\varepsilon}^*$ = the equivalent plastic strain rate/effective plastic strain rate
$T^*$ = homologous temperature = $\frac{(T - T_{room})}{T_{melt} - T_{room}}$
$T$ = Absolute temperature

The equation is divided into three bracketed components – the first set of brackets takes into account the strain when $T^* = 0$ and $\dot{\varepsilon}^* = 1$, the second set of brackets takes into account the strain rate effects, and the third set of brackets takes thermal effects into account.

Coefficients for this model come from experimental testing using both the Split-Hopkinson bar test and flyer plate experiments which allow material properties to be obtained within dynamic conditions.

### *2.6.1 Split Hopkinson Bar Test*

The Split-Bar Hopkinson test is carried out by placing a material sample in between two bars – the incident bar, and the transmission bar. A schematic of the experiment is shown below in Figure 14.

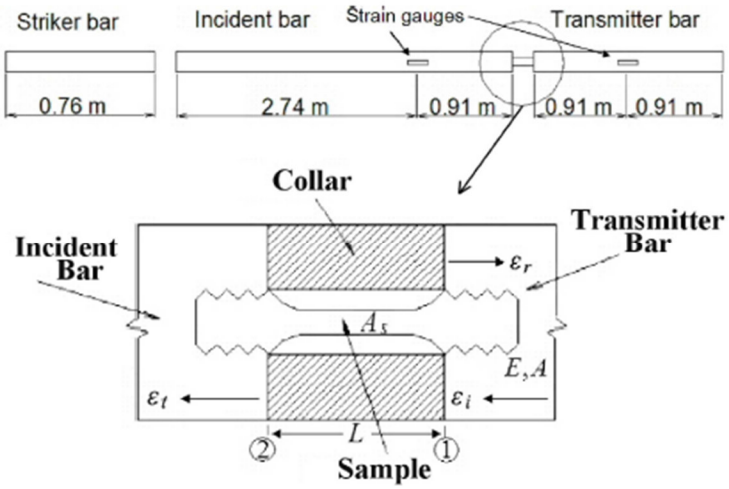


**Figure 14: Split-Hopkinson Bar Test Apparatus Schematic [37]**

The incident bar is struck by the striker bar causing an elastic pulse wave to travel through the specimen and the transmission bar. Strain gauges set up on the incident bar and the transmission bars are able to measure the strain waves that are transmitted and reflected [40]. Cinnamon in his dissertation was able to perform this test, and his experimental set up is shown in Figure 15.

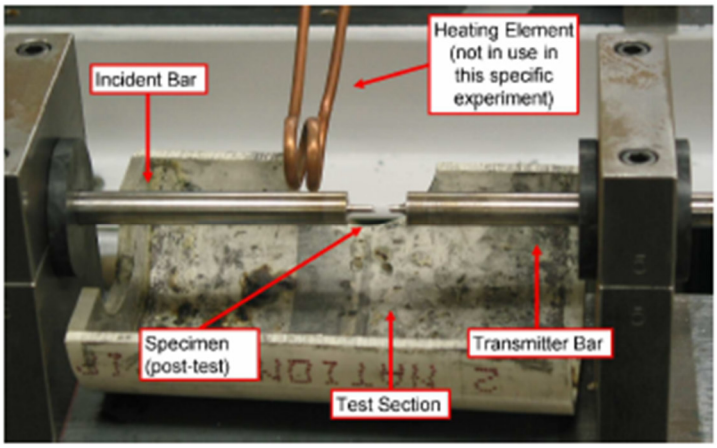


**Figure 15: Split Hopkinson Bar Apparatus Test Section at the University of Dayton [37]**

Using his results, he was able to determine the physical properties and material constants used in the Johnson and Cook Constitutive Model. His results are shown in Table 1.

**Table 1: Cinnamon's Experimental Results in the Physical Properties and Model Constants from the Split-Hopkinson Bar Test [37]**

| Property/Constant | 1080 Steel | VascoMax 300 |
|---|---|---|
| E (GPa) | 202.8 | 180.7 |
| $\nu$ | 0.27 | 0.283 |
| $T_{melt}$ (K) | 1670 | 1685 |
| $\rho$ $(kg/m^3)$ | 7800 | 8000 |
| JC: $A$ (GPa) | 0.525 | 2.17 |
| JC: $B$ (GPa) | 3.59 | 0.124 |
| JC: $C$ | 0.029 | 0.0046 |
| JC: $m$ | 0.7525 | 0.95 |
| JC: $n$ | 0.6677 | 0.3737 |

### *2.6.2 Flyer Plate Experiment*

The Split-Hopkinson Bar tests create strain rates on the order of $10^3$/second, but higher strain rates are required to fully characterize the constitutive model (on the order of $10^4$/sec-$10^5$/sec). Flyer plate impact tests reach these high strain rates, and allow for the stress to be measured with respect to time. In flyer plate experiments, it is the goal to strike a plate uniaxially with a flyer plate. A schematic of the experiment is shown below in Figure 16.

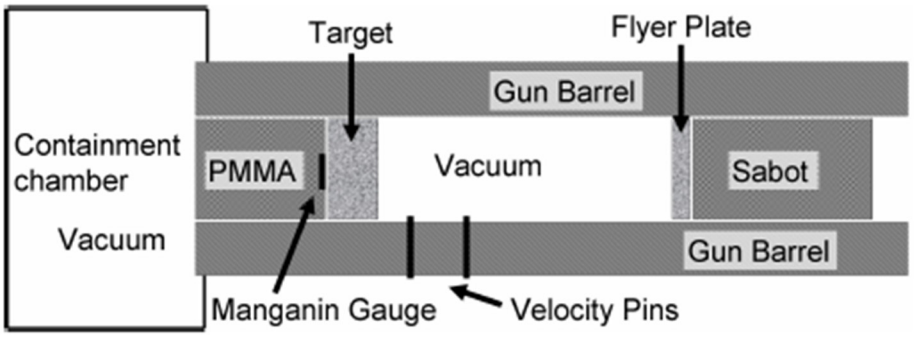


**Figure 16: Flyer Plate Experiment Schematic [37]**

Stress gauges behind the plate record the stress. The measurements should be able to pick up the plastic and elastic waves occurring and determine the peak stress and Hugoniot Elastic Limit as seen in Figure 17. [35]

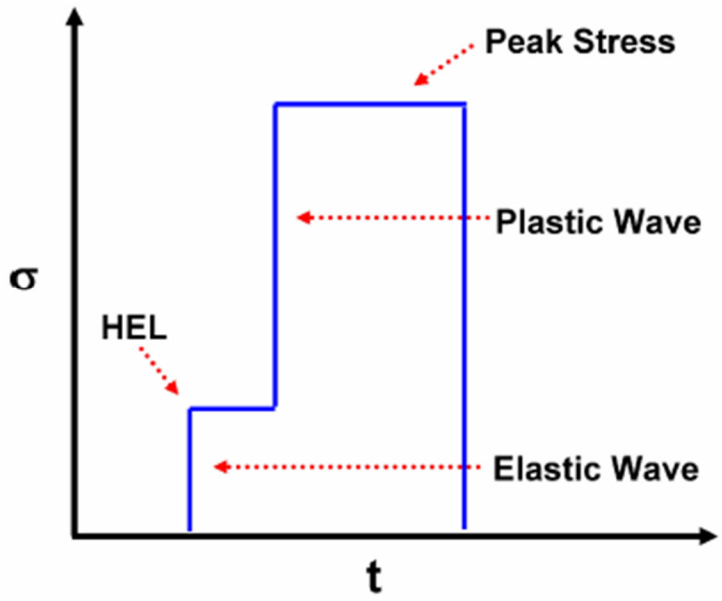


**Figure 17: Idealized Stress vs. Time Plot for a uniaxial Planar Impact [37]**

Cinnamon carried out these experiments in 2006. Figure 18 shows the flyer plate and target used in his experiment.

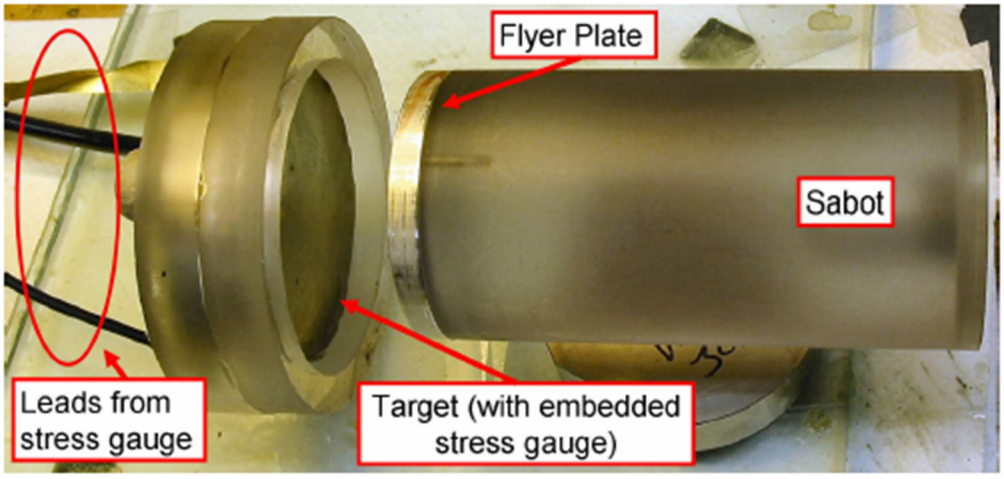


**Figure 18: Flyer Plate and Target used in University of Dayton Experiments [37]**

From data collected from these tests, all the constants can be determined. Results are seen in Table 2.

**Table 2: Cinnamon's Experimental Results in the Physical Properties and Model Constants from the Flyer Plate Tests [37]**

| Property/Constant | 1080 Steel | VascoMax 300 |
|---|---|---|
| E (GPa) | 202.8 | 180.7 |
| $\nu$ | 0.27 | 0.283 |
| $T_{melt}$ (K) | 1670 | 1685 |
| $\rho$ $(kg/m^3)$ | 7800 | 8000 |
| JC: $A$ (GPa) | 0.7 | 2.1 |
| JC: $B$ (GPa) | 3.6 | 0.124 |
| JC: $C$ | 0.017 | 0.03 |
| JC: $m$ | 0.25 | 0.8 |
| JC: $n$ | 0.6 | 0.3737 |

To obtain the final material constants to be used, the constants were adjusted to better fit experimental stress data. [37]

### *2.6.3 Johnson and Cook Constitutive Model Behavior*

A plot of the stress developed in a cell using ABAQUS gives some insight to how the stress is developing. This plot is seen in Figure 19.

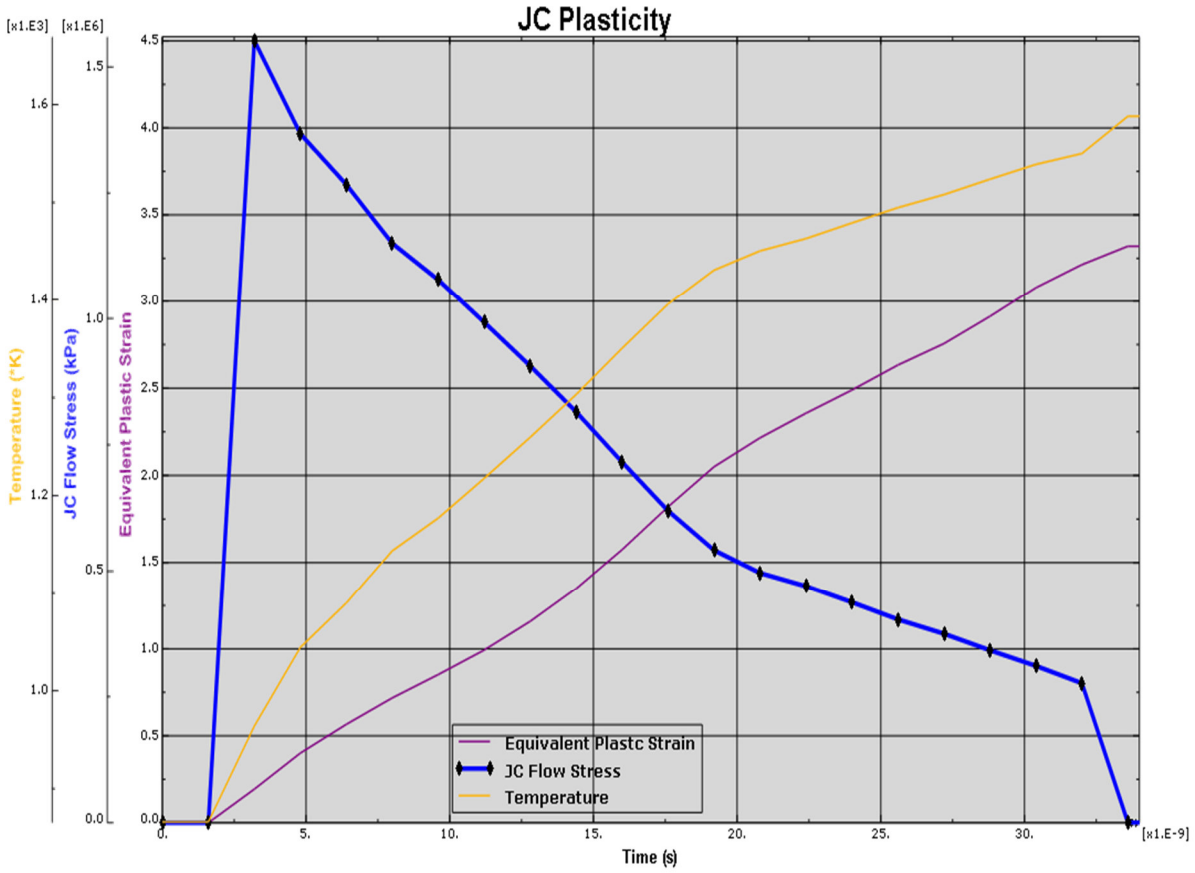


**Figure 19: Johnson and Cook Flow Stress Behavior Generated in ABAQUS [38]**

The feature of interest in Figure 19 is the blue line, which is the plot of the Johnson and Cook flow stress curve. The beginning of the curve shows the elasticity portion of stress, and is clearly linear. After hitting a maximum value, the plastic flow stress begins to develop. As the temperature and equivalent plastic strain increase, the plastic stress decreases until it hits a critical failing value. The stress drops off from there (In CTH the stress is directly set to 0)

The fact that the model includes the increase in temperature due to adiabatic heating from plastic deformation in its calculation of flow stress, takes into account the thermal softening and strain rate effects, in addition to having the material constants for

the model for our specific materials, makes this model an excellent candidate for this research. Additionally, it has its own accompanying failure criterion that is discussed in the next section.

## 2.7 Failure Criteria

The purpose of failure criteria is to predict what conditions will cause failure of a material. There are multitudes of different criteria to choose from, and each criterion will give different results for when failure occurs and how much damage accumulates. Thus, the selection of a damage criterion is a very influential part of modeling wear, as different criteria will predict different damage levels, and thus different wear levels. The differences in wear criteria are amplified even further for dynamic fracture. The flow equations are more complicated than in quasistatic fracture, and so criteria are more difficult to reliably develop for all dynamic impact cases. This research uses two failure criteria developed in previous research, as well as one new criterion that previously could only be used in ABAQUS.

### *2.7.1 Johnson and Cook Failure Criterion*

This study focuses mainly on the Johnson and Cook Failure Criterion, which is meant to be used in conjunction with the Johnson and Cook constitutive equation. It dictates when a material has failed based on strain rates. [39] It can be written as:

$$D = \int \frac{d\varepsilon}{\varepsilon^{pf}(T, p, \varepsilon, \dot{\varepsilon})} \qquad 2.28$$

Where:

D= Damage coefficient

$d\varepsilon$ = changing strain
$\varepsilon^{pf}$ = equivalent plastic strain at fracture
$T$ = absolute temperature
$p$ = pressure
$\varepsilon$ = strain
$\dot{\varepsilon}$ = equivalent deviatoric strain rate

The equivalent plastic strain is calculated with this equation wherein:

$$\varepsilon^{pf} = \left[D1 + D2\exp\left(-D3\frac{p}{Y}\right)\right]\left[\mathrm{D4} + \ln\left(\max(1,\dot{\varepsilon})\right)\right][1 + D5T^{*}] \qquad 2.29$$

Where

Y = yield stress (from Johnson and Cook model)
p = pressure
D1-D5 = experimentally determined coefficients

The equation is divided into three components: the first set of brackets denotes pressure dependence, the second set denoted strain rate dependence, and the third denotes temperature dependence. [38] The coefficients for the first set of brackets (D1-D3) are found experimentally from isothermal torsion tests, while D4 and D5 for the strain and temperature effects are found from un-notched tension tests and Hopkinson bar tests with varying temperatures. [39]

The damage coefficient (D) ranges in value from 0 to 1, where 0 indicates that no failure has occurred in the material, and 1 indicates total failure of the material. Numbers in between indicate partial failure. Once the material has failed, its tensile strength is set to 0 and it loses its ability to support shears. [39] This is a unique feature of the Johnson and Cook failure criterion that is not seen in other criteria used. It behaves much like a fluid and is essentially removed from the scenario.

### *2.7.2 Strain at Max Stress Failure Criterion*

This method determines failure based on the plastic strain at maximum stress for a given strain rate. True stress verses true strain was plotted by Hale for several strain rates, as shown below in Figure 20.

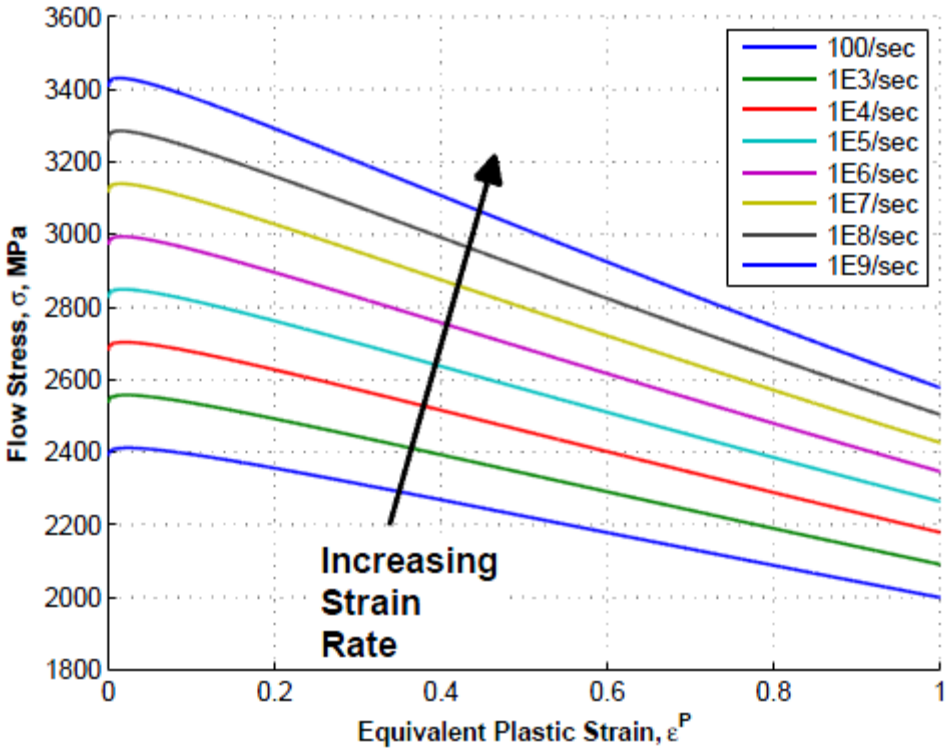


**Figure 20: True Stress-Strain Curves for Varying Strain Rates using the Johnson and Cook Constitutive Equation [3]**

The flow stress is the stress calculated using the Johnson and Cook constitutive equation. Each curve is the true stress- true strain plot of VascoMax300 at various strain rates, ranging from 100/s to 1E9 /s. The lowest strain rate produced a maximum stress of about 2.4GPa while the highest strain rate produces a maximum stress of over 3.4GPa.

These curves were developed using the Johnson-Cook constitutive equation. The critical stress is the maximum stress on the curve, and the critical equivalent plastic strain is the strain that occurs at the maximum stress value. To find the critical strain, one plots the critical plastic strain against the strain rate and fits performs a curve fit. This was done by Meador, and his resulting plot is shown below in Figure 21.

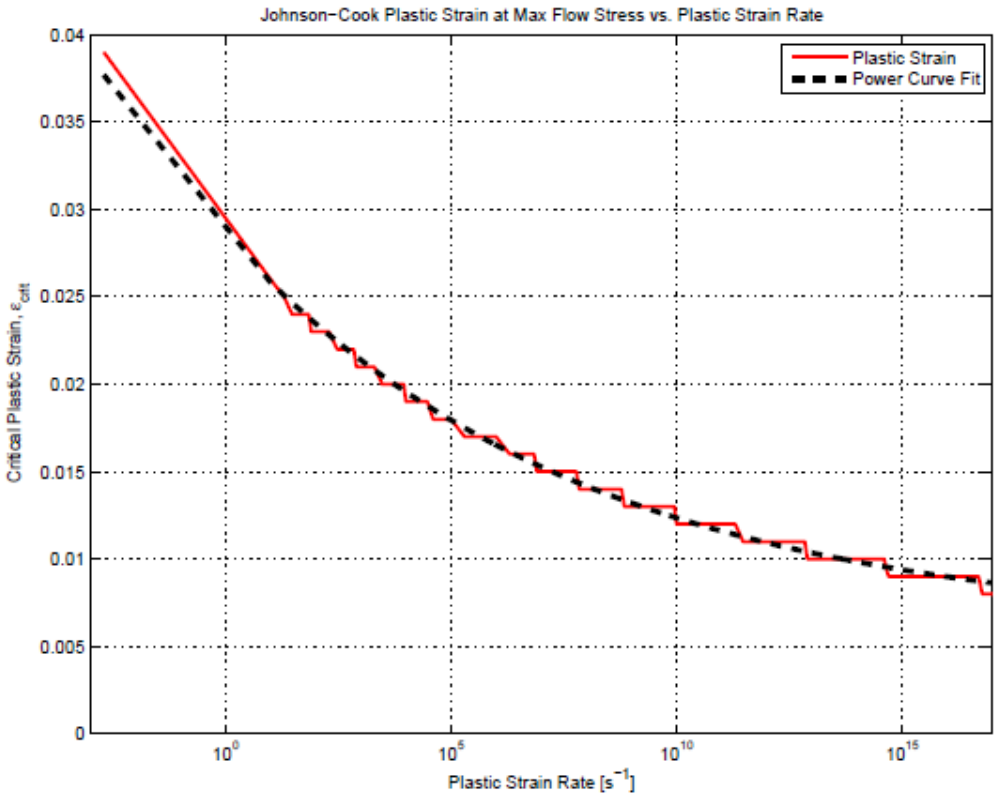


**Figure 21: Critical Plastic Strain Curve Fit [28]**

The resulting curve fit is shown in Equation 2.30.

$$\varepsilon_{crit}(x,y,t) = A_{PS}\dot{\varepsilon}(x,y,t)^{B_{PS}} + C_{PS} \qquad 2.30$$

Where $\varepsilon_{crit}$ is the critical strain, $\dot{\varepsilon}$ is the strain rate, $A_{PS}$, $B_{PS}$, and $C_{PS}$ are curve fit constants.

Table 3 shows the result of the curve fit.

**Table 3: Coefficients of Plastic Strain [4]**

| *Coefficient* | *Value* |
|---|---|
| $A_{PS}$ | 2.247E-2 MPa |
| $B_{PS}$ | -5.516E-2 |
| $C_{PS}$ | 6.044E-3 MPa |

Note that unlike the Johnson and Cook Failure Criteria, damaged material remains in the simulation.

### *2.7.3 von Mises Stress Criterion*

With the von Mises stress failure criterion, there is a maximum stress value that that once reached, counts the material as failed. This criterion was developed by Huber using work done by Hale. Hale found in his research that there were dominant strain rates for certain velocity ranges. [3] A maximum stress value from Johnson and Cook's model for VascoMax300 was determined by Hale based on the dominant strain rates. Hale's results are seen in Table 3 below:

**Table 4: Maximus Stress at Dominant Strain for VascoMax 300 [3]**

| *Velocity Range (m/s)* | *Dominant Strain Rate* | *Maximum Stress (MPa)* |
|---|---|---|
| 10-200 | $1 \times 10^5$ | 2,900 |
| 300-622 | $1 \times 10^6$ | 3,000 |
| 750-1530 | $1 \times 10^7$ | 3,130 |

Based on Hale's results, a maximum stress value of 3 GPa was set and compared to the von Mises stress calculated within CTH. As with the strain at max stress criterion, while the material is marked as failed, it is not removed from the simulation as it is with the Johnson and Cook failure criterion.

## 2.8 Hydrocodes

Due to the complexity and the sheer magnitude of the possible shock problems, it is of great help to have numerical solvers that can simultaneously solve these equations. A hydrocode is an extension of computational fluid dynamics programs. They are particularly geared for simulating dynamic events involving shocks. There are two reference frames that describe the way materials deform: Eulerian, or Lagrangian. [36]

Eulerian and Lagrangian systems vary in how they spatially represent materials in a system. Figure 22 gives a visual representation to show the difference.

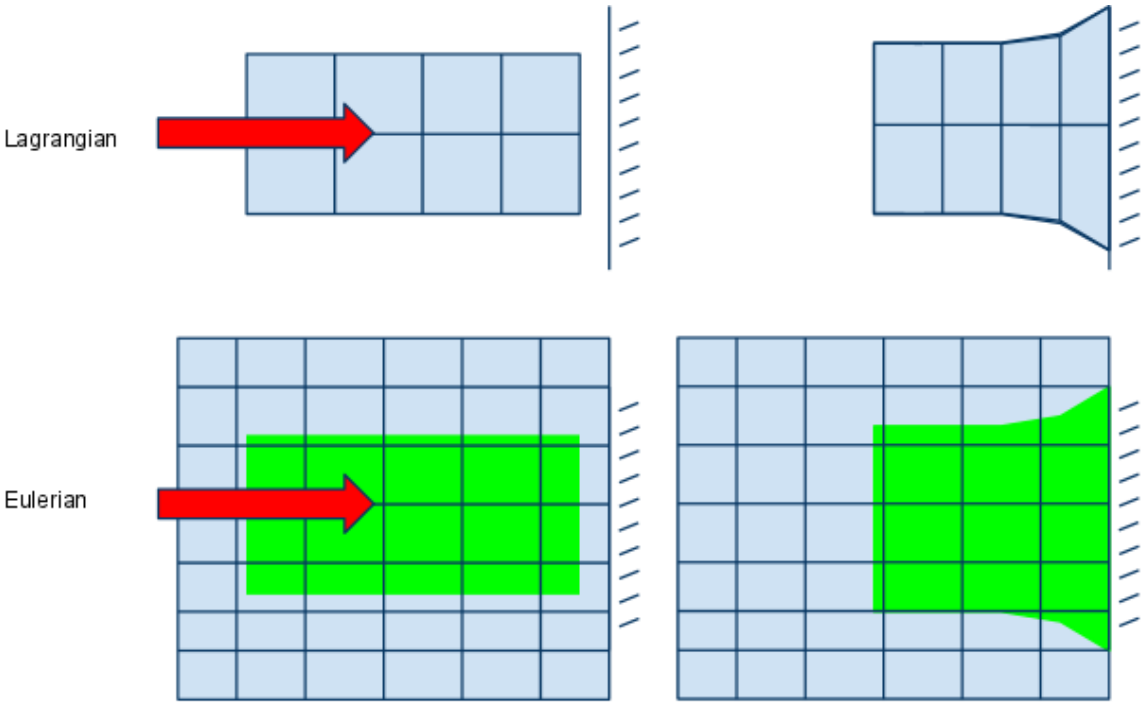


**Figure 22: Lagrangian and Eulerian Coordinate Systems [41]**

Consider the case above where a rectangle is accelerating into a wall and deforming. In the Lagrangian representation, the grid points are attached to the material and move with the material as the simulation progresses. Note how meshing is only

needed around the materials. Because the cells are allowed to deform, the volume changes, but never the mass, so thus the density is variable depending on if the cell is compressed or stretched.

In the Eulerian case, material is placed inside the mesh – which covers an entire area of action – and the grid points never move. Calculations are made based on the flow rates of materials through the cells. Thus, the volume of the cell never changes, but the amount of mass present in the cell can, and thus also the density. [36]

The equations used for each approach differ slightly due to the differing states. Below are the Lagrangian and Eulerian conservation equations used by hydrocodes. [36]

Lagrangian equations for conservation of mass, momentum, and energy respectively:

$$\frac{D\rho}{Dt} + \rho \frac{\partial v_i}{\partial x_i} = 0 \tag{2.31}$$

$$\frac{Dv_i}{Dt} = f_i + \frac{1}{\rho}\frac{\partial \sigma_{ji}}{\partial x_j} \tag{2.32}$$

$$\frac{De}{Dt} = f_i v_i + \frac{1}{\rho}\frac{\partial}{\partial x_j}(\sigma_{ij} v_i) \tag{2.33}$$

Eulerian equations for conservation of mass, momentum, and energy respectively:

$$\frac{\partial \rho}{\partial t} + \frac{\partial}{\partial x_i}(\rho v_i) = 0 \tag{2.34}$$

$$\frac{\partial v_i}{\partial t} + v_j \frac{\partial v_i}{\partial x_j} = f_i + \frac{1}{\rho}\frac{\partial \sigma_{ji}}{\partial x_j} \tag{2.35}$$

$$\frac{\partial e}{\partial t} + v_i \frac{\partial e}{\partial x_i} = f_i v_i + \frac{1}{\rho}\frac{\partial}{\partial x_j}(\sigma_{ij} v_i) \tag{2.36}$$

Where:
$v_i$ is the velocity
$\rho$ is the density
$\sigma_{ji}$ is the stress tensor
$e$ is the specific total energy
$f_i$ = the body force
$x_i$ is the Eulerian coordinate axis
i, and j are summation indices
$t$ is time

It is further noted that the total energy e can be split into the kinetic energy and the internal energy as seen in the equation below:

$$e = \frac{1}{2} v_i v_i + E \tag{2.37}$$

Where E is the specific internal energy.

With this addition, the conservation of energy equation can be written for the Lagrangian and Eulerian cases respectively as:

$$\frac{DE}{Dt} = \frac{P}{\rho^2}\frac{D\rho}{Dt} + \frac{1}{\rho} s_{ij}\dot{\varepsilon}_{ij} \tag{2.38}$$

$$\frac{\partial E}{\partial t} + v_i \frac{\partial E}{\partial x_i} = \frac{P}{\rho^2}\left(\frac{\partial \rho}{\partial t} + v_i \frac{\partial \rho}{\partial x_i}\right) + \frac{1}{\rho} s_{ij}\dot{\varepsilon}_{ij} \tag{2.39}$$

Where $s_{ij}$ is the stress deviators, $\dot{\varepsilon}_{ij}$ is the strain rates, and P is the hydrostatic pressure.

The Lagrangian and Eulerian equations are interchangeable by use of the substantial derivative, where:

$$\frac{D}{Dt} = \frac{\partial}{\partial t} + v_i \frac{\partial}{\partial x_i} \tag{2.40}$$

The program that is used in this research, CTH, is based primarily in the Eulerian system, but it does use the Lagrangian conservation equations before mapping them back over to the Eulerian system. This will be further addressed in the following sections.

Both sets of equations calculate solutions at grid points of meshes that are defined in the code.

Both systems have different advantages and disadvantages. The Lagrangian system can show the shape of the deformed materials much more accurately, and can work more easily with constitutive equations and failure criteria, because it is able to record the time history of the material. However, if events are too dynamic and the cells become extremely distorted, the Lagrangian system can struggle with making said calculations. The Eulerian system is much better in this case and is able to allow for these extreme cases to occur. However, the material position is only vaguely known, because once a material enters a cell, it is considered present in the entire cell. Thus the calculations for the constitutive equations and failure criteria are doable, but not as accurate in a Lagrangian system. Additionally, since materials are prone to mixing, the boundary conditions can be a bit trickier in an Eulerian system.

## 2.9 CTH

The specific hydrocode used in this research attempts to bring together the best of both worlds. It was developed by Sandia National Laboratories to model ballistic problems, so excels at modeling strong shock wave physics. It is an Eulerian-based system, but uses a Lagrangian step in its solving. [39] The solving process uses explicit integration based on a time step In the process of making calculations, first CTH takes a

Lagrangian step and solves the Lagrangian conservation equations for the given time step, then the deformed mesh is re-mapped back to the Eulerian mesh. A new time step is then calculated to satisfy the stability of the solution. [25]

### *2.9.1 Lagrangian Step*

During the Lagrangian step, the mesh is distorted to follow the motion of the material in Lagrangian using the Lagrangian conservation equations. The conservation of mass is already fulfilled since mass cannot exit the cell. Energy and momentum are calculated using finite volume representations. Care must be taken to select a time step that is small enough to prevent a wave from completely crossing a cell in one step. Mass, volume, momentum, and energy are all calculated. In the event that the conservation equations cannot be satisfied, CTH will always choose to satisfy the momentum equation.

### *2.9.2 Remap Step*

Calculations made in the Lagrangian step are transferred and new calculations are made to align them with the Eulerian mesh. Change in volume from the old cell to the new cell and where the changing masses end up are determined by an interface tracking algorithm set in CTH. Mass and internal energy is shifted between old and new cells. Using data from the tracking algorithm, momentum and kinetic energy is divided between cells based on the movement of mass. After the re-map step is complete, the next time step is calculated.

### *2.9.3 Boundary Conditions*

Boundary conditions are also an essential part of bringing a numerical model together. CTH has 6 different types of acoustic wave oriented boundary conditions and

two of them are used in this model. The mesh that is set up is surrounded by a secondary outer mesh consisting of "ghost cells." [39] These cells are used purely for numerical calculations, and the set boundary conditions determine how mass, momentum, and energy fluxes across boundaries.

The Type 0 boundary is the symmetry boundary condition, which models rigid boundaries and symmetrical geometry. This is particularly handy for cylindrical and spherical geometries. Velocity between the ghost cell and the interior mesh cell is set to 0 and the kinetic energy is converted to internal energy; there is no flux across the boundary.

The Type 1 boundary is the sound speed based absorbing boundary condition, which simulates and infinite/semi-infinite medium. Mass is allowed to flow in and out of the mesh. This type is used on the bottoms of the x and y meshes in our scenario, where the material is situated.

The Type 2 boundary is the outflow boundary condition. It allows mass to leave the system. When mass flows into the ghost cells, the ghost cells are automatically set to void. This is the condition places on the top of the x and y axis, where there is no material initially.

The Type 3 boundary condition is the inflow boundary condition, where mass can enter the interior of the mesh from the outside. The properties of the incoming mass are extrapolated from adjacent interior cells.

The Type 4 Boundary condition is the outflow extrapolation boundary condition. It linearly extrapolates the boundary pressure from the interior of them mesh. If the

extrapolated pressure turns out to be positive, then it is set to zero. Mass can flow in and out of the mesh. This condition is good for letting parts of the problem flow out while maintaining pressure,

The Type 5 boundary condition is similar to the Type 0 condition. It is symmetric, but mass is not allowed to flow in.

Type 6 boundary is periodic. This one is particularly unique because it has specific processor requirements (at least 2 processors must be in the periodic direction), and the boundaries must be set to be symmetrical, so the top and the bottom must both be periodic. It is used for modeling infinite or semi-infinite materials with an explicit microstructure.

While there are many options for boundary conditions in CTH, only type 1 and type 2 are used in our simulation to simulate the infinite air medium and to allow the slipper to exit the mesh.

### *2.9.4 Mixed Materials*

What does CTH do when more than one material occupies a cell? CTH has a few different options for how to deal with it. With mixed cell option 1 (Mix 1), the strength in the cell is a weighted average based on the volume fractions of the materials in the cells. Mix 5 sets the yield strength to 0 when materials mix. Mix 3 is like mix 1 in that it bases the yield strength on the mix of the materials, but divided by the sum of the volume fraction of the materials that support shears. This is what generally gives the best results and what is used in our model. [39] If the reader is curious what happened to mixes 2 and 4, they were options in previous generations of CTH but have since been removed.

### *2.9.4 Material Interface*

There are two options for how material will behave when it comes into contact with another material. The options are to allow for a sliding interface ("slide"), where there is no friction, or to call for a "no slide" condition, where the materials are essentially "welded together." [39] The materials will not move forward until the averaged fracture pressure of the materials in the cells has been reached. The reason for this very on/off approach to materials interacting is that in strong shock wave scenarios the normal stresses are usually much stronger than shear stresses, so typically fine tuning them is rarely necessary. Sadly, this means that the friction properties for sliding are non-negotiable. However, using the no slide condition gives an upper bound for wear because far more damage to the slipper must take place for the slipper to even move, and the slipper is continually taking additional damage as it is sliding. Dave Huber did work comparing the slide and no slide conditions, and as expected, wear rates using the no slide condition were always much higher than those using the slide condition. [29]

### *2.9.5 Tracers*

Tracer points can be set up within CTH to track the progress of variables. They are set at initial Lagrangian points and record requested data, such as the velocity, the pressure, the yield stress, the temperature, and any other data the user may want. The user can even define variables and have CTH perform calculations during the simulation and output them via tracer points. The data collected is what allows for post-processing and calculation of wear values to occur.

To track what exactly is happening as CTH progresses, let us examine the process of the failure of a cell using the Johnson and Cook failure criterion. At the initial stage, a velocity is imposed on the material along with a given time step. The first Lagrangian step occurs and the mesh deforms while state variables and flow stress are calculated, along with the plastic strain and the plastic strain at failure for the damage criteria. The mesh is then re-mapped back to its original position, and the calculated variables are also shifted into the Eulerian system. The failure criteria is checked – has it reached its critical value? If not, the next time step is calculated and the process repeats itself until. When using the Johnson and Cook failure criterion, if the critical value has been reached, the strength of the material in that cell is set to 0, so it can no longer support other material and behaves essentially like a fluid. If not, then the cell will fail based on when a fracture pressure of the materials is reached.

**2.10 Defining Wear**

Our research is interested in bringing together all of these pieces to determine wear. Wear here is the volume of material removed from the slipper. Wear rates are a ratio of the volume of material removed to the distance slid. Additionally wear rates per unit area, are used, which is the wear area divided by the distance slid.

Wear is defined at the volume of material removed. To obtain values for the wear rate in $mm^3/mm$, one runs a simulation and determines the number of failed cells based on whatever fracture criterion is being used, uses that number to calculate a volume and divides it by the distance slid.

## 2.11 Summary of Theory

In this section, the background behind the equations being used in this analysis has been reviewed, including wave mechanics through elastic, plastic, and shock waves, fundamental conservation equation reviewed, Lagrangian and Eulerian states explained, equations of states, constitutive equations, and failure criterion reviewed. Following this, a brief overview of how CTH applied these building blocks in its solving procedure was given. Now that the problem background and theory have been addressed, let us move on to previous wear results that this research attempts to match.

# III. Comparative Data

## 3.1 Chapter Overview

This research is focused around comparing wear results to experimental and other modeled data. Major Buentello has been working on an ABAQUS FEA model that models the same scenario as the CTH model. His model considers a few different collision scenarios, and is able to incorporate Coulomb's friction model (using a coefficient of friction determined in previous research by Montgomery) and uses Mie-Grüneisen EOS rather than the SESAME tables. [10] As such, he also has additional thermal considerations that are outside the scope of the CTH model. The idea in this research is to see if some of the refinement incorporated into the finite element approach is really necessary. Therefore, the approach used herein is to make use of a simple plane strain model with corrections and evaluate wear volume with the defined damage relations. The end result will then be compared without a thermal environment to the finite element solution.

## 3.2 2008 Experimental DADS Data

The HHTSS data this research is attempting to compare to come from a 2008 experiment. The set-up for the particular experiment can be seen in Figure 23.

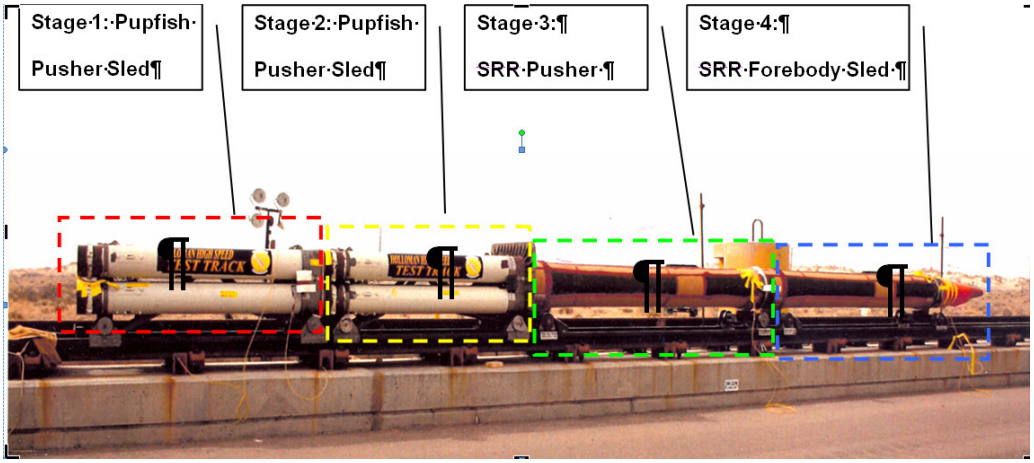


**Figure 23: Rocket Stages for the 2008 HHSTT Experiment [3]**

It consisted of the front forebody sled, which carried the experiment payload, and three pusher sleds, which carried rockets that propelled the experiment up to 1,530m/s. The entire experiment occurred in 8.14 seconds and over a distance of 5,816 m. [38] The front two sleds were fitted with slippers made from VascoMax300, but the back two sleds' slippers were made from AISI4130 Steel. One of the VascoMax300 slippers from stage 3 was recovered and it is the one focused on in the research. A diagram of the slipper can be seen in Figure 24.

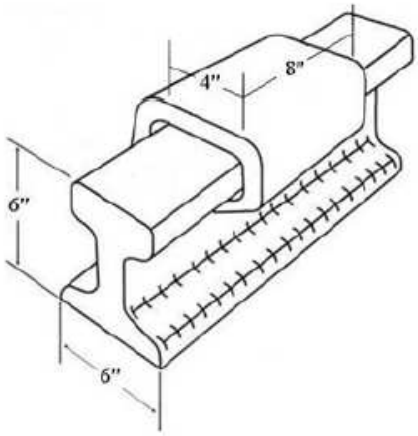


**Figure 24: Slipper and Rail dimensions [3]**

From technical drawings, the un-used slipper is assumed to have a nominal thickness of 14.7 mm. The area of the slipper subjected to wear damage was determined to be 103.5 $mm^2$, and the width of the slipper was determined to be 10.1 mm. [38] The total volumetric wear was determined to be 10.52 $cm^3$, or 3.49% of the initial top volume (300.9$cm^3$). The velocity profile of the slipper is shown below in Figure 25.

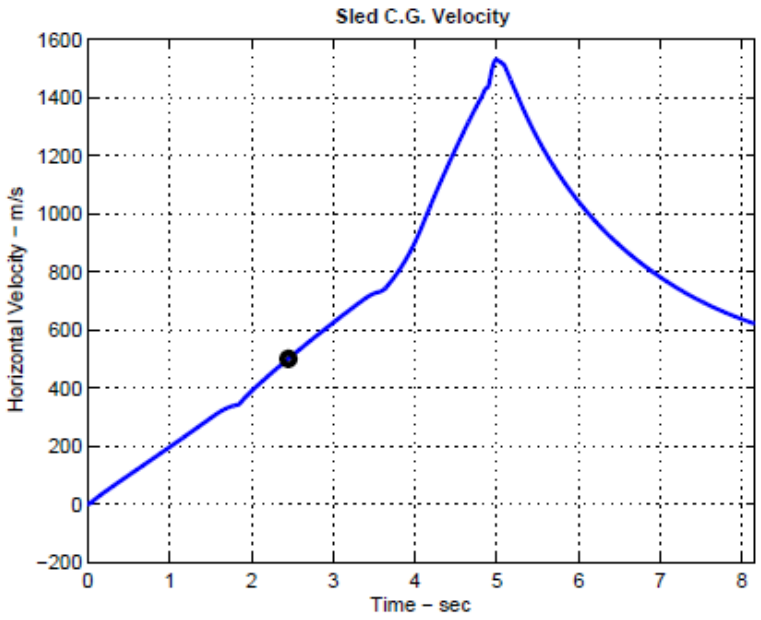


**Figure 25: Horizontal Sled Velocity of a stage 3 slipper from the 2008 HHSTT Experiment [3]**

Though one would like to imagine the entire trip is a smooth ride, there are some complications to consider. For one thing, the slipper does not stay in consistent contact with the rail. Figure 26 shows an incriminating shot of the slipper during a similar experiment in 2003.

(a) 80X-G1 Test Mission, April 2003, V = 2,853 m/s.

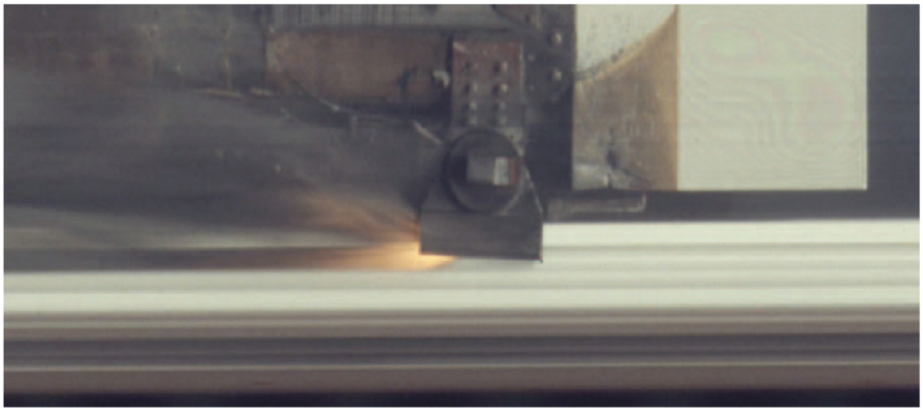

(b) 80X-G1 Test Mission, April 2003, V = 2,861 m/s.

**Figure 26: 2003 HHSTT Experiment showing Slipper Pitch**

As the picture shows, the slipper is pitched forward, so the majority of the wear is occurring at the front of the slipper. Additionally, due to the aerodynamics of the experiment, lift is generated, causing the slipper to bounce on the rail.

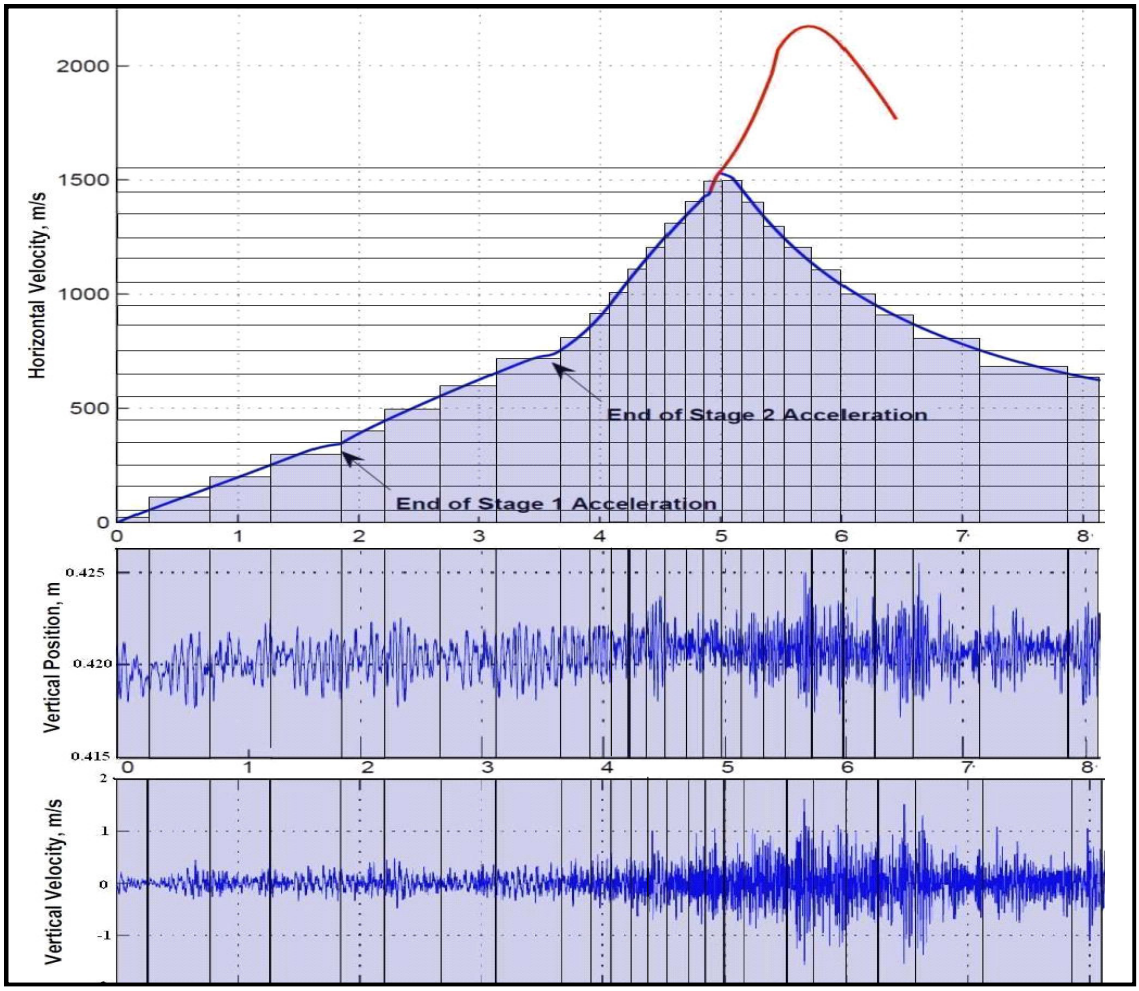


**Figure 27: Discretized Horizontal Velocity, Vertical Position, and Vertical Velocity of a Stage 3 Slipper [3]**

This figure shows the vibration while the slipper runs along the track. This means that the bottom of the slipper is not in contact with the rail 100% of the time. This has already affected research with Meador where he discovered that due to the bouncing the thermal distribution coefficient needed to be adjusted. [28] It is a major consideration that Buentello is attempting to account for in his ABAQUS model.

### 3.3 3D Abaqus Model

Major Buentello has created a model in ABAQUS to attempt to model the wear. It models the same scenario as the CTH model – a slipper colliding with single asperity. His model uses the Johnsons and Cook flow stress model, implements the Mie-Grüneisen EOS as opposed to SESAME tables, and implements a contact algorithm between the two materials and uses Coulomb's Friction Model as seen below in Equation 3.1.

$$F_f \leq \mu F_n \tag{3.1}$$

Where

$F_f$ = Friction force
$\mu$ = Friction coefficient
$F_n$ = Normal force

The friction coefficient used is based on Montgomery's previous work. [10]

$$V_d = \sum_{n=1}^{n} W_{uA_n} A_{c_n} D_{S_n} \%Cont_n \tag{3.2}$$

Where:

$V_d$= Damage volume
$W_{uAn}$= Wear per unit area
$A_c$ = Area of contact
$D_s$ = Sliding distance
%Cont = Percent of contact time the slipper had with the rail.

The results are shown below in Table 5.

**Table 5: ABAQUS Volume Damage Calculations [38]**

| | Avg. Vel (m/s) | $W_{uAi}$ (mm^3/mm^2) | width (mm) | Avg Worn length $l_i$ (mm) | Sliding Distance $D_i$ | % Contact | Predicted Vol. Damage $V_i$ | Measured $V_i$ |
|---|---|---|---|---|---|---|---|---|
| Stage 1 | 175 | 1.67E-6 | 101 | 70 | 323000 | .3063 | 1168.1 | 6716.5 |
| Stage 2 | 500 | 1.81E-6 | 101 | 35 | 1016000 | .3063 | 1993.9 | 1684.2 |
| Stage 3 | 1100 | 2.65E-6 | 101 | 22.5 | 1356000 | .3063 | 2501.2 | 1010 |
| Desa 1 | 1250 | 2.78E-6 | 101 | 10 | 1265000 | .3063 | 1086.0 | 252.5 |
| Desa 2 | 750 | 2.2E-6 | 101 | 25 | 1680000 | .3063 | 2858.5 | 909 |
| | | | | Totals | 5816000 | | 9607.8 | 10572 |

The $W_{uA}$ numbers are generated from Buentello's ABAQUS model using a 2um asperity for the collision. The width is known from technical drawings and the sliding distance and is known from the DADS data. The percent contact is assumed to be 0.3063 from previous work. The predicted volume damage was calculated using equation 3.2. The measured volume came from calculations made by Buentello. Looking over work done by Hale, Buentello noted that there were 5 general worn areas on the slipper and was able to identity which area would have worn away based on each acceleration or deceleration stage. This is illustrated in Figure 28.

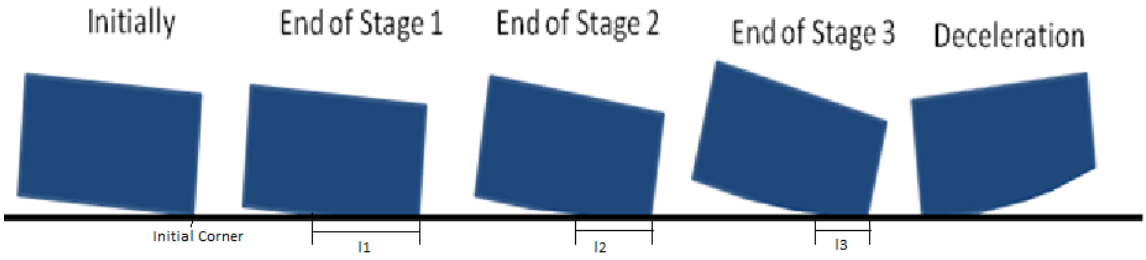


**Figure 28: Wear Areas based on Acceleration State [38]**

From this observation, he calculated the observed removed volume for each stage. The total wear calculated from this method closely matched with the total wear removed from the slipper (10.52 $cm^3$ compared to 10.57 $cm^3$). This research attempts to compare its results to the Stage 2, 500mps wear area rate and wear volume.

### 3.4 Differences between ABAQUS and CTH

Previously the workings of CTH were described, but how exactly are the differences from the ABAQUS code used? The most obvious difference is that CTH is an Eulerian-based system, but ABAQUS is Lagrangian based system. This means CTH has an advantage at higher velocities because its mesh won't distort too much to be able to perform calculations, but ABAQUS had better defined boundary conditions between materials. While CTH uses acoustic wave boundary conditions, ABAQUS boundary conditions are based on stress and displacement. Additionally they're more easily defined since its mesh is attached to materials separately, and materials aren't sharing as in CTH. Not only will it more accurately predict specific shapes of material deformation, but it can also have a defined friction force between materials.

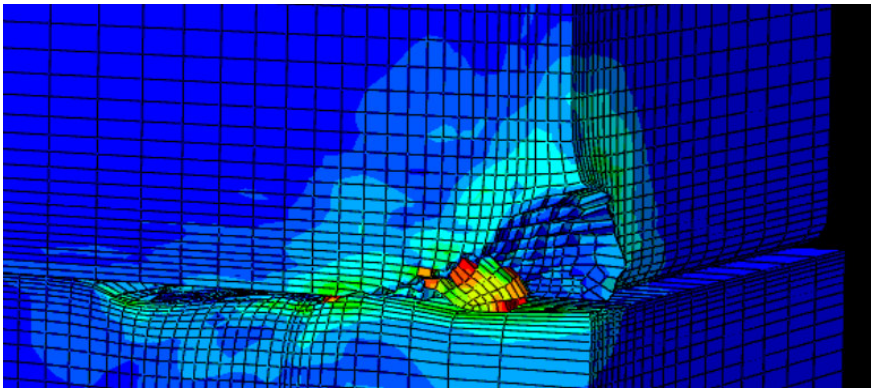

**Figure 29: ABAQUS Model showing damage occurring to the slipper [38]**

Thus, ABAQUS is better able to take into account adhesion and abrasion wear, while CTH's ability to add it in is crude at best. Additionally the way the two programs make their calculations differ. CTH uses finite volume calculations by explicitly integrating at the edges of the cells to get its data. ABAQUS uses finite difference methods to get its data.

### 3.5 Wolfson Experimental Data

Wolfson in his experiments was able vary the sliding materials he used, velocities, normal forces, track conditions, and bearing pressures. As such not all of his experiments are applicable to this study, but of the 60 runs, 2 of them are comparable. They use stainless steel sliders on a bare steel track. The wear was originally in units of in./ft, but by multiplying the results by the slider area and converting units the data is comparable to this study's results. The conversion is shown in Equation 3.3.

$$Wear_{rate} = W_{wolfson} A_n \qquad 3.3$$

Where $W_{wolfson}$ is the measured wear rate and $A_n$ is 1 $in.^2$ (645.16$mm^2$)

The values used are seen in Table 6.

**Table 6: Wolfson Data Conversion**

| Sliding Velocity | | Average Wolfson Wear Rate | | Converted Average Wear Rate |
|---|---|---|---|---|
| ft/s | m/s | in./ft | mm/mm | $mm^3/mm$ |
| 825 | 251.46 | 9.50E-6 | 7.92E-7 | 5.11E-4 |
| 2500 | 762 | 7.50E-6 | 6.25E-7 | 4.03E-4 |

### 3.6 Previous AFIT Work

Both Chad Hale and Dave Huber have done previous work that this research will compare against. Chad Hale developed a global and a local submodel finite element analysis. The results from his local submodel are used to compare to our results. He ran 12 different target velocities using a 6um asperity. His model dimensions can be seen in Figure 30.

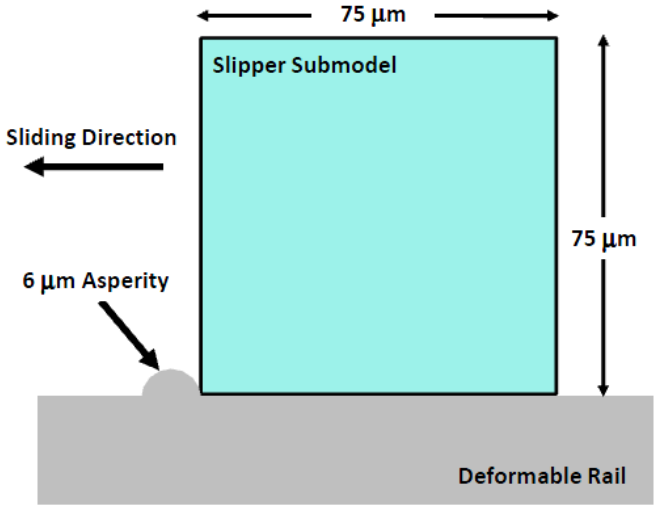


**Figure 30: Hale's Plain Strain ABAQUS Model Dimensions**

Hale uses the Mie-Grüneisen EOS, the Johnson and Cook constitutive Viscoplastic model, and also uses the Johnson and Cook failure criterion. The results from his work are shown below in Table 7.

**Table 7: Hale's Wear Volume Rate Results**

| Velocity | Hale (FEA) |
|---|---|
| (m/s) | mm^3/mm |
| 10 | 2.63E-05 |
| 20 | 3.44E-05 |
| 40 | 3.79E-05 |
| 100 | 4.88E-05 |
| 200 | 8.42E-05 |
| 300 | 1.20E-04 |
| 500 | 2.00E-04 |
| 622 | 2.13E-04 |
| 750 | 1.93E-04 |
| 1000 | 1.87E-04 |
| 1250 | 1.67E-04 |
| 1530 | 1.37E-04 |

Huber used a model near identical to the model used in this research. The difference between his work and this work is the use of the Johnson and Cook Failure Criterion, and the ability to pinpoint maximum wear. Huber's work, simulations were run using the following equation:

$$t_{sim} = \frac{(1.1)r_a}{v_{slide}} \qquad 3.4$$

Where $t_{sim}$ is the simulation time, $r_a$ is the asperity radius, and $v_{slide}$ is the sliding velocity.

This equation was used so that the slipper would run over the maximum height of the asperity, however it was found in this research that the time for maximum wear varied

based on failure criteria and slipper size. The data used from Huber's work is shown in Table 8.

**Table 8: Huber's Wear Volume Rate Results**

| **Velocity** | Slide Line Strain at $\sigma_{max}$ | Slide Line von Mises stress |
|---|---|---|
| m/s | mm^3/mm | mm^3/mm |
| 200 | 7.49E-05 | 3.71E-05 |
| 300 | 8.34E-05 | 6.16E-05 |
| 400 | 1.05E-04 | 1.09E-04 |
| 500 | 1.45E-04 | 1.70E-04 |
| 600 | 1.70E-04 | 2.04E-04 |
| 700 | 1.86E-04 | 2.42E-04 |
| 800 | 2.06E-04 | 2.79E-04 |
| 900 | 2.20E-04 | 3.03E-04 |
| 1000 | 2.32E-04 | 3.21E-04 |
| 1100 | 2.44E-04 | 3.33E-04 |
| 1200 | 2.58E-04 | 3.44E-04 |
| 1300 | 2.62E-04 | 3.63E-04 |
| 1400 | 2.64E-04 | 3.61E-04 |
| 1500 | 2.67E-04 | 3.45E-04 |

# IV. Analysis and Results

## 4.1 Goal

The aim of this research is to implement a 2D plane strain model in CTH using the Johnson and Cook fracture criterion to represent a 3D wear event, to validate it by comparing it to previous studies' wear results.

## 4.2 Plane Strain Model

It is of interest to use a 2D plane strain model because of its simplicity.

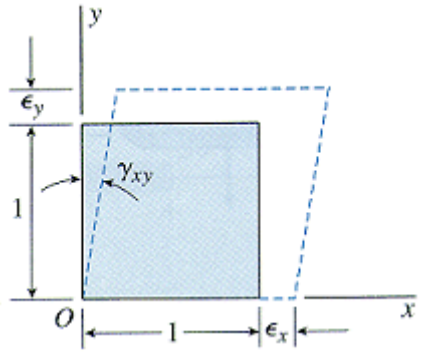


**Figure 31: Plane Strain Diagram [X]**

By placing the model in a 2D coordinate system, the model completely ignores strains in the z direction and shear strains in the xz and yx planes.

The 2D plane strain model consists of a 0.0125cm by 0.0649cm slipper sliding along a 0.0200cm by 0.850cm rail with a constant velocity. The total model is seen in Figure 32.

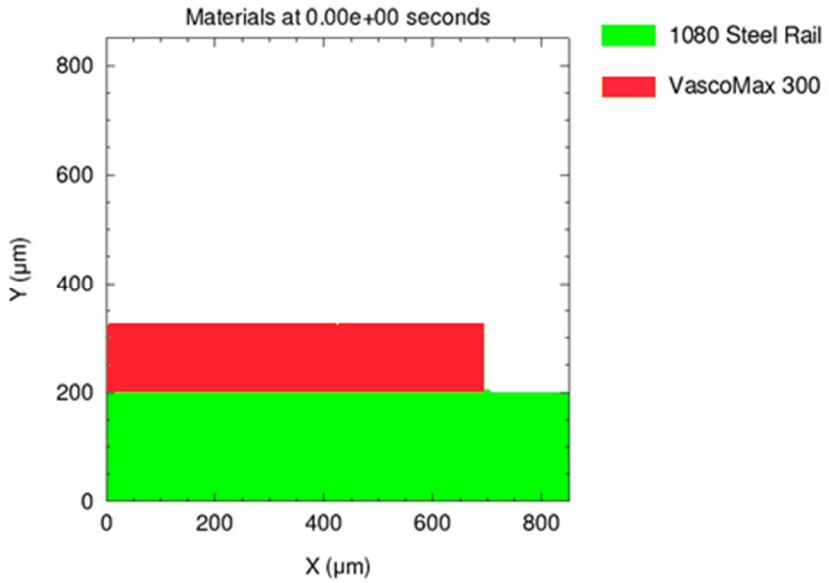


**Figure 32: CTH Plane Strain Model**

The slipper collides with an asperity placed in front of it, which range in size from 6um to 2um.1295 cells are traced throughout the simulation, and recorded are the position, yield stress, cell volume fraction (fraction of material volumes present in each cell), strain rate, and optionally the Johnson and Cook damage coefficient. In this research velocities varied between 200m/s and 1500m/s.

To get an idea of how the material collision looks in CTH, Figures 33-36 show the progress of the material flow over time.

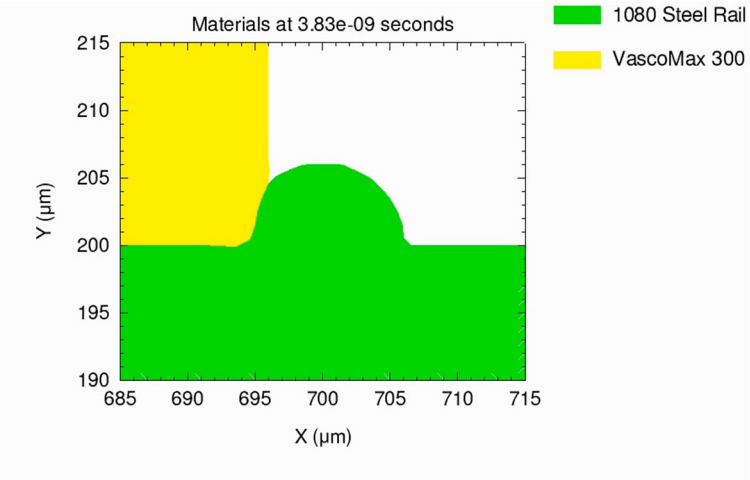


**Figure 33: Material Flow Stage 1**

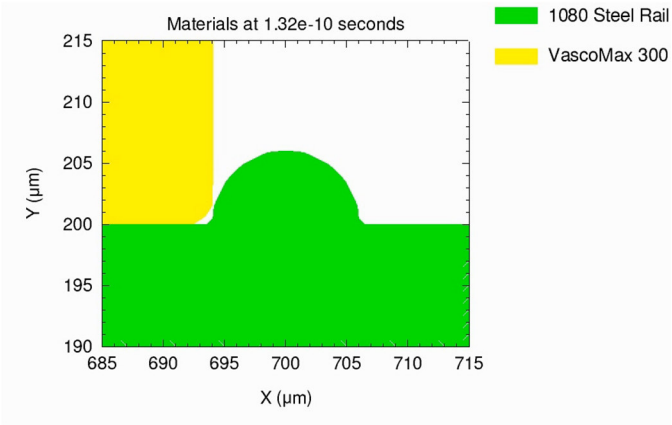


**Figure 34: Material Flow Stage 2**

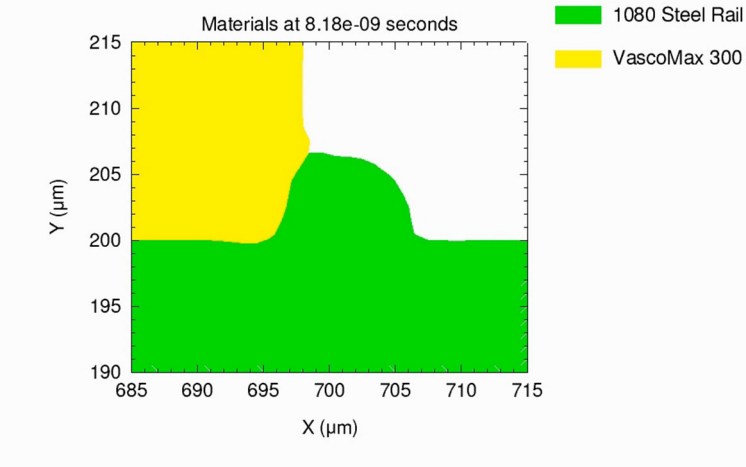


**Figure 35: Material Flow Stage 3**

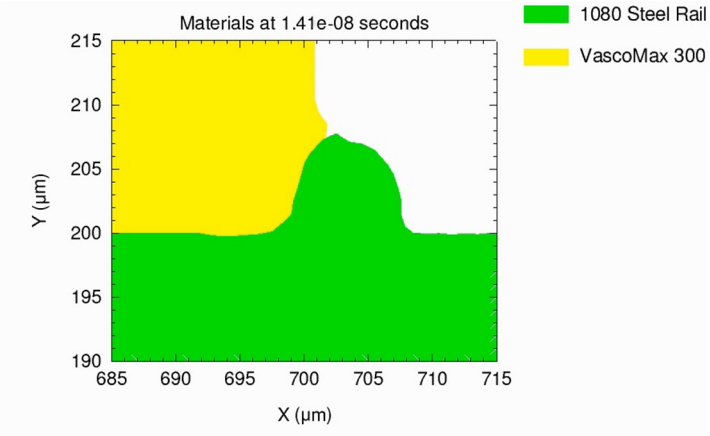


**Figure 36: Material Flow Stage 4**

It is seen that the boundaries between the materials aren't exactly crisp, as is characteristic of an Eulerian system. Deformation is not really occuring, but the materials are flowing together.

As the impact occurs, the pressure in the materials increases dramatically. Figures 37-40 show how this progresses in the simulation.

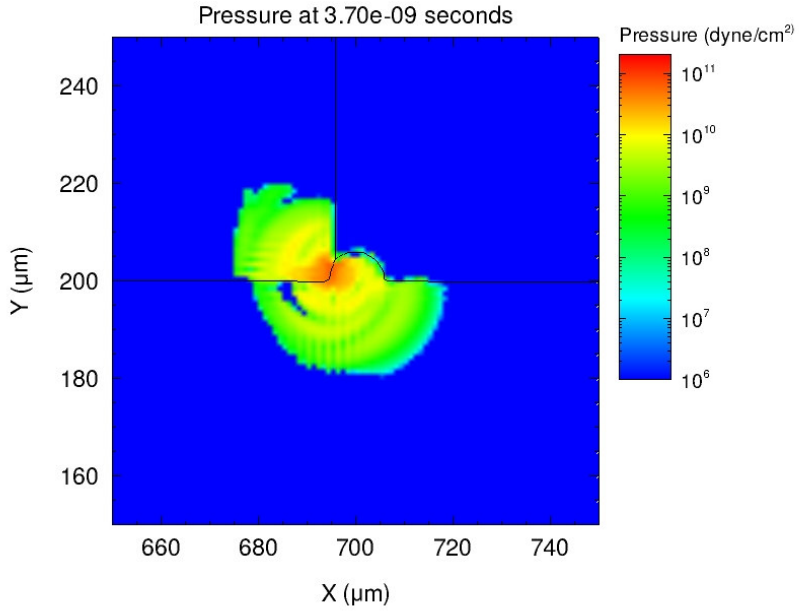


**Figure 37: Pressure Development Stage 1**

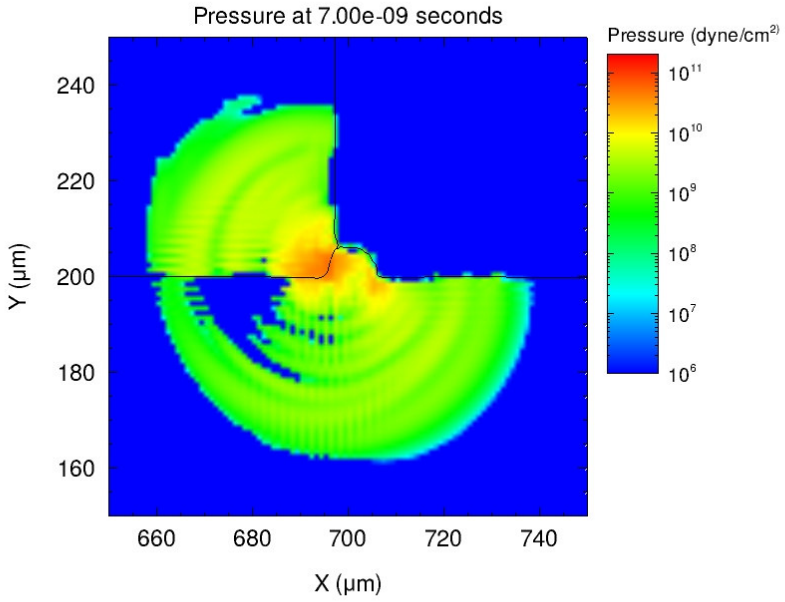


**Figure 38: Pressure Development Stage 2**

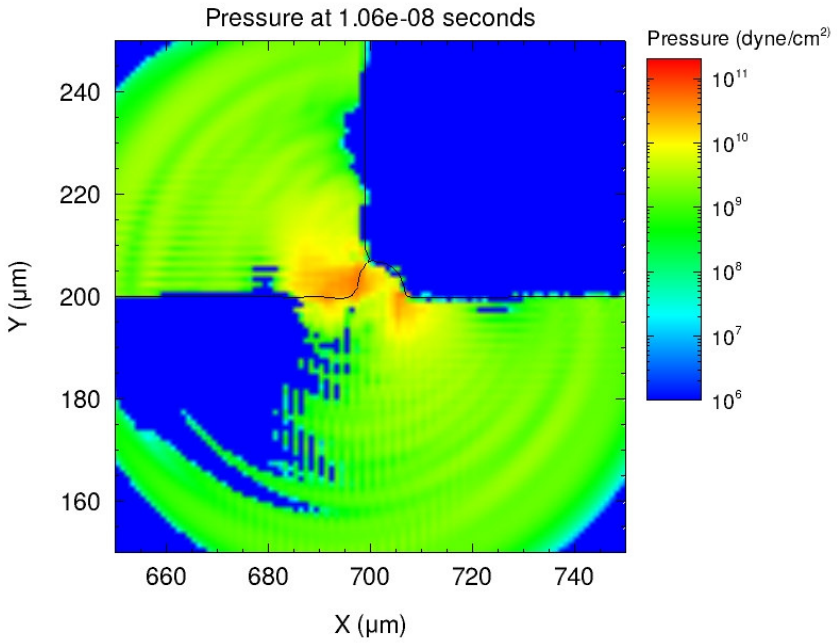


**Figure 39: Pressure Development Stage 3**

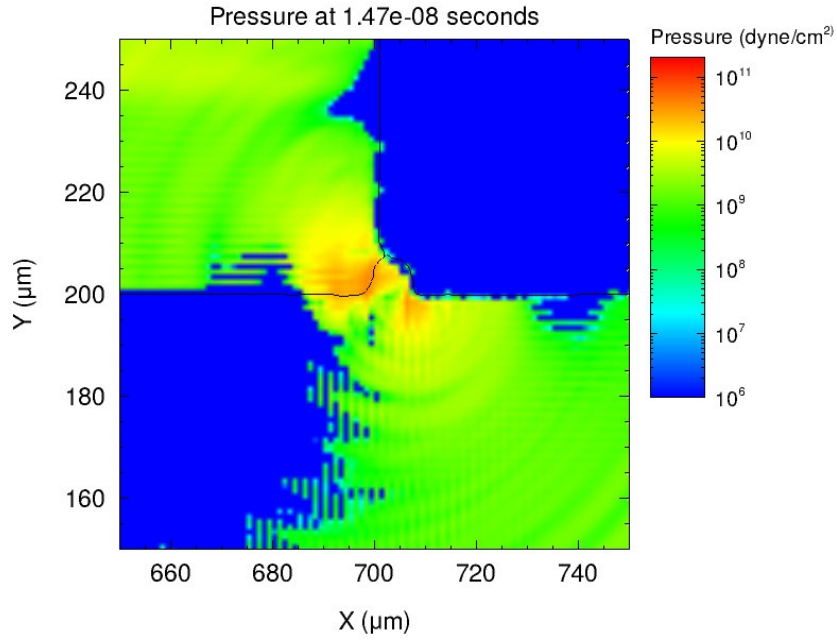


**Figure 40: Pressure Development Stage 4**

As the figures show, pressure propagates progressively in a wave pattern in both the slipper and the asperity, with the less intense elastic waves traveling more quickly than the stronger plastic waves. As time continues the strength begins to dissipate,

The materials for the slipper and rail are Vascomax300 and 1080 steel respectively, to mirror what is actually used at HHSTT. The properties of these materials are listed below.

**Table 9: VascoMax300 and 1080 Steel Material Properties**

| *Property* | *VascoMax 300* | *1080 Steel* |
|---|---|---|
| **Melt Temperature, $T_{melt}$** | 1,685K | 1,670 K |
| **Density, ρ** | 8, 000 kg/m$^3$ | 7,800 kg/m$^3$ |
| **Poisson's Ratio, $\nu$** | 0.283 | 0.270 |
| **Modulus of Elasticity, E** | 180.7 GPa | 202.8 GPa |
| **Hardness, H** | 200 GPa | - |

The Johnson and Cook plasticity model and failure criterion are also used in the model, with constants as shown below.

$$\sigma = (A + B\varepsilon^n)(1 + C \ln \dot{\varepsilon}^*)\,(1 - T^{*m}) \qquad 2.27$$

**Table 10: Johnson and Cooke Constitutive Model Material Constants**

| *Constant* | *VascoMax 300* | *Steel 1080* |
|---|---|---|
| A | 2.1E10 | 0.7E10 |
| B | 0.124E10 | 3.6E10 |
| C | 0.03 | 0.17 |
| M | 0.8 | 0.25 |
| N | .3737 | 0.6 |

$$D = \int \frac{d\varepsilon}{\varepsilon^{pf}(T, p, \varepsilon, \dot{\varepsilon})} \qquad 2.28$$

$$\varepsilon^{pf} = \left[D1 + D2 \exp\left(-D3\frac{p}{Y}\right)\right]\left[\mathrm{D4} + \ln\left(\max(1, \dot{\varepsilon})\right)\right][1 + D5T^*] \qquad 2.29$$

**Table 11: Johnson and Cook Failure Criterion Material Constants**

| *Constant* | *VascoMax 300* |
|---|---|
| D1 | -0.09 |
| D2 | 0.27 |
| D3 | -0.48 |
| D4 | 0.014 |
| D5 | 3.870 |

One thing to note about the Johnson and Cook Failure Criterion constants is that D3 is negative in CTH. The way the equation in arranged in ABAQUS, D3 is positive.

### 4.3 Wear Calculation Road Map

Wear is defined at the volume of material removed. To obtain values for the wear rate in $mm^3/mm$, one runs a simulation and determines the number of failed cells based on whatever fracture criteria being used, uses that number to calculate an area and divides it by the distance slid. This number is then multiplied by a spherical correction factor (SCF). Specifics for how this is done follow.

To give an overview of what is to be presented, first, how the damaged areas for each failure criteria will be presented and then used to calculate wear per unit width ($mm^2/mm$) in section 4.4. Results for these calculations are presented graphically. The next topic introduced is how to calculate the SCF in section 4.5, which entails how to calculate single asperity wear. Results for the single asperity wear and the SCFs are given. Finally in section 4.6, wear volume rates ($mm^3/mm$) are given and results are compared to prior work.

## 4.4 Wear Per unit Width Calculaitions

### *4.4.1 Plastic Strain at Max Stress Criterion*

In CTH, the strains and strain rate data are extracted from the simulation. Then the critical strain equation is applied to the strain rate data, and if the strain is over the critical strain value, then the cell is marked as failed with a "1," non-failed cells are set to "0." The table of failed-non-failed cells is then multiplied by the volume fraction of the slipper, so that only the slipper failed cells are counted and not any rail failures. The finally result is summed up to then apply to an area.

### *4.4.2 von Mises Stress Criterion*

Based on Hale's results, a maximum stress value of 3 GPa was set and compared to the von Mises stress calculated within CTH. [29] Once again, cells that reached the critical value are set to 1 and all other cells are set to 0. The failed slipper cells are isolated by multiplying by the slipper volume fraction. The final result is summed up into a single value

### *4.4.3 Johnson and Cook Fracture Criterion*

Johnson and Cook's Fracture Criterion was addressed previously, and is conveniently calculated within CTH. It is easier to use as a criterion because it is already in a 0-1 range, allows partially failed cells to be added into the calculation, and is already only tracking the slipper material, so does not need to be isolated out from the rail material with the volume fraction. The final damage numbers in the simulation are simply summed.

### *4.3.4 Damage Area*

Once the damage sums are calculated based on each stress criteria, these numbers are converted to an area ($mm^2$) by multiplying the by the mesh area of the traced cells. A wear rate can be obtained by dividing the wear area by the distance slid to have a final result in terms of $mm^2/mm$. However, to make comparison with 3D models, the wear rate needs to be in $mm^3/mm$ units. Thus a correction factor is needed to apply to the results.

### *4.3.5 Putting it all together*

To obtain the wear per unit width, the damage area is calculated depending on what failure criteria is being used, and then divided by the distance slid. [3]

$$W_{uw} = \frac{A_d}{D_s} \qquad 4.1$$

Where $W_{uw}$ is the wear per unit width, $A_d$ is the damage area which varies depending on the failure criterion in use, and $D_s$ is the sliding distance of the slipper.

Previously the wear per unit width values were calculated using equation 3.4, but by plotting the wear rate against time, it has been observed that this time is not when the maximum damage to the slipper has occurred. Work has been done in ABAQUS to find the time when the maximum damage has occurred and no additional damage is done to the slipper. Similar efforts were made using CTH, but the results are inconclusive. The specific CTH and MATLAB codes used can be found in Appendix A, B.1 and B.2. Figures 41-43 show some examples of the damage area per time results.

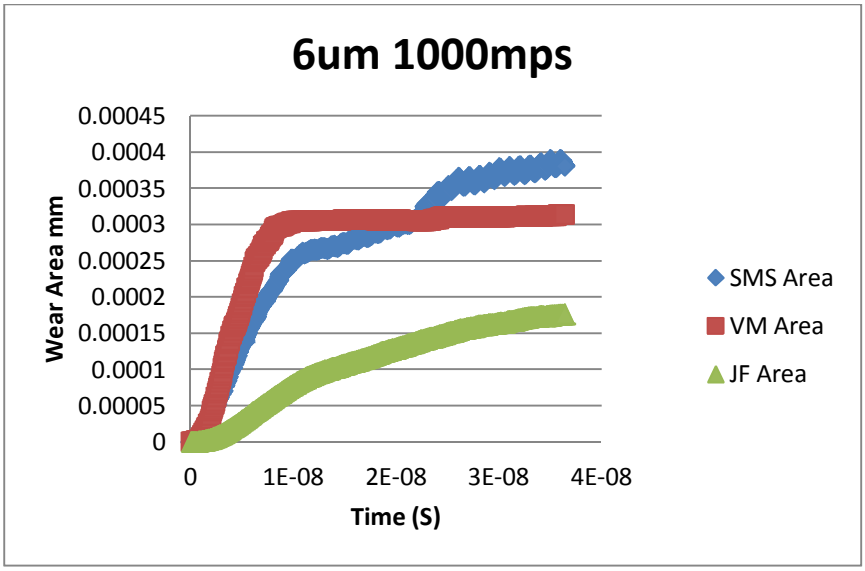


**Figure 41: 6um 1000mps**

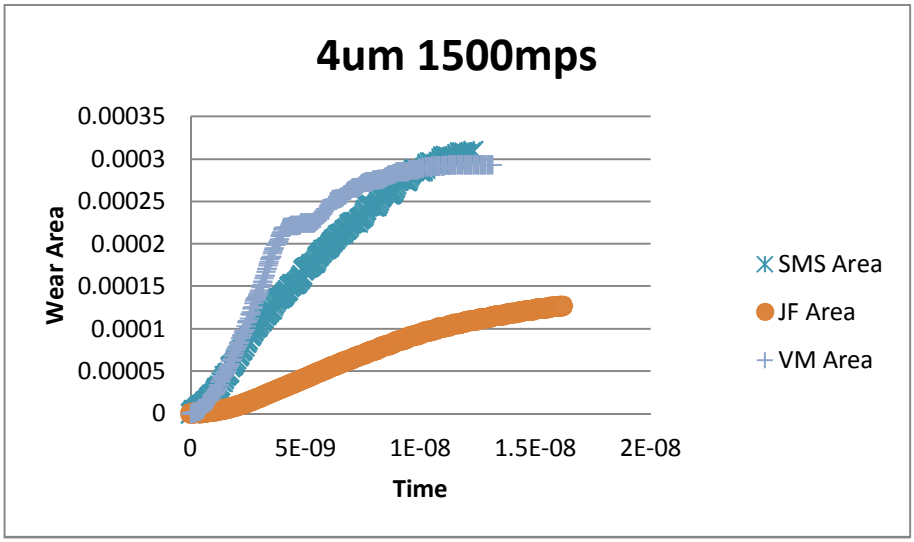


**Figure 42: 4um 1500mps**

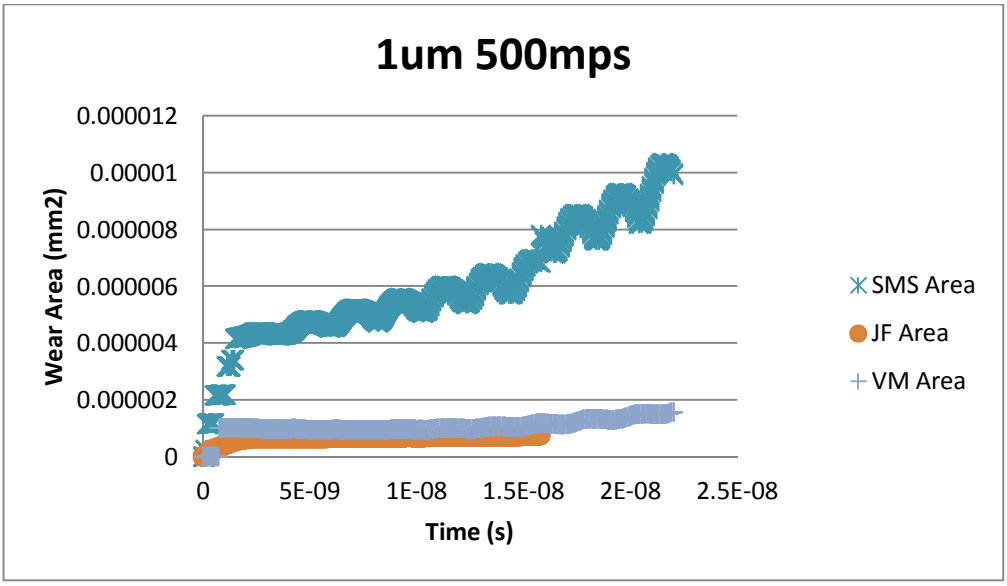


**Figure 43: 1um: 500mps**

These plots show different asperity sizes and different collision speeds. No two plots are exactly alike. When the maximum damage has been reached, the wear area should level off to a flat line. In Figure 41, the von Mises damage area is very clearly exhibiting this behavior. However, the strain at max stress and Johnson and Cook damage areas do not level off and are continuing to increase. Thus it is thought that simulations will need to be run for longer simulation times to try to capture maximum damage area for the other two criteria. The results for the simulations that were run can be found in Appendix C.

### 4.5 Spherical Correction Factor

There is a lot that can be done with the wear per unit width data. Chad Hale and Dave Huber were able to compare their work to Wolfson's experimental data. But how were they able to convert their data from $mm^2/mm$ to $mm^3$? They needed a way to transition their results from a 2D scenario to a 3D scenario. Hale was able to do this by

developing a conversion factor, which in this research is referred to as the spherical correction factor.

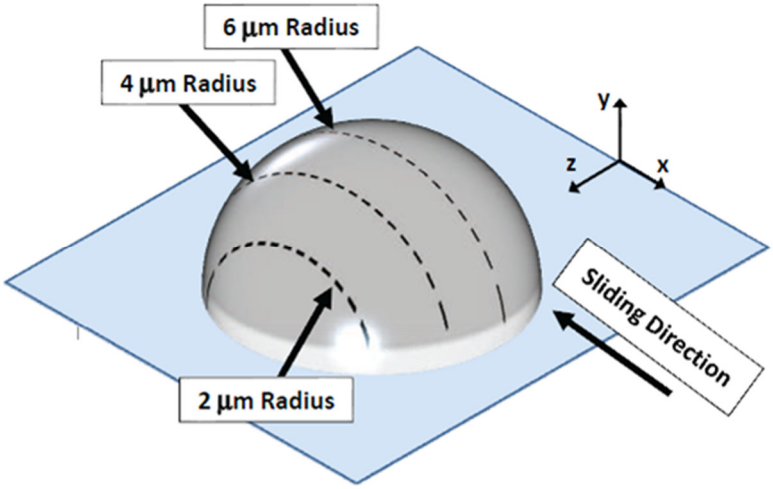


(a) Hemispherical Asperity

Hale found this constant by finding the wear of a single asperity, and dividing it by the wear rate per unit width of the asperity of interest (in his case, 6um).

$$SCF = \frac{W_{sa}}{W_{uw}} \qquad 4.2$$

Where $W_{sa}$ is the single asperity wear and $W_{uw}$ is the wear per unit width.

This was done for multiple heights along the total asperity size of interest for multiple collision velocities. The results were then averaged together for a final result.

Hale developed this constant in ABAQUS and Huber used it in his work in CTH. However since the number can have a very large impact on the end wear results, it was of interest to see how the correction factor would turn out if it were calculated in CTH using different failure criteria.

### *4.5.1 Single Asperity Wear Rates*

To be able to get the correction factor, the wear rate for a single asperity is needed. The single asperity wear represents the wear occurring as a function of height of the asperity.

$$W_{sa} = 2\int_{0}^{\substack{asperity \\ radius}} W_{uw}(y)\, dy \qquad 4.3$$

To make this calculation, wear rates per unit widths were calculated for different heights along the asperity – for a 6um correction factor, heights 2, 4, and 6 were used. For a 2um asperity factor, 0.5, 1, and 2 microns were used. All of these wear rates were calculated at 200, 500, 1000, and 1500 m/s in contrast to Chad Hale, who used 10, 100, 500, 1000, and 1530 m/s. Lower velocities were excluded from CTH calculation because CTH does not handle low velocities well due to its lack of friction modeling. These results were then plotted according to their wear rate and the location along the asperity laterally, which was calculated in the yz plane using the equation below:

$$z = \sqrt{r^2 - y^2} \qquad 4.4$$

Where z is the asperity distance in the z plane, r is the asperity radius, and y is the asperity height in the y plane.

This was done and the results are as follows for a 2um asperity using the strain at max stress and the Johnson and Cook Failure criteria.

**Table 12: 2um Wear per Unit Width Data for Single Asperity Calculations using the Strain at Max Stress Failure Criterion**

| | 2um Strain at Max Stress Failure Criteria | | | | |
|---|---|---|---|---|---|
| | Wear rate per unit width ($W_{uw}$) | | | | |
| | 200 | 500 | 1000 | 1500 | Distance |
| 2 microns | 0.002711 | 0.002715 | 0.003031 | 0.010604 | 0.00 |
| 1 micron | 0.002113 | 0.000901 | 0.002536 | 0.004896 | 1.73 |
| 0.5 microns | 0.001604 | 0.001573 | 0.000706 | 0.001017 | 1.93 |
| 0microns | 0 | 0 | 0 | 0 | 2 |

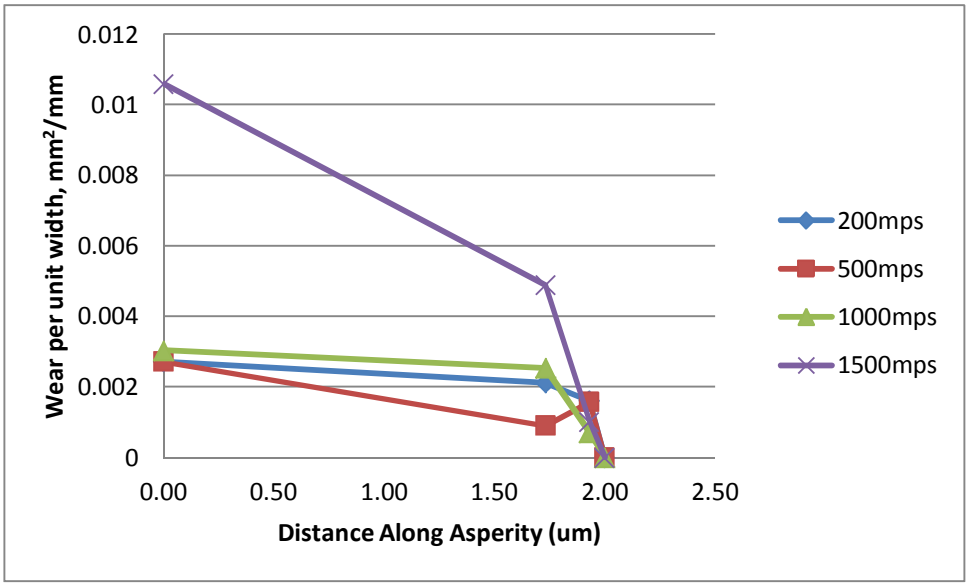


**Figure 44: Single Asperity formation using SMS Failure Criteria**

**Table 13: 2um Wear per Unit Width Data for Single Asperity Calculations using the Johnson and Cook Failure Criterion**

| | 2um Johnson and Cook Failure Criteria | | | | |
|---|---|---|---|---|---|
| | Wear rate per unit width ($W_{uw}$) | | | | |
| | 200 | 500 | 1000 | 1500 | Distance |
| 2 microns | 0.000907 | 0.000771 | 0.000940 | 0.002536 | 0.00 |
| 1 micron | 0.000049 | 0.000095 | 0.000000 | 0.000498 | 1.73 |
| 0.5 microns | 0.000000 | 0.000043 | 0.000036 | 0.000069 | 1.93 |
| 0 microns | 0 | 0 | 0 | 0 | 2 |

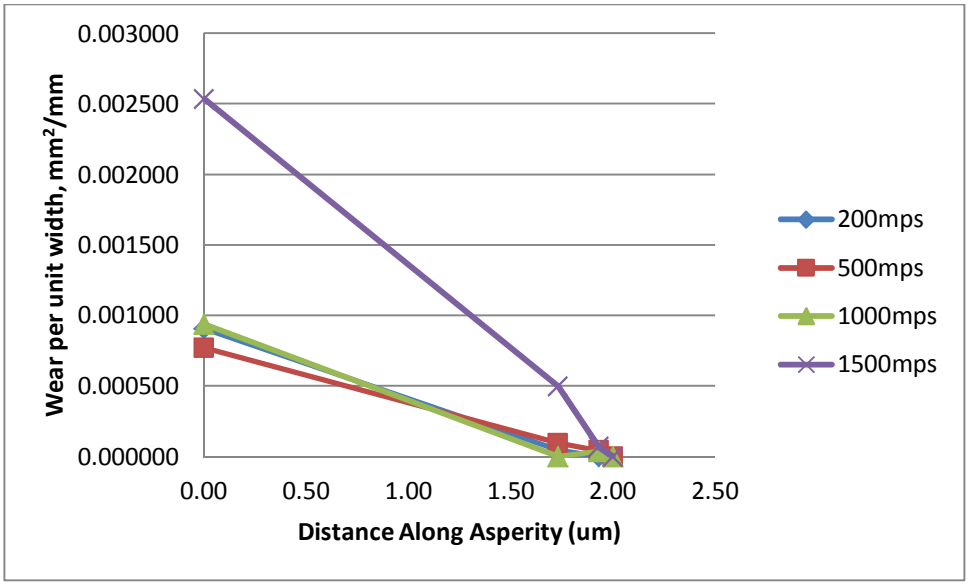


**Figure 45: Single Asperity formation using JC Failure Criteria**

The single asperity rates for each of these velocities was obtained by finding the average area under the curve and multiplying by 2, as established in equation 4.3. To find the correction factor, one divides the single asperity rate found by the wear per unit width of the radius of the asperity. Finally by taking the average of all of the velocities single asperity rates, one arrives at a value that can be used generally for any velocity. Those results are seen below in Tables 14 and 15.

**Table 14: Spherical Correction Factor Calculations for a 2um asperity using the Strain at Max Stress Failure Criterion**

| Velocity | Single asperity wear rate ($W_{sa}$) | $W_{uw}$ (2um) | Ratio ($W_{sa}/W_{uw}$) |
|---|---|---|---|
| m/s | $mm^3/mm$ | $mm^2/mm$ | mm |
| 200 | 9.203E-03 | 2.71E-03 | 3.39E+00 |
| 500 | 6.862E-03 | 2.72E-03 | 2.53E+00 |
| 1000 | 1.033E-02 | 3.03E-03 | 3.41E+00 |
| 1500 | 2.809E-02 | 1.06E-02 | 2.65E+00 |
| | | Average: | 3.00E+00 |

**Table 15: Spherical Correction Factor Calculations for a 2um asperity using the Johnson and Cook Failure Criterion**

| Velocity | Single asperity wear rate ($W_{sa}$) | $W_{uw}$ (2um) | Ratio ($W_{sa}/W_{uw}$) |
|---|---|---|---|
| m/s | $mm^3/mm$ | $mm^2/mm$ | mm |
| 200 | 1.666E-03 | 9.07E-04 | 1.84E+00 |
| 500 | 1.530E-03 | 7.71E-04 | 1.98E+00 |
| 1000 | 1.637E-03 | 9.40E-04 | 1.74E+00 |
| 1500 | 5.372E-03 | 2.54E-03 | 2.12E+00 |
| | | Average: | 1.92E+00 |

### *4.5.2 Spherical Correction Factor Comparison*

This was done for both a 6um asperity and a 2um asperity. The 6um asperity was originally done by Chad Hale and is useful for comparing to previous work. Hale assumed that the correction factor was linearly scalable based on the asperity size. The 2um correction factor was of interest to compare to Buentello's ABAQUS simulation, where a 2um asperity was being used for calculations. All of the calculations performed to arrive at the final numbers are included in Appendix D. Here are the comparative results:

**Table 16: Comparative Spherical Correction Factors**

| **Source** | ABAQUS [3] | CTH | CTH |
|---|---|---|---|
| **Failure Criteria** | Johnson and Cook | Strain at Max Stress | Johnson and Cook |
| **6um Asperity Radius** | 8.29 | 10.1 | 9.58 |
| **2um Asperity Radius** | 2.76 | 3.00 | 1.92 |

The new CTH values are higher than the ABAQUS factor the 6 micron correction factor, and are above and below the ABAQUS values for the 2 micron asperity. The CTH numbers do seem reasonable when compared to the ABAQUS results. This is particularly

encouraging as it confirms that the two programs, despite their differences, can produce competitive results. However CTH's results do not confirm that the correction factor can be scaled based on asperity size. Now that the spherical correction factor has been calculated, wear volumes can be found.

### 4.6 Wear Results and Comparison

For the results section, the failure criteria will be abbreviated to SMS (strain at max stress), VM (von Mises), and JCF (Johnson and Cook Fracture) as a space saving measure. The wear volume rate in $mm^3/mm$ is found using the following equation:

$$WVR = \frac{W_{uw} SCF}{D_s} \qquad 4.6$$

Previous work by Hale and Huber used 6um asperities, so for the moment 6um wear results will only be used. However, now there are different failure criteria to throw into the mix, so those will also be compared. Below are the results found in this study:

**Table 17: Wear Volume Rates using Various Failure Criteria and SCF**

| | Wear Volume Rate (mm^3/mm) | | | | | | | | |
|---|---|---|---|---|---|---|---|---|---|
| | ABAQUS correction Factor (8.29*10^-3) | | | SMS correction Factor (10.1*10^-3) | | | JCF Correction Factor (9.58*10^-3) | | |
| | SMS | VM | JCF | SMS | VM | JCF | SMS | VM | JCF |
| 200 | 9.32E-05 | 5.14E-05 | 2.45E-05 | 1.13E-04 | 6.24E-05 | 2.97E-05 | 1.08E-04 | 5.95E-05 | 2.83E-05 |
| 500 | 6.16E-05 | 5.49E-05 | 3.08E-05 | 7.48E-05 | 6.66E-05 | 3.74E-05 | 7.13E-05 | 6.35E-05 | 3.57E-05 |
| 1000 | 8.72E-05 | 2.78E-04 | 4.02E-05 | 1.06E-04 | 3.37E-04 | 4.87E-05 | 1.01E-04 | 3.22E-04 | 4.64E-05 |
| 1500 | 9.99E-05 | 3.29E-04 | 4.65E-05 | 1.21E-04 | 3.99E-04 | 5.64E-05 | 1.16E-04 | 3.80E-04 | 5.37E-05 |

Graphically, they look something like this:

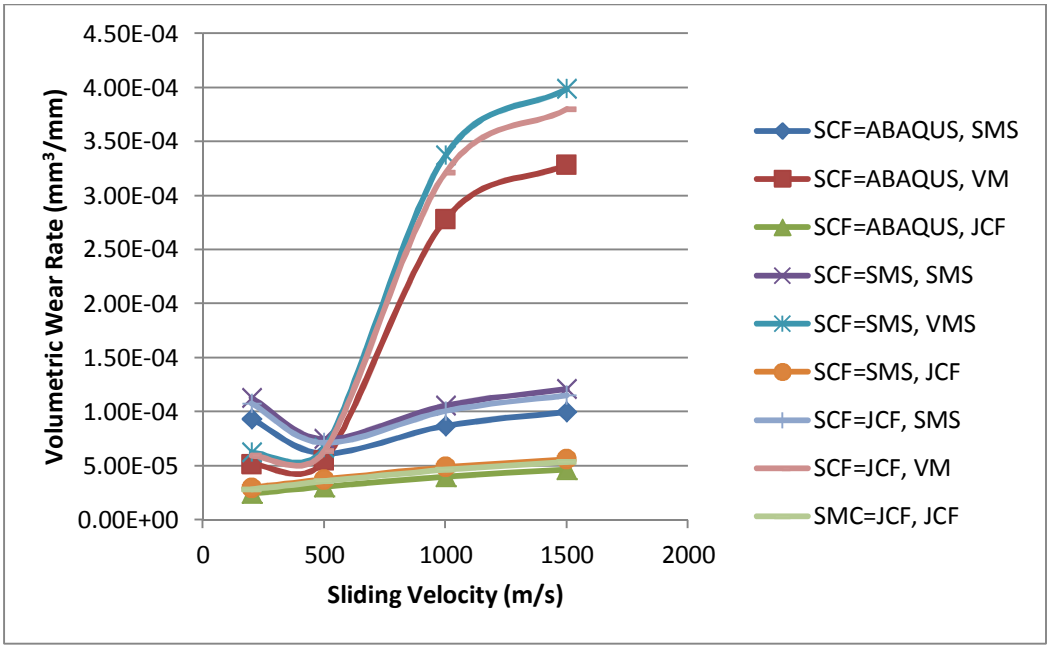


**Figure 46: Graphical Wear Volume Comparison**

To unpack this graph a bit, there seems to be two major groups, an upper wear bound and a lower wear bound. The three grouped lines at the very bottom of the graph are wear rates using the Johnson and Cook failure criterion. The group of three lines above the Johnson and Cook failure criterion values are the wear rates using the strain at max stress failure criteria. Finally, the three lines grouped at the top of the graph are all the wear rates generated using the von Mises failure criterion. Applying the spherical correction factors provides an upper bound and a lower bound of possible wear rates, with the strain at max stress correction factor providing the upper bound value and the Johnson and Cook correction factor providing the lower bound value.

The Johnson and Cook wear rates are all lower than the von Mises and strain at max stress wear rates. This is because of the feature of the Johnson and Cook failure criterion to allow the strength of damaged materials to be set to zero during the simulation. Removing the material strength lessens the pressure in the slipper and reduces

the overall wear. When material is not allowed to leave, pressure accumulates more and the wear rate is increased.

How do these results stack up against previous work results? Here is a visual comparison of this research's work (prefaced with LW in the legend, the author's initials) to Huber, Hale, and Wolfson's data:

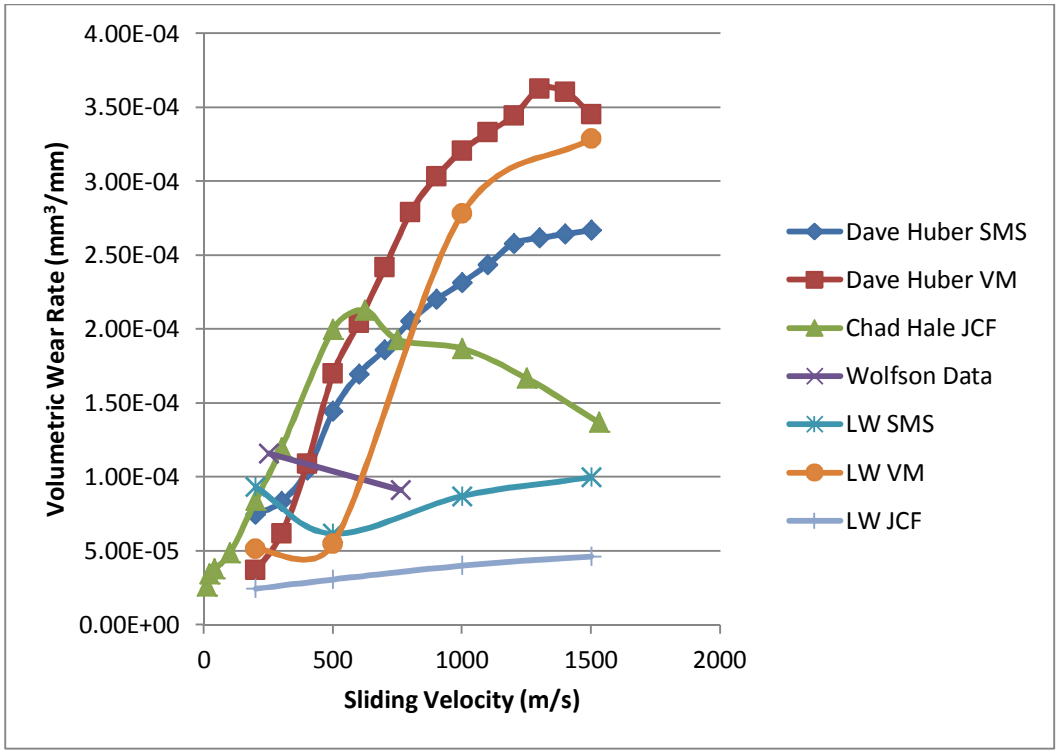


**Figure 47: Comparison of Wear Volume Rates**

For this comparison, only wear rates using the ABAQUS spherical correction factor were used in an attempt to reduce clutter on the graph and show the median of possible wear volume rate results. The new strain at max stress and von Mises wear volume rates line up very closely with the work done by Huber. The new values differ from previous work with the CTH model because the simulation in this research was run for a longer period of time. In the slower velocity regimes, Huber's, Hale's, and the new

strain at max stress and von Mises values seem to be rather close to the Wolfson experimental data. The Johnson and Cook failure criterion seems to under-predict the wear here. This may be an indication that friction wear is more relevant in the 200mps velocity regime. However, as the velocity increases, the von Mises wear increases much more compared to the other strain rates. There is also a significant difference in the strain at max stress failure criterion results from previous research. This clearly indicated that finding when the maximum damage area occurs will change the results. The difference is not as dramatic in between the von Mises criteria because the von Mises damage area reaches an asymptote earlier than any of the other criterion being used.

Finally it is of interest to try to compare with Rodolfo Buentello's 3D ABAQUS model. This study's results can compare to his calculations at 500mps. In his work he found:

**Table 18: Buentello 3D ABAQUS Damage Volume Calculations**

| Stage | Ave. Vel (m/s) | $W_{uA}$ ($mm^3/mm$) | Width (mm) | Ave. Worn length | Sliding Distance | % Contact | Predicted Volume Damage ($mm^3$) | Measured Volume Damage ($mm^3$) |
|---|---|---|---|---|---|---|---|---|
| 2 | 500 | 1.81E-6 | 101 | 35 | 1016000 | 0.30 | 1993.9 | 1684.2 |

Where the volume of damage was found using the following equation:

$$V_d = \sum_{n=1}^{n} W_{uA_n} A_{c_n} D_{S_n} \%Cont_n \qquad 3.2$$

To be able to compare to these numbers, the wear volume per unit area is needed. Using an equation developed by Buentello, the following equation is used:

$$WuA = \frac{A_D \; SCF \times 10}{Measured \; Area} \qquad 4.7$$

Where $A_D$ is the damage area, the measured area is the 0.16mm$^2$ and 10 is the number of asperities found in the 0.16 area

The results using each of the spherical correction factors are shown below:

**Table 19: Wear Area Rate Calculations**

| | Fracture Criteria | mm$^3$/mm$^2$ | mm$^3$ |
|---|---|---|---|
| 3D ABAQUS | JCF | 1.81E-06 | 2.90E-08 |
| | SMS | 5.15E-06 | 8.25E-08 |
| | VM | 2.70E-06 | 4.33E-08 |
| SCF = SMS | JCF | 1.46E-06 | 2.34E-08 |
| | SMS | 3.30E-06 | 5.29E-08 |
| | VM | 1.73E-06 | 2.77E-08 |
| SCF = JCF | JCF | 9.39E-07 | 1.50E-08 |
| | SMS | 4.76E-06 | 7.61E-08 |
| | VM | 2.49E-06 | 3.99E-08 |
| SCF = ABAQUS | JCF | 1.35E-06 | 2.16E-08 |

Interestingly enough, the closest CTH results are the ones using the von Mises failure criterion. They actually are extremely close.

It is also possible to attempt to match the volume of wear that Buentello predicted. Using Equation 3.2 and using the same sliding distance, %contact, and area of contact, the following results are generated:

**Table 20: Comparative Predicted Volume Damage**

| Spherical Correction Factor used | Fracture Criteria used | Wear per unit area (mm$^3$/mm$^2$) | Predicted Volume Damage | Measured Volume Damage | % Difference |
|---|---|---|---|---|---|
| ABAQUS | SMS | 4.76E-06 | 5127.5 | 1684.2 | 204.5 |
| | VM | 2.49E-06 | 2687.2 | 1684.2 | 59.6 |
| | JCF | 1.35E-06 | 1456.6 | 1684.2 | 13.5 |
| SMS | SMS | 5.1581E-06 | 5557.7 | 1684.2 | 230.0 |
| | VM | 2.7032E-06 | 2912.6 | 1684.2 | 72.9 |

| | | | | | |
|---|---|---|---|---|---|
| | JCF | 1.46526E-06 | 1578.8 | 1684.2 | 6.3 |
| JCF | SMS | 3.30623E-06 | 3562.4 | 1684.2 | 111.5 |
| | VM | 1.73269E-06 | 1866.9 | 1684.2 | 10.84 |
| | JCF | 9.39201E-07 | 1011.9 | 1684.2 | 39.9 |
| 3D simulation | JCF | 1.81E-06 | 1950.2 | 1684.2 | 15.8 |

Admittedly, most of the results are not exactly spot-on. However, for the two of the Johnson and Cook wear rates, the results are actually better than those predicted with the 3D ABAQUS simulation.

The comparison seems to indicate that some failure criteria may be more appropriate for modeling certain velocity ranges than others. Certainly in the comparative data, the Johnson and Cook data was predicting values much lower than the experimental data at lower values, but the SMS and von Mises data was much closer. It seems that keeping the material from being removed in the simulation can actually compensate for the lack of frictional representation at lower velocities. However, using a combination of failure criteria is rather cumbersome, and not exactly the streamlined simple solution that is sought. Also this assumption is based on the 3D Abaqus data behaves like the Wolfson experimental data, which is a relationship that has not officially been established. Thus this postulation cannot be confirmed without additional data to back it up.

### 4.7 Wear Results Summary

To summarize what was done in this section, the background for the wear per unit width, single asperity wear rate, spherical correction factor, and wear volume were all reviewed, and results of these calculations were presented. It was show that during the simulation, a maximum damage area will occur, but not all of the maximum damage areas have been found yet using CTH. Following this, single asperity rates were

calculated, which showed that wear of a single asperity increases with increasing velocity and asperity size. The spherical correction factor was calculated, and the results found by Hale's plane strain model in ABAQUS within the range of results produced by the CTH Johnson and Cook failure criterion. The strain at max stress correction factor produced higher values, as was expected since there is no material removal with that criterion. Wear volume rates were calculated using the new spherical correction factors and compared to past work done by Huber, Hale, and Wolfson. The wear volume rates calculated using the old criteria matched up with previous work fairly well, and the Johnson and Cook criterion produced lower wear volume rates, which were closer in value to the Wolfson experimental data for higher velocities. At lower velocities, the strain at max stress and von Mises wear volume rates appeared to be closer to the experimental Wolfson Data than the Johnson and Cook wear volume rates. Finally, wear area rates and wear volume was calculated and compared to a 3D ABAQUS simulation results. The Johnson and Cook failure criterion seemed to produce the best results, but produced smaller results when used in combination with the Johnson and Cook spherical correction factor.

# V. Conclusions

## 5.1 Research Summary

This project set about attempting to demonstrate the validity of a 2D plane strain hydrocode model to model the wear of a slipper in a high velocity environment. The CTH model was advanced by engaging the Johnson and Cook failure criterion, by re-calculating spherical correction factors previously developed by Chad Hale, and by using a wear data collected from longer simulation runs. The study shows that the wear results are comparable to those calculated by ABAQUS.

## 5.2 Conclusions

This study has allowed us to reach several conclusions. It was our goal to determine if using a 2D plane strain scenario with the Johnson and Cook fracture criterion would improve previous models predictions of wear. Happily it can be said that that the results showed an overall improvement of wear results closer to those seen in an ABAQUS 3D model over other failure criteria used previously.

One of the questions that this model raises is if the asperity collision is the driving factor of the wear, since in this CTH model friction cannot contribute anything. Based on the results, asperity collisions can account for the majority of the wear, as it predicts wear closer than those seen in experimental data. More data from ABAQUS is needed to confirm this when comparing simulation models.

There had been concern that a 2D plane strain model might be over-simplified and not be able to capture enough of the wear event to make it a competitive model. However since the results are in the range as those produced in 3D simulations and

compared to data from HHSTT, it seems the simplified model will work well given the right failure criterion is in place.

One theory that was confirmed was that engaging the Johnson and Cook failure criterion in CTH would lead to lower predicted wear than previously found using other failure criteria. This in fact turned out to be true and was reflected in the results in that the Johnson and Cook wear was lower than the Wolfson data and ABAQUS data.

Some would worry about how far one can extend a single asperity collision to an overall wear event, but our results coincide with the previous research that concludes that this is reasonable approach that produces realistic results.

One thing that can be noted is that CTH, while fantastic at speeds greater than 500mps, seems to misbehave at lower velocities. It is very promising for research that will want to go to speeds greater than those in this research, but for lower velocities, it may be best that another program that can model friction better be used.

When determining the spherical correction factor, it was found that CTH and ABAQUS both created similar results. This is fantastic because it shows how compatible the two modeling programs are, and further confirms that they both should predict similar values despite using different solving methods. Using the CTH-determined spherical correction factors provided an upper and lower bound for wear rate calculations. Additionally, it was found that the idea that the spherical correction factor can be scaled based on asperity size may not actually be true.

In most cases, the wear rate increased with increasing velocities.

## 5.1 Future Work

As with most research, as results come in, more questions arise. In the future it would be beneficial to further investigate the differences in the ABAQUS 3D model and the CTH model for additional velocities and asperity sizes.

For the failure criterion damage areas, simulations will need to be run longer to find when the maximum damage occurs. Once that is done, it would be interesting to take the data and see if the maximum damage occurred at predictable distances. This would be helpful so that one would not have to guess at how long a simulation needs to run to obtain the maximum damage.

While the spherical correction factor was validated between plane strain models in CTH and ABAQUS, it would be interesting to do more work in the 3D coordinate system. CTH has 3D capabilities, and a 3D model is already in development. It would be very interesting to finish developing this model and make comparisons between plane strain simulation and the 3D ABAQUS simulation.

Additionally, there are several modifications that might be made to the model itself. There is work going on investigating the true initial temperature of the materials in the model, so it would be of interest implement a more accurate number there. Another possible modification would be to move away from the Johnson and Cook Constitutive Model and investigate other potential constitutive models and make comparisons. An additional modification would be implementing the Mie-Grüneisen Equation of state in the CTH model in place of the SESAME tables to see if results closer match the ABAQUS predictions.

## Appendix A – CTH Input File

Below is the input file that was imported into CTH for this research. Parameters that were changed were the velocity, simulation times, and size of asperity, along with turning off the Johnson and Cook fracture criterion by commenting out its parameters. It has been updated to be compatible with CTH version 10.2.

```
*********************************************
*eor* cthin
*********************************************
*
* cthin input with Spymaster graphics for slipper wear simulation
*
* filename: slipperwear.in
*
* 1. File modified by Steve Meador (MS-10M)
* 2. File converted to CTH v8.1 by Maj Chad Hale, PhD-09S, Aug
2008
* 3. new format based on CTH Course (4-7 Aug 08) in Albuquerque,
NM
* 4. modifies Cameron's 393 m/s, No Coating, Asperity, T=297
input file
*
*          _________________
*         |       ----->    |
*         |       |         |
*         |       v        /
*  ----------------------------
*
*
*  vx=varies, vy=-1 m/s  V300 Steel Slider, 1080 Steel Rail, No
Atm.
*  No Slide line. mix=1 frac=1 Rounded corner.
*  Added mass on top to simulate sled mass

*********************************************
* title record set
*********************************************

Horizontal Velocity = 500 m/s, Vertical Velocity = -0.50 m/s

*********************************************
* control input set
*********************************************
control
```

```
  mmp3                  * enable multiple material temperatures
and pressures in each cell
  tstop = 4.40e-9     * stopping criteria for time level - this
is total simulation time
  nscycle = 100000     * maximum number of cycles to be run
*  rdumpf = 3600.       * time for back-ups of restart file
updates
  tbad = 1e30          * maximum number of thermodynamics
warnings
*  dtcourant = 0.6      * Courant condition multiplier
  ygravity = -980      * Acceleration due to gravity = -9.80
m/s^2
endcontrol

*******************************************
* mesh input set
*******************************************
*  geom=2DR(rectangular x,y)
*  geom=2DC(cylindrical x=radius, y=axis)
*  geom=3DR(rectangular x,y,z)
*  type=e (Eulerian) - now the default (CTHv8.1)
*  x#=coordinate range for plot
*  y#=coordinate range for plot
*  dxf=width of first cell in the region
*  dxl=width of last cell in the region
*  n=number of cells added in this region
*  w=total width of this region in centimeters
*  r=ratio of adjacent cell widths
*******************************************

mesh
  block 1  geom=2dr             * coordinates for 2D rectangular
Eulerian mesh
    x0 = 0.0000
      x1 w = 850e-4 dxf = 1.0e-4 dxl = 1.0e-4
    endx

    y0 = 0.0000
      y1 w = 850e-4 dyf = 1.0e-4 dyl = 1.0e-4
    endy
  endblock
endmesh

*******************************************
* EOS input set
*******************************************
eos
  material1 ses iron          * 1080 steel rail
  material2 ses steel_v300    * VascoMax 300 slipper
endeos
```

```
*******************************************
* elastic-plastic input set
*******************************************
epdata
  vpsave        * cell yield stress and plastic strain rate data
is saved
  lstrain       * compute and save Lagrangian strain tensor
components
  mix = 3       * volume averaged yield strength normalized by
sum of volume fractions



 matep = 1     * 1080 Steel rail
    JO USER
    AJO 0.7e10        * A
    BJO 3.6e10        * B
    CJO 0.17          * C
    MJO 0.25          * m
    NJO 0.6           * n
    TJO 0.14391       * Melting temperature
    poisson 0.27

  matep = 2      * VascoMax 300 slipper
    JO USER
    AJO = 2.1e10      * A
    BJO = 0.124e10    * B
    CJO = 0.03        * C
    MJO = 0.8         * m
    NJO = 0.3737* n
    TJO = 0.145202    * Melting temperature
    poisson 0.283

*     JFRAC USER
*     JFD1 = -0.09     * D1
*     JFD2 = 0.27      * D2
*     JFD3 = 0.48      * D3
*     JFD4 = 0.014     * D4
*     JFD5 = 3.870     * D5
*     JFTM = 0.145202  * Melting temperature
*     JFPF0 = -7.45e10* =PFRAC2



 SLIDE 1 2

endepdata
```

```
*********************************************
* diatom input set
*********************************************
diatom
  block 1

      package '1080 steel rail'
      material 1
      numsub 100
      temperature = 2.55935e-2 * eV = 74.93F = 297 K
      velocity 0.0, 0.0
      insert box
       p1 0 0
       p2 850e-4 200e-4
      endinsert
      delete circle
       center 695e-4 200e-4
       radius 2e-4
      enddelete
      insert circle
       center 695e-4 200e-4
       radius 2e-4
      endinsert
    endpackage

   package 'slipper'
      material 2
      numsub 100
      temperature = 0.0184558
      velocity = 500e2, -0.50e2
      insert box
         p1 0.0 200e-4
         p2 694e-4 325e-4
      endinsert
      delete box
       p1 692e-4 200e-4
       p2 694e-4 202e-4
     enddelete
      delete circle
       center 692e-4 202e-4
       radius 2e-4
      enddelete
     insert circle
      center 692e-4 202e-4
      radius 2e-4
      endinsert
   endpackage

  endblock
enddiatom
```

```
*********************************************
* tracer input set
*********************************************
tracer
      add 0.06755, 0.01905 to 0.07115, 0.01905 n=37
      add 0.06755, 0.01915 to 0.07115, 0.01915 n=37
      add 0.06755, 0.01925 to 0.07115, 0.01925 n=37
      add 0.06755, 0.01935 to 0.07115, 0.01935 n=37
      add 0.06755, 0.01945 to 0.07115, 0.01945 n=37
      add 0.06755, 0.01955 to 0.07115, 0.01955 n=37
      add 0.06755, 0.01965 to 0.07115, 0.01965 n=37
      add 0.06755, 0.01975 to 0.07115, 0.01975 n=37
      add 0.06755, 0.01985 to 0.07115, 0.01985 n=37
      add 0.06755, 0.01995 to 0.07115, 0.01995 n=37
      add 0.06755, 0.02005 to 0.07115, 0.02005 n=37
      add 0.06755, 0.02015 to 0.07115, 0.02015 n=37
      add 0.06755, 0.02025 to 0.07115, 0.02025 n=37
      add 0.06755, 0.02035 to 0.07115, 0.02035 n=37
      add 0.06755, 0.02045 to 0.07115, 0.02045 n=37
      add 0.06755, 0.02055 to 0.07115, 0.02055 n=37
      add 0.06755, 0.02065 to 0.07115, 0.02065 n=37
      add 0.06755, 0.02075 to 0.07115, 0.02075 n=37
      add 0.06755, 0.02085 to 0.07115, 0.02085 n=37
      add 0.06755, 0.02095 to 0.07115, 0.02095 n=37
      add 0.06755, 0.02105 to 0.07115, 0.02105 n=37
      add 0.06755, 0.02115 to 0.07115, 0.02115 n=37
      add 0.06755, 0.02125 to 0.07115, 0.02125 n=37
      add 0.06755, 0.02135 to 0.07115, 0.02135 n=37
      add 0.06755, 0.02145 to 0.07115, 0.02145 n=37
      add 0.06755, 0.02155 to 0.07115, 0.02155 n=37
      add 0.06755, 0.02165 to 0.07115, 0.02165 n=37
      add 0.06755, 0.02175 to 0.07115, 0.02175 n=37
      add 0.06755, 0.02185 to 0.07115, 0.02185 n=37
      add 0.06755, 0.02195 to 0.07115, 0.02195 n=37
      add 0.06755, 0.02205 to 0.07115, 0.02205 n=37
      add 0.06755, 0.02215 to 0.07115, 0.02215 n=37
      add 0.06755, 0.02225 to 0.07115, 0.02225 n=37
      add 0.06755, 0.02235 to 0.07115, 0.02235 n=37
      add 0.06755, 0.02245 to 0.07115, 0.02245 n=37
endtracer


*********************************************
* convection control input set
*********************************************
Convct                  * enable convection of internal energy
  convection = 1        * use slope of internal energy and mass
density, discard KE residual
  interface = smyra     * scheme for interface tracker
```

```
endconvct


*********************************************
* fracture input set
*********************************************
Fracts                  * enable fracture data (dynes/cm^2)
  pressure
  pfrac1 = -2.0e10
  pfrac2 = -7.45e10
endfracts
*********************************************
* edits input set
*********************************************

edit
  exact
  shortta              * short edits based on time
    time = 0.0  , dt = 4.40e-11
  ends
  longt                * long edits based on time
    time = 0.0e0  , dt = 4.40e-11
  endl
  plott                * plot dumps based on time
    time  0.0e-6  dtfrequency 4.40e-11
  endp
  histt                * tracer history based on time
    time  0.0e-6  dtfrequency 4.40e-11
    htracer all
  endhistt
ende

*********************************************
* boundary condition input set
*********************************************
* 0=symmetry
* 1=sound speed based absorbing
* 2=extrapolated pressure with no mass allowed to enter
* 3=extrapolated pressure but mass is allowed to enter
*********************************************

boundary                       * enable boundary condition data
  bhydro                       * enable hydrodynamic boundary
conditions
    block 1
      bxbot = 1 , bxtop = 2
      bybot = 1 , bytop = 2
    endb
  endh
endb
```

```
maxdt            * maximum allowable time step in mesh
   time = 0.0 dt = 4.40e-11
endm


* CSH: Attempt to get data for Spymaster

spy

 PlotTime(0.0, 4.40e-11);
 SaveTime(0.0, 4.40e-11);

Save("VOID,VOLM,M,P,XXDEV,YYDEV,XYDEV,VX,VY,T,TK,PM,TM,YLD,Q2,J2P
");

define main()
 {
%   pprintf(" PLOT: Cycle=%d, Time=%e\n",CYCLE,TIME);
%   XLimits(400e-4,725e-4);
%   YLimits(175e-4,300e-4);
%   Image("Materials");
%    Window(0,0,0.75,1);
%    Label(sprintf("Materials at %6.2e seconds", TIME));
%    Plot2DMats(0.3);
%    ULabel("Test: (cm)");
%    Draw2DMesh();              % toggle on/off mesh
%    MatColors(RED,GREEN,YELLOW,NO_COLOR);
%    MatNames("Epoxy Coating","1080 Steel Rail","VascoMax 300
Slipper","");
%    DrawMatLegend("",0.71,0.2,0.99,0.9);
%   EndImage;

%   XLimits(650e-4,750e-4);
%   YLimits(150e-4,250e-4);
%   Image("VonMisesStress");
%    Window(0,0,0.75,1);
%    ColorMapRange(0,4000);
%    ColorMapClipping(OFF,OFF);
%    Label(sprintf("von Mises Stress at %6.2e seconds", TIME));
%    Plot2D("J2P");
%    Draw2DMatContour;
%    DrawColorMap("vonMises Stress (MPa)", 0.7,0.4,0.9,0.9);
%   EndImage;

%   XLimits(650e-4,750e-4);
%   YLimits(150e-4,250e-4);
%   Image("PlasticStrainRate");
%    Window(0,0,0.75,1);
```

```
%    ColorMapRange(1e6,1e15,LOG_MAP);
%    ColorMapClipping(OFF,OFF);
%    Label(sprintf("Plastic Strain Rate at %6.2e seconds",
TIME));
%    Plot2D("PSR");
%    Draw2DMatContour;
%    DrawColorMap("Plastic Strain Rate (1/sec)",
0.7,0.4,0.9,0.9);
%   EndImage;

   XLimits(685e-4,715e-4);
   YLimits(190e-4,215e-4);
   Image("Materials_small");
    Window(0,0,0.75,1);
    Label(sprintf("Materials at %6.2e seconds", TIME));
    Plot2DMats(0.3);
    Label( "Test Label: Distance (cm)" );
%    Draw2DMesh();              % toggle on/off mesh
    MatColors(GREEN,YELLOW);
    MatNames("1080 Steel Rail","VascoMax 300 Slipper");
    DrawMatLegend("",0.71,0.2,0.99,0.9);
   EndImage;

   XLimits(650e-4,750e-4);
   YLimits(150e-4,250e-4);
   Image("Pressure");
    Window(0,0,0.75,1);
    ColorMapRange(1e6,2e11,LOG_MAP);
    ColorMapClipping(OFF,OFF);
    Label(sprintf("Pressure at %6.2e seconds", TIME));
    Plot2D("P");
    Draw2DMatContour;
    DrawColorMap("Pressure (dyne/cm^2)", 0.7,0.4,0.9,0.9);
   EndImage;

 }

SaveHis("POSITION,Q2,PSR,VOLM+2,J2P,YLD");
%SaveHis("POSITION,Q2,PSR,VOLM+2,J2P,DMG2");
%SaveHis("POSITION,YLD,Q3,PSR,VOLM+3,P,XXDEV,YYDEV,J2P,DMG3");
% SaveHis("POSITION,YLD,VOLM+3,P,XXDEV,YYDEV,XYDEV");
% SaveHis("POSITION,Q3,PSR,VOLM+3");
% SaveHis("POSITION,VOLM+3,DMG3");
 SaveTracer(ALL);
 HisTime(0,4.40e-11);

 define spyhis_main()
 {
  HisLoad(1,"hscth");
  Label("EFP Velocity (Tracer 1)");
```

```
  TPlot("VY.1",1,AUTOSCALE);
 }

endspy
```

## Appendix B.1 Strain at Max Stress MATLAB Post-Processing File

Below is the post-processing file used to calculate the wear per unit with per time for the strain at max stress failure criterion.

```
% Lauren Wuertemberger
% AFIT
% 7 Aug 2012
% Importing Wear data

clear all
close all
clc

velocity = 500;
meshSize = 1.0e-4*1.0e-4;

% Load wear data file
dataFile = '2um500mpsData-2.txt';
data = load(dataFile);
disp('Data Imported...')

% Start grabbin' stuff

time = data(:,1);

CycleNum = length(time);
TracerPoints = (size(data,2)-1)/7;
xLoc = 2;
yLoc = 3;
yieldLoc = 4;
J2PLoc = 5;
vfLoc = 6;
srLoc = 7; %PSR
sLoc = 8; %Q

for iter = 1:TracerPoints
    xPoints(:,iter) = data(:,xLoc);
    yPoints(:,iter) = data(:,yLoc);
    yieldData(:,iter) = data(:,yieldLoc);
    J2PData(:,iter) = data(:,J2PLoc);
    vfData(:,iter) = data(:,vfLoc);
```

```
    srData(:,iter) = data(:,srLoc);
    strainData(:,iter) = data(:,sLoc);

    xLoc = xLoc + 7;
    yLoc = yLoc + 7;
    yieldLoc = yieldLoc+7;
    J2PLoc = J2PLoc + 7; %%
    vfLoc = vfLoc + 7;
    srLoc = srLoc + 7; %%
    sLoc = sLoc + 7;
end

% EVALUATE STRAIN RATES FOR ZEROS

for r = 1:size(srData,1)
    for c = 1:size(srData,2)
        if srData(r,c)<.002
            srData(r,c) = .002;
        end

         if srData(r,c)>10e17
             disp('Temp:'),disp(temp)
             disp('H Vel:'),disp(velocity)
             disp('V Vel:'),disp(vVel)
             disp('Row:'),disp(r)
             disp('Col:'),disp(c)
             disp('Strain Rate'),disp(srData(r,c))
             error('Strain Rate Out of Range')
         end
    end
end



% EVALUATE STRAIN AT MAX STRESS FAILURE AREA

failureSMS = zeros(CycleNum,TracerPoints);

failureSumSMS = zeros(CycleNum,1);

A = 2.24700e-2;
B = -5.5160e-2;
C = 6.04400e-3;

failureCritSMS = A*(srData.^B) + C;

for row=1:r
    for col=1:c
        if row>1 && failureSMS(row-1,col)==1
            failureSMS(row,col)=1;
        end
        if strainData(row,col)>=failureCritSMS(row,col)
            failureSMS(row,col)=1;
```

```
        end
    end
end

failureSMS = failureSMS.*vfData; %unitless

for iter = 1:length(failureSumSMS)
    failureSumSMS(iter,1) = sum(failureSMS(iter,:)); %unitless
end

damAreaSMS = failureSumSMS*meshSize; %mm^2

for i = 2:CycleNum
    distanceSlid = velocity*time(i)*1000;
    WR_SMS(i) = 100*damAreaSMS(i)/distanceSlid;
end

SMS_Average = 100*damAreaSMS(end)/distanceSlid
%WR_SMS = 100*damAreaSMS/distanceSlid; %mm^2/mm
disp('Strain at Max Stress Failure Mechanism Evaluated...')

%Calculate Wear at each interval
plot(time, WR_SMS)
xlabel('Time (s)')
ylabel('Wear Rate per Unit Width (mm^2/mm)')
title('2um Asperity Wear')

figure
plot(time,damAreaSMS)
xlabel('Time (s)')
ylabel('Area of Damaged Elements(mm^2)')
title('2um Asperity Damage Area')
```

## Appendix B.2 Johnson-Cook Failure Criteria Post-Processing MATLAB File

Below is the post-processing file used to calculate the wear per unit with per time for the Johnson and Cook failure criterion.

```
% Lauren Wuertemberger
% AFIT
% 7 Aug 2012
% Importing Wear data

clear all
close all
```

```
clc

velocity = 1500;
meshSize = 1.0e-4*1.0e-4;

% Load wear data file
dataFile = '2um1500mpsJFData-2.txt';
data = load(dataFile);
disp('Data Imported...')

% Start grabbin' stuff

time = data(:,1);

CycleNum = length(time);
TracerPoints = (size(data,2)-1)/8;
xLoc = 2;
yLoc = 3;
JFLoc = 4;
yieldLoc = 5;
J2PLoc = 6;
vfLoc = 7;
srLoc = 8; %PSR
sLoc = 9; %Q

for iter = 1:TracerPoints
    xPoints(:,iter) = data(:,xLoc);
    yPoints(:,iter) = data(:,yLoc);
    JFData(:,iter) = data(:,JFLoc);
    yieldData(:,iter) = data(:,yieldLoc);
    J2PData(:,iter) = data(:,J2PLoc);
    vfData(:,iter) = data(:,vfLoc);
    srData(:,iter) = data(:,srLoc);
    strainData(:,iter) = data(:,sLoc);

    xLoc = xLoc + 8;
    yLoc = yLoc + 8;
    JFLoc = JFLoc + 8;
    yieldLoc = yieldLoc+8;
    J2PLoc = J2PLoc + 8; %%
    vfLoc = vfLoc + 8;
    srLoc = srLoc + 8; %%
    sLoc = sLoc + 8;
end

%% EVALUATE STRAIN RATES FOR ZEROS
%
% for r = 1:size(srData,1)
%     for c = 1:size(srData,2)
%         if srData(r,c)<.002
%             srData(r,c) = .002;
%         end
%
%          if srData(r,c)>10e17
```

```
%    %          disp('Temp:'),disp(temp)
%     %         disp('H Vel:'),disp(velocity)
%      %        disp('V Vel:'),disp(vVel)
%       %       disp('Row:'),disp(r)
%        %      disp('Col:'),disp(c)
%         %     disp('Strain Rate'),disp(srData(r,c))
%              error('Strain Rate Out of Range')
%          end
%     end
% end
%
%
%%
% EVALUATE STRAIN AT MAX STRESS FAILURE AREA

% failureSMS = zeros(CycleNum,TracerPoints);
%
% failureSumSMS = zeros(CycleNum,1);
%
% A = 2.24700e-2;
% B = -5.5160e-2;
% C = 6.04400e-3;
%
% failureCritSMS = A*(srData.^B) + C;
%
% for row=1:r
%     for col=1:c
%         if row>1 && failureSMS(row-1,col)==1
%             failureSMS(row,col)=1;
%         end
%         if strainData(row,col)>=failureCritSMS(row,col)
%             failureSMS(row,col)=1;
%         end
%     end
% end
%
% failureSMS = failureSMS.*vfData; %unitless
%
% for iter = 1:length(failureSumSMS)
%     failureSumSMS(iter,1) = sum(failureSMS(iter,:)); %unitless
% end
%
% damAreaSMS = failureSumSMS*meshSize; %mm^2

for i = 2:CycleNum
    distanceSlid = velocity*time(i)*1000;
    %WR_SMS(i) = 100*damAreaSMS(i)/distanceSlid;
end

%SMS_Average = 100*damAreaSMS(end)/distanceSlid
%WR_SMS = 100*damAreaSMS/distanceSlid; %mm^2/mm
%disp('Strain at Max Stress Failure Mechanism Evaluated...')

%% Evaluate JFrac Data - method 2
```

```
final_cells = JFData([end],:);
failureJF = final_cells.*vfData(101,:);
failureSumJF = sum(failureJF);
damAreaJF = failureSumJF*meshSize;

WR_JF = 100*damAreaJF(end)/distanceSlid;

%for i = 2:CycleNum
%    distanceSlid = velocity*time(i)*1000;
%    WR_JF(i) = 100*damAreaSMS(i)/distanceSlid;
%end

JF_Average = 100*damAreaJF(end)/distanceSlid
disp('Johnson-Cook Fracture Criterion Evaluated...')
%%

%Calculate Wear at each interval
plot(time, WR_JF)
xlabel('Time (s)')
ylabel('Wear Rate per Unit Width (mm^2/mm)')
title('2um Asperity Wear')

figure
plot(time,damAreaJF)
xlabel('Time (s)')
ylabel('Area of Damaged Elements(mm^2)')
title('2um Asperity Damage Area')
```

## Appendix C. Wear Damage Area vs. Time Plots

Below are all of the figures generated from looking up the maximum wear damage over the simulation time. At the end of the section the maximum values are included tabularly, along with the sliding distance that each maximum occurred at.

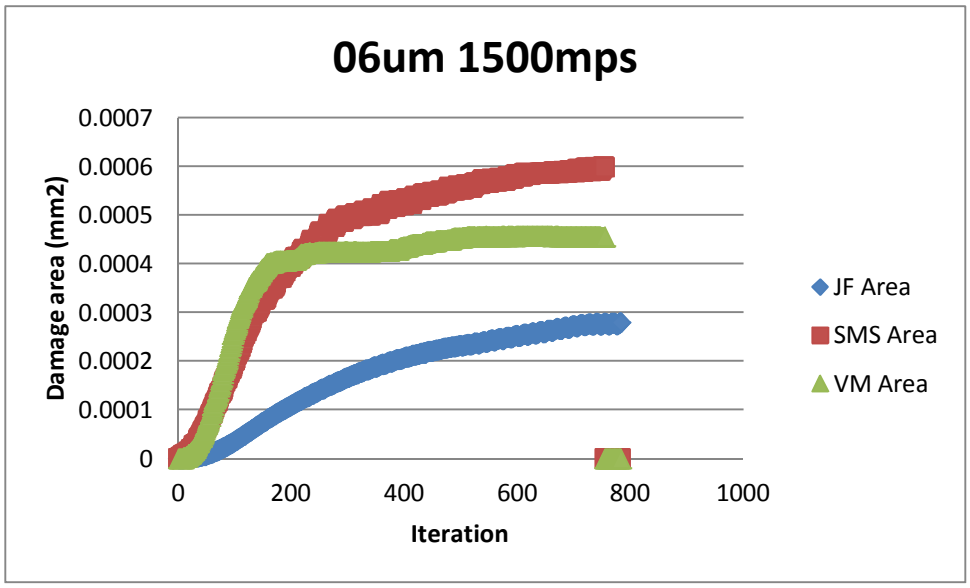

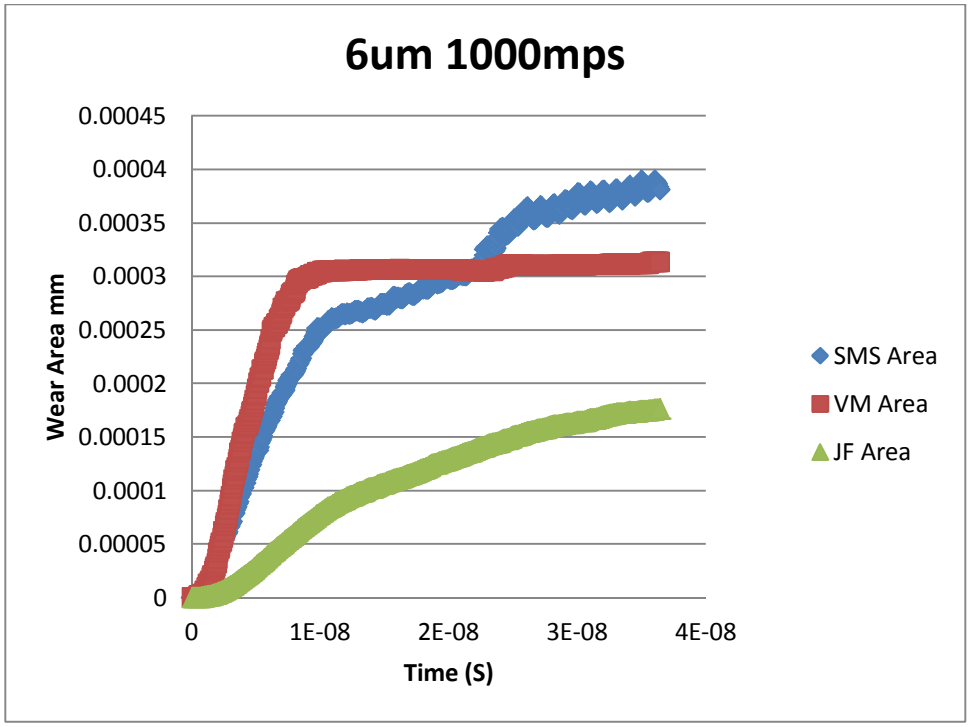
6um 1000mps
0.00045
0.0004
0.00035
0.0003
0.00025
0.0002
0.00015
0.0001
0.00005
0
Wear Area mm
0
1E-08
2E-08
3E-08
4E-08
Time (S)
SMS Area
VM Area
JF Area

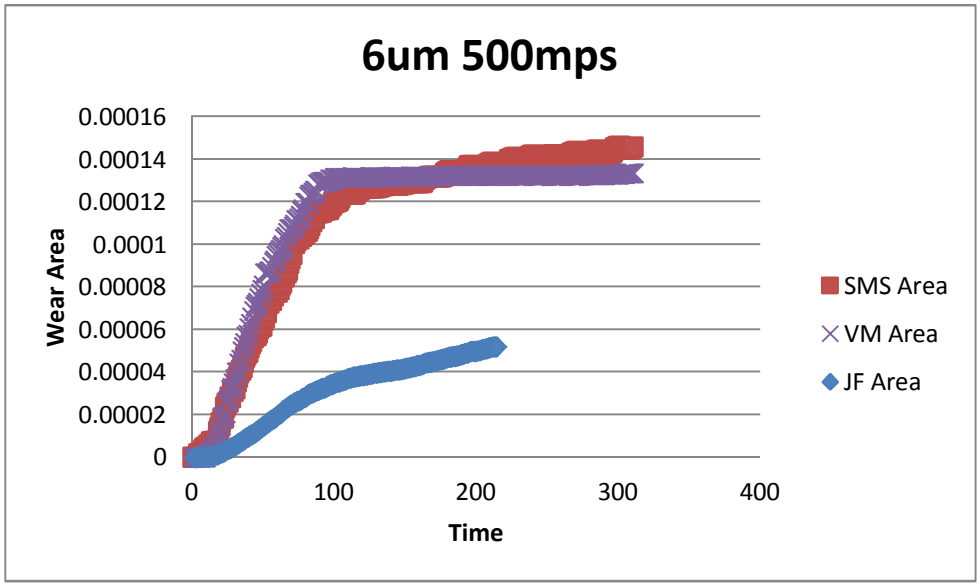
6um 500mps
0.00016
0.00014
0.00012
0.0001
0.00008
0.00006
0.00004
0.00002
0
Wear Area
0
100
200
300
400
Time
SMS Area
VM Area
JF Area

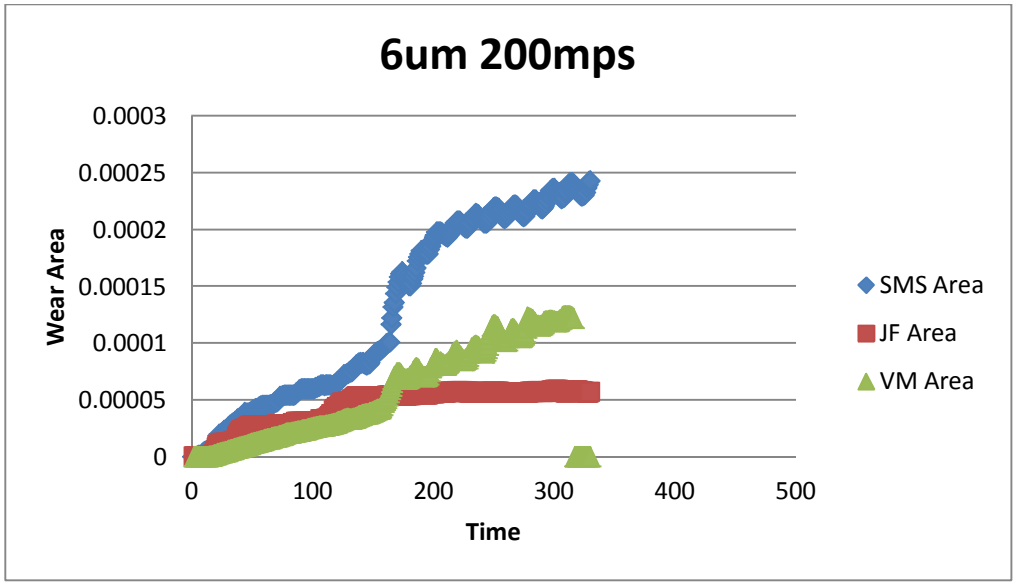
6um 200mps
0.0003
0.00025
0.0002
0.00015
0.0001
0.00005
0
Wear Area
0
100
200
300
400
500
Time
SMS Area
JF Area
VM Area

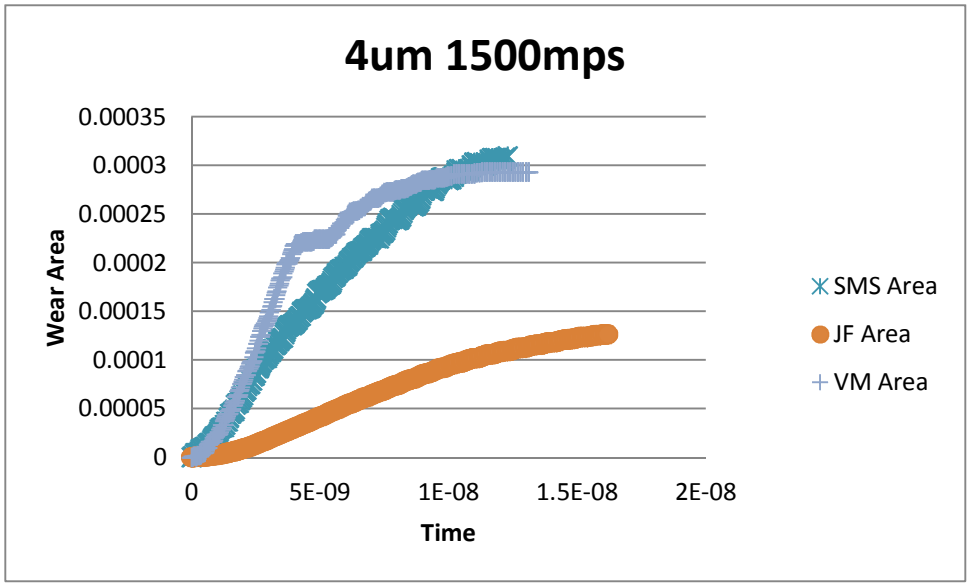
4um 1500mps
0.00035
0.0003
0.00025
0.0002
0.00015
0.0001
0.00005
0
Wear Area
0
5E-09
1E-08
1.5E-08
2E-08
Time
SMS Area
JF Area
VM Area

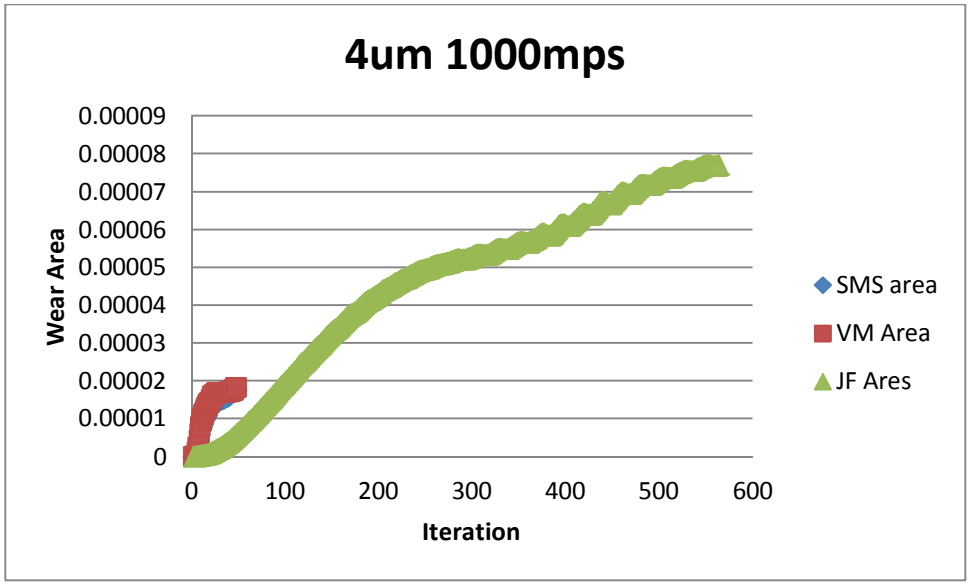
4um 1000mps
Wear Area
0.00009
0.00008
0.00007
0.00006
0.00005
0.00004
0.00003
0.00002
0.00001
0
0
100
200
300
400
500
600
Iteration
SMS area
VM Area
JF Ares

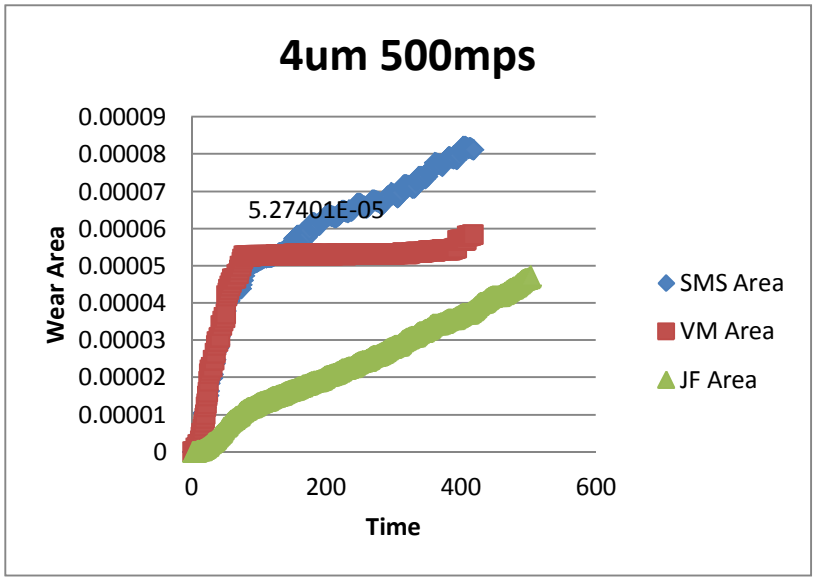
4um 500mps
Wear Area
0.00009
0.00008
0.00007
0.00006
0.00005
0.00004
0.00003
0.00002
0.00001
0
5.27401E-05
0
200
400
600
Time
SMS Area
VM Area
JF Area

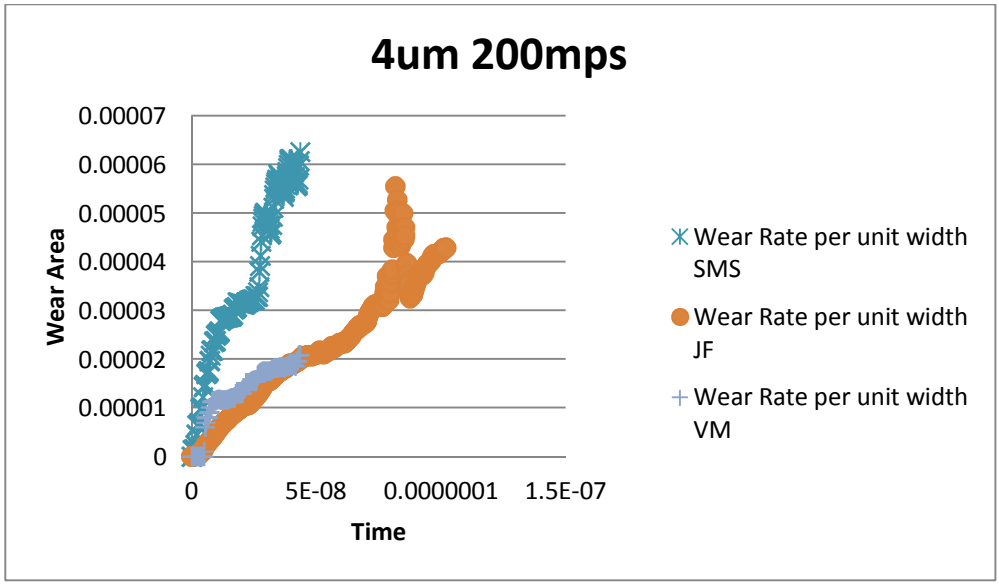
4um 200mps
0.00007
0.00006
0.00005
0.00004
0.00003
0.00002
0.00001
0
Wear Area
0
5E-08
0.0000001
1.5E-07
Time
Wear Rate per unit width SMS
Wear Rate per unit width JF
Wear Rate per unit width VM

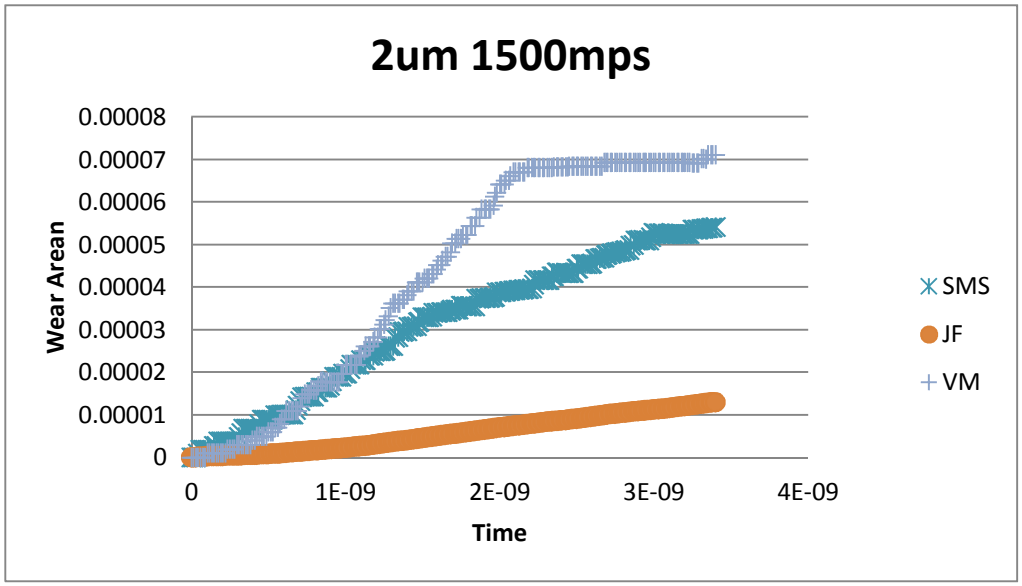
2um 1500mps
0.00008
0.00007
0.00006
0.00005
0.00004
0.00003
0.00002
0.00001
0
Wear Arean
0
1E-09
2E-09
3E-09
4E-09
Time
SMS
JF
VM

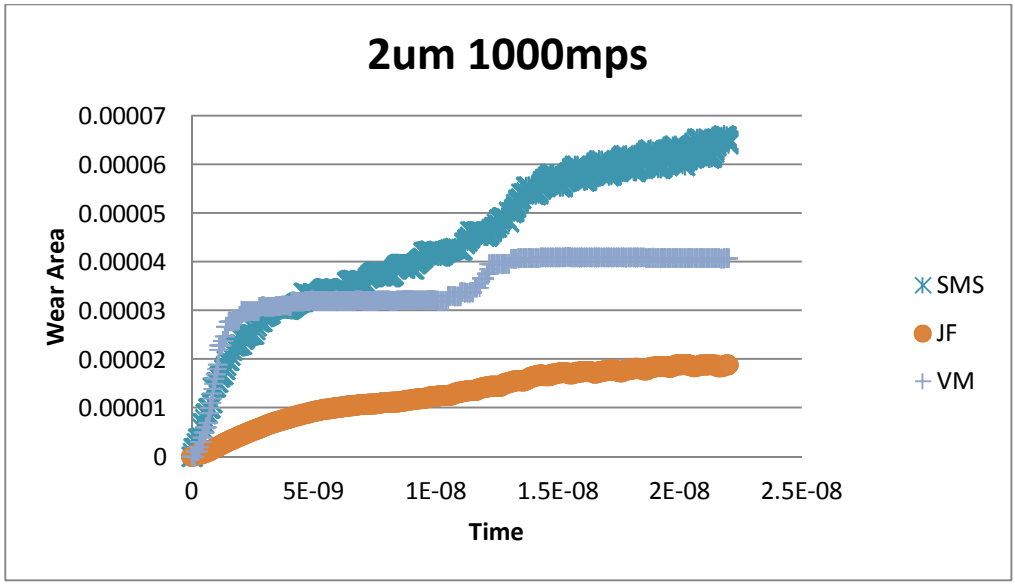
2um 1000mps
0.00007
0.00006
0.00005
0.00004
0.00003
0.00002
0.00001
0
Wear Area
0
5E-09
1E-08
1.5E-08
2E-08
2.5E-08
Time
SMS
JF
VM

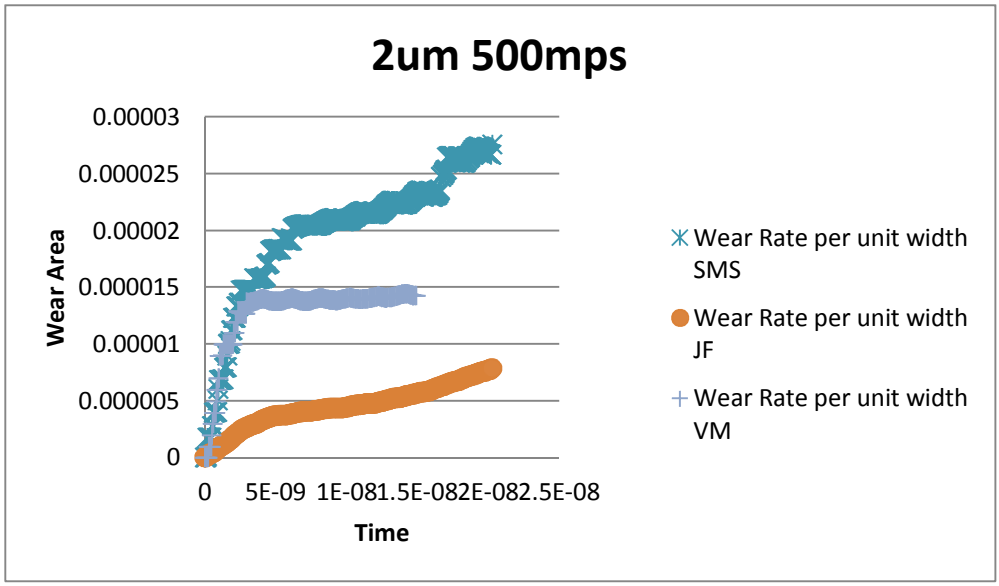
2um 500mps
0.00003
0.000025
0.00002
0.000015
0.00001
0.000005
0
Wear Area
0
5E-09
1E-08
1.5E-08
2E-08
2.5E-08
Time
Wear Rate per unit width SMS
Wear Rate per unit width JF
Wear Rate per unit width VM

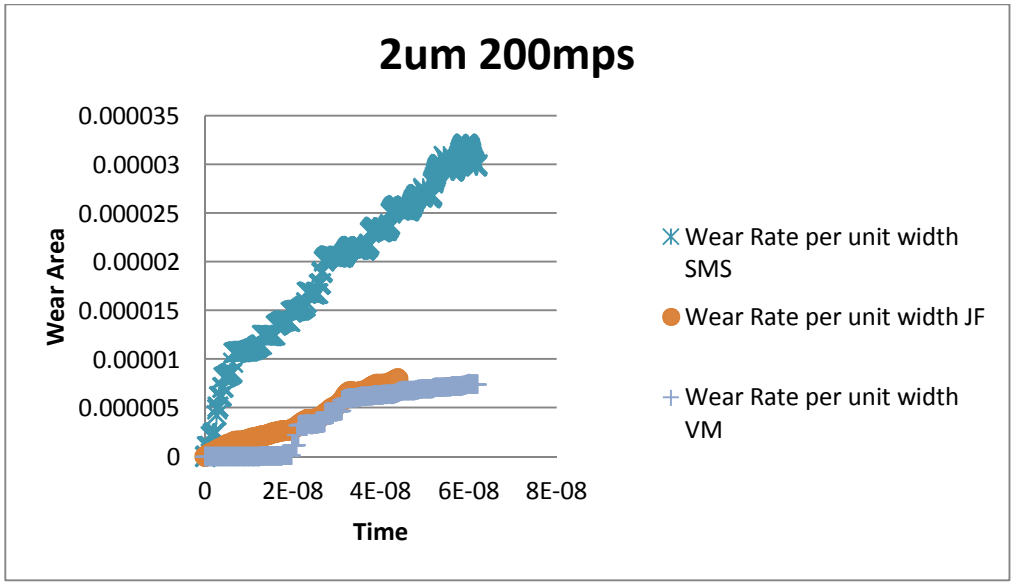
2um 200mps
0.000035
0.00003
0.000025
0.00002
0.000015
0.00001
0.000005
0
Wear Area
0
2E-08
4E-08
6E-08
8E-08
Time
Wear Rate per unit width SMS
Wear Rate per unit width JF
Wear Rate per unit width VM

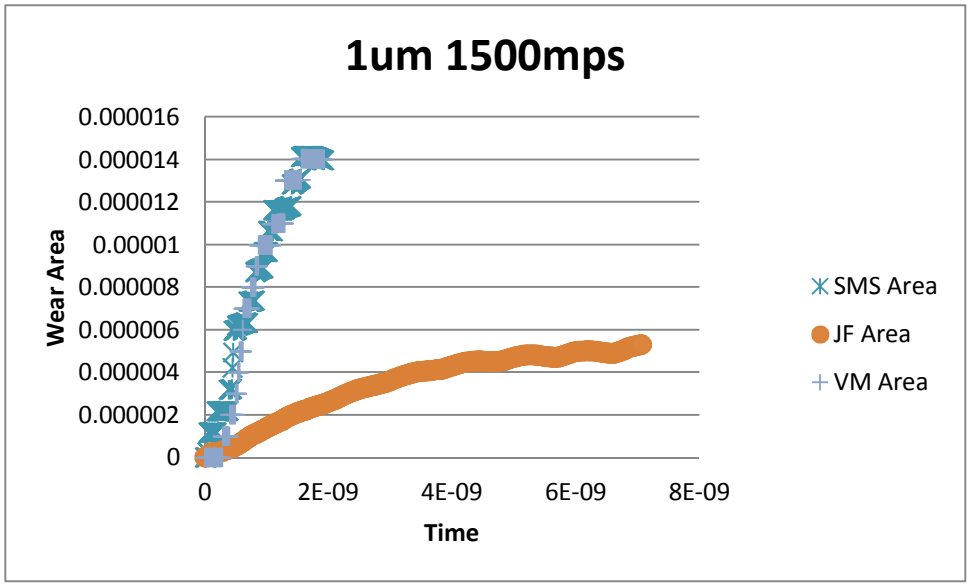
1um 1500mps
0.000016
0.000014
0.000012
0.00001
0.000008
0.000006
0.000004
0.000002
0
Wear Area
0
2E-09
4E-09
6E-09
8E-09
Time
SMS Area
JF Area
VM Area

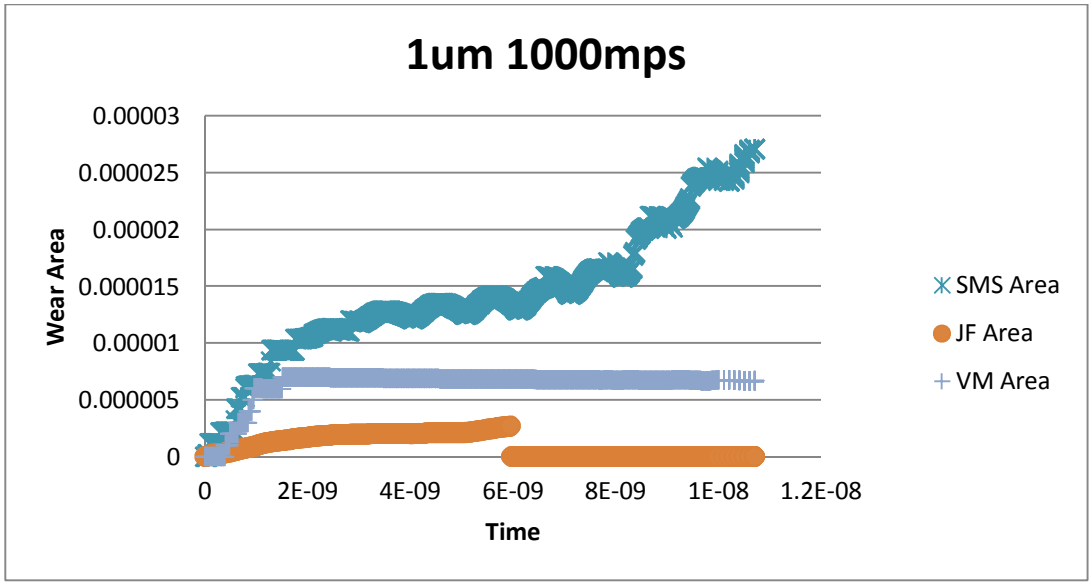
1um 1000mps
0.00003
0.000025
0.00002
0.000015
0.00001
0.000005
0
Wear Area
0
2E-09
4E-09
6E-09
8E-09
1E-08
1.2E-08
Time
SMS Area
JF Area
VM Area

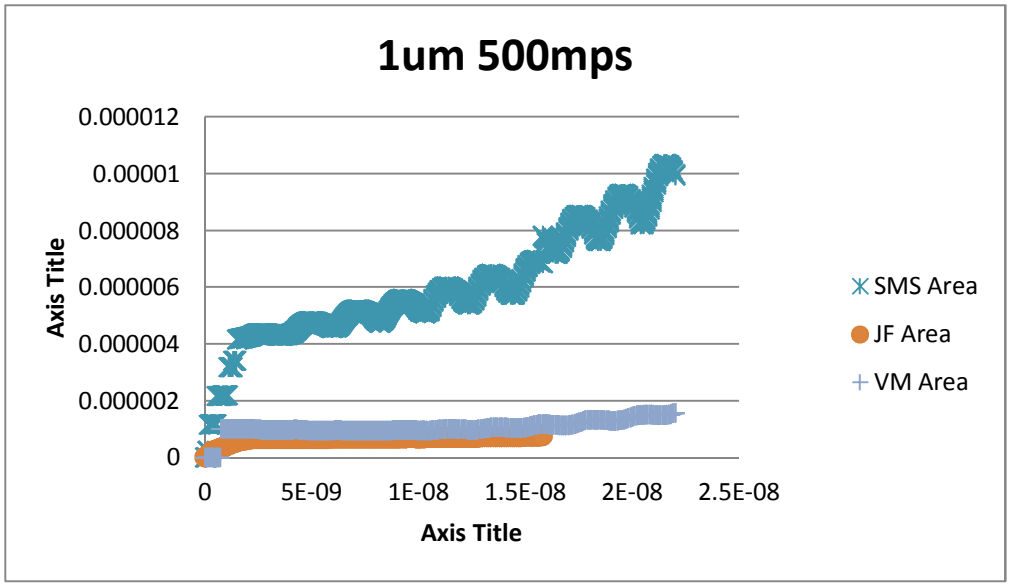
1um 500mps
0.000012
0.00001
0.000008
0.000006
0.000004
0.000002
0
Axis Title
0
5E-09
1E-08
1.5E-08
2E-08
2.5E-08
Axis Title
SMS Area
JF Area
VM Area

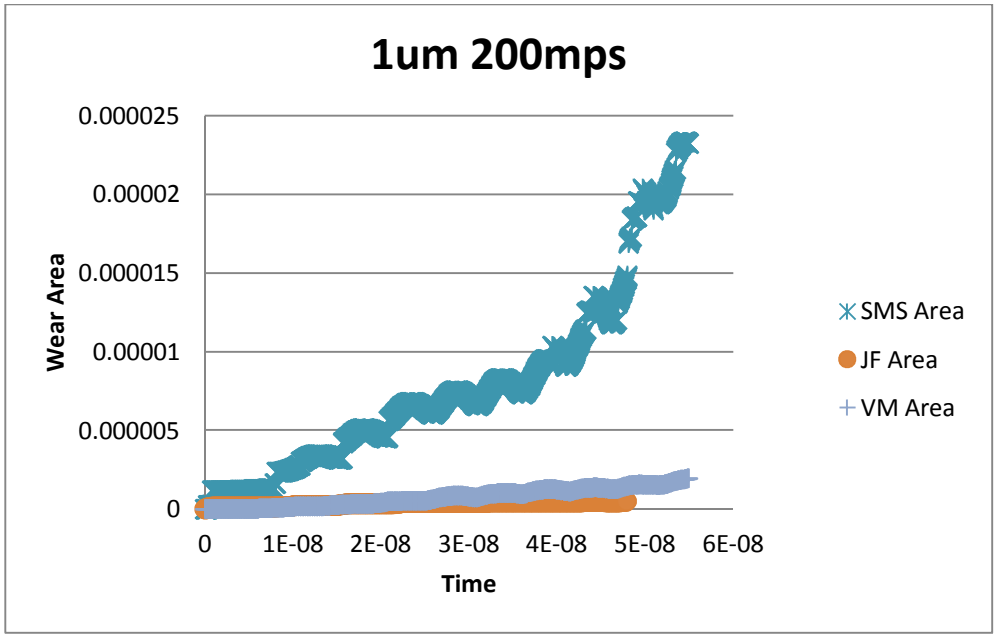
1um 200mps
0.000025
0.00002
0.000015
0.00001
0.000005
0
Wear Area
0
1E-08
2E-08
3E-08
4E-08
5E-08
6E-08
Time
SMS Area
JF Area
VM Area

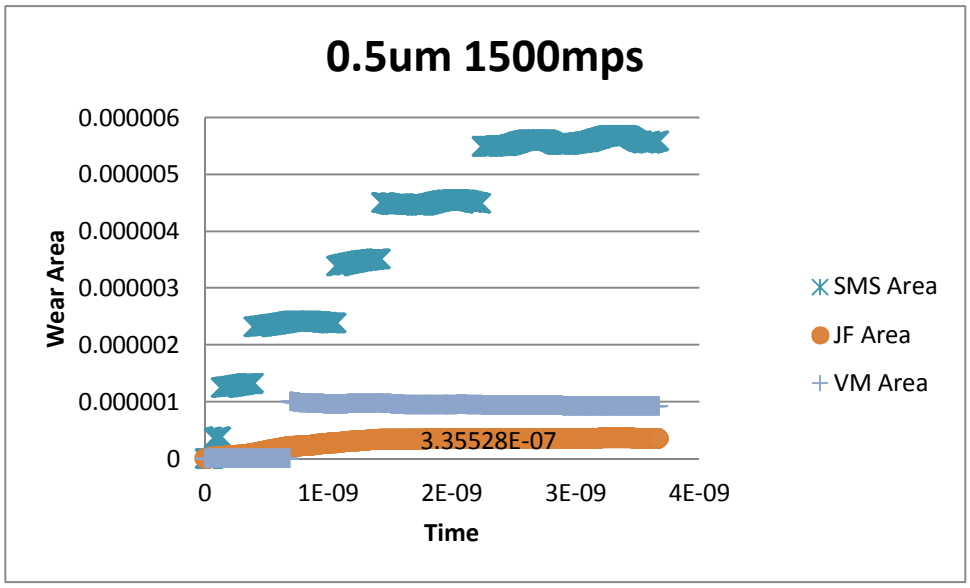
0.5um 1500mps
0.000006
0.000005
0.000004
0.000003
0.000002
0.000001
0
Wear Area
3.35528E-07
0
1E-09
2E-09
3E-09
4E-09
Time
SMS Area
JF Area
VM Area

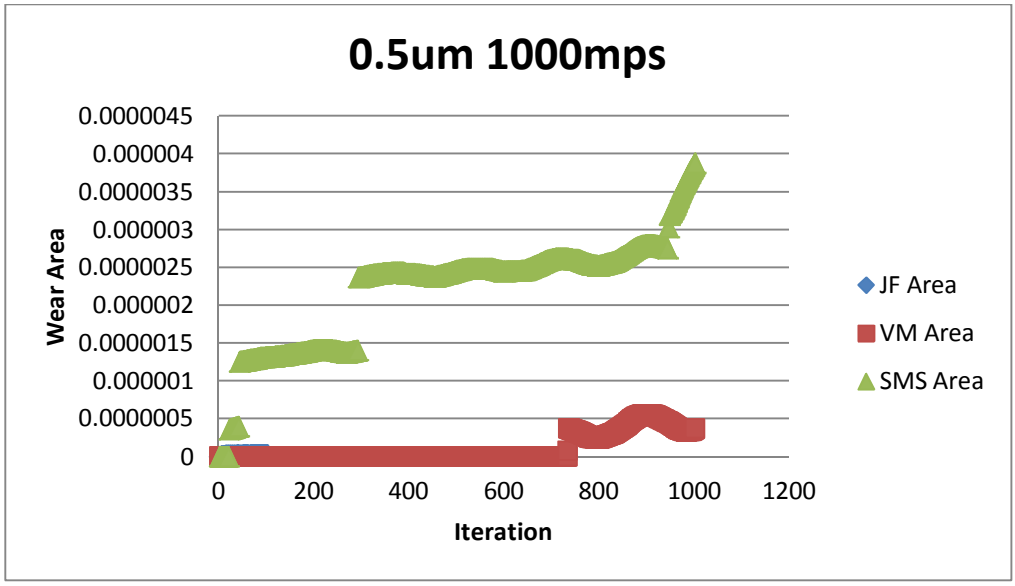
0.5um 1000mps
Wear Area
0.0000045
0.000004
0.0000035
0.000003
0.0000025
0.000002
0.0000015
0.000001
0.0000005
0
0
200
400
600
800
1000
1200
Iteration
JF Area
VM Area
SMS Area

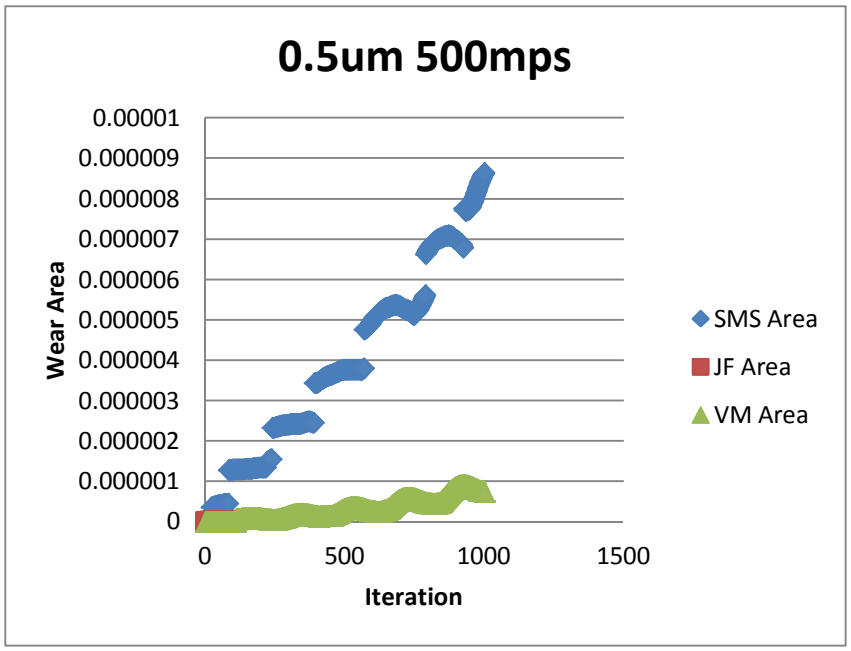
0.5um 500mps
Wear Area
0.00001
0.000009
0.000008
0.000007
0.000006
0.000005
0.000004
0.000003
0.000002
0.000001
0
0
500
1000
1500
Iteration
SMS Area
JF Area
VM Area

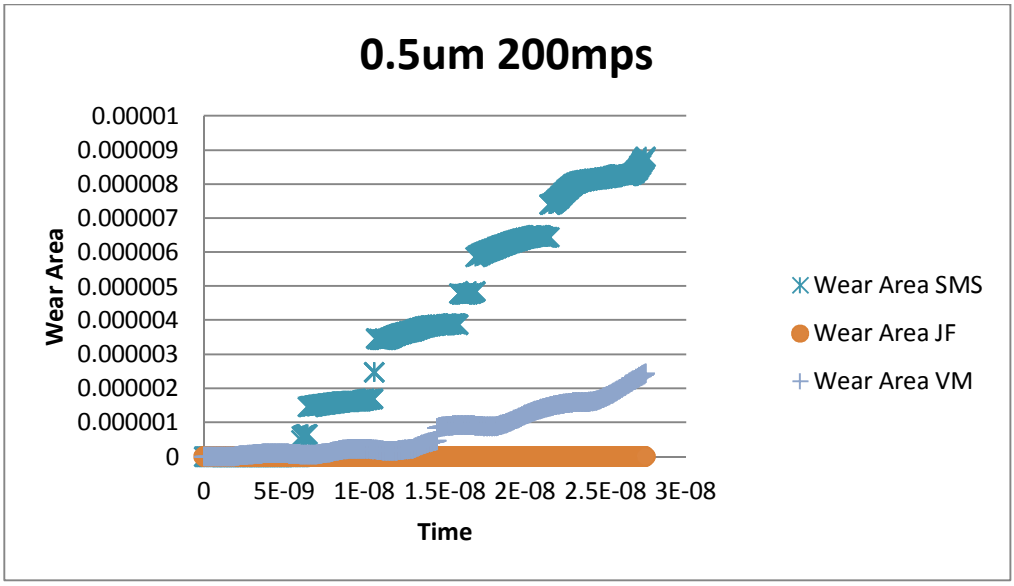
0.5um 200mps
Wear Area
0.00001
0.000009
0.000008
0.000007
0.000006
0.000005
0.000004
0.000003
0.000002
0.000001
0
0
5E-09
1E-08
1.5E-08
2E-08
2.5E-08
3E-08
Time
Wear Area SMS
Wear Area JF
Wear Area VM

| | Wear per unit width (mm^2/mm)* | | | | | | | | | | | |
|---|---|---|---|---|---|---|---|---|---|---|---|---|
| | Strain at Max Stress | | | | vonMises | | | | Johnson and Cook Fracture | | | |
| | **200mps** | **500mps** | **1000mps** | **1500mps** | **200mps** | **500mps** | **1000mps** | **1500mps** | **200mps** | **500mps** | **1000mps** | **1500mps** |
| 6micron | 0.000243 | 0.000146 | 0.000383 | 0.000599 | 0.000124 | 0.000134 | 0.000299 | 0.000395 | 5.85E-05 | 5.21E-05 | 0.000176 | 0.000278 |
| 4micron | 6.26E-05 | 8.21E-05 | 1.77E-05 | 0.00031 | 2.09E-05 | 5.27E-05 | 1.83E-05 | 0.000294 | 5.55E-05 | 4.73E-05 | 7.71E-05 | 0.000126 |
| 2micron | 3.22E-05 | 2.76E-05 | 6.61E-05 | 5.41E-05 | 7.46E-06 | 1.44E-05 | 4.1E-05 | 7.11E-05 | 7.98E-06 | 7.83E-06 | 1.89E-05 | 1.29E-05 |
| 1micron | 2.32E-05 | 9.91E-06 | 2.71E-05 | 1.42E-05 | 1.93E-06 | 1.57E-06 | 6.98E-06 | 1.41E-05 | 4.67E-07 | 7.47E-07 | 2.67E-06 | 5.28E-06 |
| 0.5micron | 8.82E-06 | 8.65E-06 | 3.88E-06 | 5.6E-06 | 2.44E-06 | 7.43E-07 | 3.67E-07 | 9.18E-07 | 0 | 2.36E-08 | 1.98E-08 | 3.56E-07 |

| | Distance slid at maximum wear (mm)* | | | | | | | | | | | |
|---|---|---|---|---|---|---|---|---|---|---|---|---|
| | Strain at Max Stress | | | | vonMises | | | | Johnson and Cook Fracture | | | |
| | **200mps** | **500mps** | **1000mps** | **1500mps** | **200mps** | **500mps** | **1000mps** | **1500mps** | **200mps** | **500mps** | **1000mps** | **1500mps** |
| 6micron | 0.0216 | 0.01965 | 0.0364 | 0.04965 | 0.02 | 0.02015 | 0.00891 | 0.00996 | 0.0198 | 0.014 | 0.0364 | 0.04965 |
| 4micron | 0.00872 | 0.0183 | 0.00202 | 0.01845 | 0.00872 | 0.0033 | 0.00202 | 0.000293 | 0.01636 | 0.022 | 0.0247 | 0.0243 |
| 2micron | 0.01186 | 0.01015 | 0.0218 | 0.0051 | 0.0124 | 0.00715 | 0.0153 | 0.005025 | 0.0088 | 0.01015 | 0.0201 | 0.0051 |
| 1micron | 0.011 | 0.011 | 0.0107 | 0.002895 | 0.011 | 0.011 | 2.29E-03 | 0.002895 | 0.00958 | 0.0079 | 1.31E+04 | 0.010605 |
| 0.5micron | 0.0055 | 0.0055 | 0.0055 | 0.005505 | 0.0055 | 0.0055 | 0.0055 | 0.005505 | 0.00E+00 | 0.00055 | 0.00055 | 0.00513 |

## Appendix D. Single Asperity Wear Rates and Wear Volume Calculations

The following tables contain the wear rates generated from CTH that describe the maximum wear rates at 200, 500, 1000, and 1500 meters per second for asperities with 6, 4, 2, 1, and 0.5 radii. These wear rates are then used to calculate single asperity wear rates and averaged together to calculate spherical correction factors. These calculations are also shown in the tables in this section.

**Table 21: 06micron Wear Rates using Johnson and Cook Failure Criterion**

| | Wear rate per unit width (Wuw) | | | | | |
|---|---|---|---|---|---|---|
| | 200 | 500 | 1000 | 1500 | Distance | |
| 06 microns | 0.002952 | 0.003721 | 0.004844 | 0.005605 | 0.00 | sqrt(6^2-6^2) |
| 04 microns | 0.003395 | 0.002148 | 0.003122 | 0.005203 | 4.47 | sqrt(6^2-4^2) |
| 02 microns | 0.000907 | 0.000771 | 0.00094 | 0.002536 | 5.66 | sqrt(6^2-2^2) |
| 0 microns | 0 | 0 | 0 | 0 | 6 | |

**Table 22: Area under the Curve Calculations for 6micron Wear Rates using Johnson Cook Failure Criterion**

| | Area | | | |
|---|---|---|---|---|
| | 200mps | 500mps | 1000mps | 1500mps |
| | -0.000988709 | 0.003515341 | 0.003847749 | 0.000898107 |
| | 1.52E-02 | 9.60E-03 | 1.40E-02 | 2.33E-02 |
| | 0.001479842 | 0.000819275 | 0.00129852 | 0.001586831 |
| | 1.08E-03 | 9.18E-04 | 1.12E-03 | 3.02E-03 |
| | 0.000154255 | 0.000131099 | 0.000159772 | 0.000431165 |
| Total area | 0.016898643 | 0.014985418 | 0.02038077 | 0.029192578 |
| x2 | 0.033797286 | 0.029970836 | 0.04076154 | 0.058385155 |

**Table 23: Spherical Correction Factor Calculations for 6micron using Johnson and Cook Failure Criterion**

| m/s | Single asperity wear rate (Wsa) mm^3/mm | Ratio (Wsa/Wuw) um |
|---|---|---|
| 200 | 3.380E-02 | 1.14E+01 |
| 500 | 2.997E-02 | 8.05E+00 |
| 1000 | 4.076E-02 | 8.42E+00 |
| 1500 | 5.839E-02 | 1.04E+01 |
| | | 9.58E+00 |

**Table 24: 6micron Wear Rates using the Strain at Max Stress Criterion**

| | Wear rate per unit width (Wuw) | | | | | |
|---|---|---|---|---|---|---|
| | 200 | 500 | 1000 | 1500 | Distance | |
| 06 microns | 0.011247 | 0.007437 | 0.010513 | 0.012055 | 0.00 | sqrt(6^2-6^2) |
| 04 microns | 0.007182 | 0.004489 | 0.008758 | 0.016797 | 4.47 | sqrt(6^2-4^2) |
| 02 microns | 0.002711 | 0.002715 | 0.003031 | 0.010604 | 5.66 | sqrt(6^2-2^2) |
| 0 microns | 0 | 0 | 0 | 0 | 6 | |

**Table 25: Area under the Curve Calculations for 6micron Wear Rates using Strain at Max Stress Criterion**

| | 200mps | 500mps | 1000mps | 1500mps |
|---|---|---|---|---|
| | 0.009085256 | 0.006588593 | 0.003922881 | -0.010598313 |
| | 3.21E-02 | 2.01E-02 | 3.91E-02 | 7.51E-02 |
| | 0.002659861 | 0.001055453 | 0.003407672 | 0.00368475 |
| | 3.23E-03 | 3.23E-03 | 3.61E-03 | 1.26E-02 |
| | 0.000460915 | 0.000461502 | 0.000515226 | 0.001802663 |
| Total area | 0.047534267 | 0.03140004 | 0.05060028 | 0.08258925 |
| x2 | 0.095068535 | 0.06280008 | 0.101200561 | 0.1651785 |

**Table 26: Spherical Correction Factor Calculations for 6micron using Strain at Max Stress Failure Criterion**

| m/s | Single asperity wear rate (Wsa) mm^3/mm | Ratio (Wsa/Wuw) um |
|---|---|---|
| 200 | 9.507E-02 | 8.45E+00 |
| 500 | 6.280E-02 | 8.44E+00 |
| 1000 | 1.012E-01 | 9.63E+00 |
| 1500 | 1.652E-01 | 1.37E+01 |
| | | 1.01E+01 |

**Table 27: 2micron Wear Rates using Johnson and Cook Failure Criterion**

| | Wear rate per unit width (Wuw) | | | | | |
|---|---|---|---|---|---|---|
| | 200 | 500 | 1000 | 1500 | Distance | |
| 2 microns | 0.000907 | 0.000771 | 0.000940 | 0.002536 | 0.00 | sqrt(2^2-2^2) |
| 1 micron | 0.000049 | 0.000095 | 0.000000 | 0.000498 | 1.73 | sqrt(2^2-1^2) |
| 0.5 microns | 0.000000 | 0.000043 | 0.000036 | 0.000069 | 1.93 | sqrt(2^2-0.5^2) |
| 0 microns | 0 | 0 | 0 | 0 | 2 | sqrt(2^2-0) |

**Table 28: Area under the Curve Calculations for 2micron Wear Rates using Johnson Cook Failure Criterion**

| | Area | | | |
|---|---|---|---|---|
| | 200mps | 500mps | 1000mps | 1500mps |
| | 0.000743604 | 0.00058599 | 0.000813896 | 0.001765468 |
| | 8.44E-05 | 1.64E-04 | 3.54E-10 | 8.62E-04 |
| | 4.82306E-06 | 5.10522E-06 | -3.56493E-06 | 4.24019E-05 |
| | 0.00E+00 | 8.50E-06 | 7.13E-06 | 1.37E-05 |
| | 0 | 1.50285E-06 | 1.26034E-06 | 2.42596E-06 |
| Total area | 0.000832806 | 0.000764784 | 0.000818722 | 0.002685889 |
| x2 | 0.001665613 | 0.001529569 | 0.001637444 | 0.005371778 |

**Table 29: Spherical Correction Factor Calculations for 2micron using Johnson and Cook Failure Criterion**

| m/s | Single asperity wear rate (Wsa) mm^3/mm | Ratio (Wsa/Wuw) um |
|---|---|---|
| 200 | 1.666E-03 | 1.84E+00 |
| 500 | 1.530E-03 | 1.98E+00 |
| 1000 | 1.637E-03 | 1.74E+00 |
| 1500 | 5.372E-03 | 2.12E+00 |
| | | 1.92E+00 |

**Table 30:2micron Wear Rates using the Strain at Max Stress Criterion**

| | Wear rate per unit width (Wuw) | | | | | |
|---|---|---|---|---|---|---|
| | 200 | 500 | 1000 | 1500 | Distance | |
| 2 microns | 0.002711 | 0.002715 | 0.003031 | 0.010604 | 0.00 | sqrt(2^2-2^2) |
| 1 micron | 0.002113 | 0.000901 | 0.002536 | 0.004896 | 1.73 | sqrt(2^2-1^2) |
| 0.5 microns | 0.001604 | 0.001573 | 0.000706 | 0.001017 | 1.93 | sqrt(2^2-0.5^2) |
| 0microns | 0 | 0 | 0 | 0 | 2 | sqrt(2^2-0) |

**Table 31: Area under the Curve Calculations for 2micron Wear Rates using Strain at Max Stress Failure Criterion**

| | Area | | | |
|---|---|---|---|---|
| | 200mps | 500mps | 1000mps | 1500mps |
| | 0.000518283 | 0.001570781 | 0.000428277 | 0.004942856 |
| | 3.66E-03 | 1.56E-03 | 4.39E-03 | 8.48E-03 |
| | 5.04025E-05 | -6.65686E-05 | 0.000181203 | 0.000384037 |
| | 3.18E-04 | 3.12E-04 | 1.40E-04 | 2.01E-04 |
| | 5.61284E-05 | 5.50652E-05 | 2.47053E-05 | 3.55967E-05 |
| Total area | 0.004601684 | 0.003431116 | 0.00516664 | 0.014044108 |
| x2 | 0.009203367 | 0.006862233 | 0.01033328 | 0.028088217 |

**Table 32: Spherical Correction Factor Calculations for 2micron using Strain at Max Stress Failure Criterion**

| m/s | Single asperity wear rate (Wsa) mm^3/mm | Ratio (Wsa/Wuw) um |
|---|---|---|
| 200 | 9.203E-03 | 3.39E+00 |
| 500 | 6.862E-03 | 2.53E+00 |
| 1000 | 1.033E-02 | 3.41E+00 |
| 1500 | 2.809E-02 | 2.65E+00 |
| | | 3.00E+00 |

## Bibliography


1. *holloman-high-speed-test-track-hhstt*. 2008. Mobility & Email BlogWeb. 20 Nov 2012. <http://mail2web.com/blog/2008/02/holloman-sets-new-land-speed-record/>.

2. *Test Track 1*. 2008. From the U.S. to Hong Kong. Web. 20 Nov 2012. <http://angiepalmer.files.wordpress.com/2008/01/test-track-1.jpg>.

3. Hale, Chad S. Consideration of Wear Rates at High Velocities, AFIT/DS/ENY/10-08. Ph.D. Thesis, Air Force Institute of Technology, Wright Patterson AFB, OH, 2009.

4. Cinnamon, J. D. *Analysis and Simulation of Hypervelocity Gouging Impacts* AFIT/DS/ENY/06-01. Ph.D. Dissertation, Air Force Institute of Technology, Wright-Patterson AFB, OH, 2006.

5. Stemlicth, B., and H. Apkarian. "Investigation of Melt Wear." *Tribology Transactions*. 2.2 (1959): 248-256. Print.

6. Bayer, R. G. Wear Analysis for Engineers. HNB Publishing, New York, 2002.

7. Archard, J.F. "Contact and Rubbing of Flat Surfaces." *Journal of Applied Physics*. 24.8 (1953): 981-988.

8. Graff, K.F., and B.B. Dettloff. "The Gouging Phenomenon Between Metal Surfaces at High Sliding Speeds." *Wear*. 14. (1969): 87-97. Print.

9. Schmitz, CP and Schmitz RP, 'Slipper Wear/Gouging Analytical Tool', Phase I SBIR Final Report Contract No F08365-97-c-0046, AZ Technology Report No. 97-4-351-001 (1998).

10. Montgomery, R. S. *"Muzzle Wear of Cannon,"* Wear, 33(2):359–368, July 1975

11. Archard, J.F. "The Temperature of Rubbing Surfaces." *Wear*. 2. (1958): 438-459.

12. Blok, H. "The Flash Temperature Concept." *Wear*. 6. (1963): 483-494. Print.

13. Korkegi, R.H., and R.A. Briggs. "The Hypersonic Slipper Bearing – A Test Track Problem." *Journal of Spacecraft and Rockets*. 6.2 (1969): 210-212. Print.

14. Challen, J.M., and P.L.B. Oxley. "An Explanation of the Different Regimes of Friction and Wear Using Asperity Deformation Models." *Wear*. 53. (1979): 229-243. Print.

15. Lim, S. C. and M. F. Ashby. "Wear-Mechanism Maps." *Acta Metallurgica*, 35(1):1–24, January 1987.

16. Barber, J.P., and D.P. Bauer. "Contact Phenomena at Hypervelocities." *Wear*. 78. (1982): 163-169. Print.

17. Meng, H.C., and K.C Ludema. "Wear Models and Predictive Equations: Their Form and Content." *Wear*. 181. (1995): 443-457. Print

18. Gray, G.T., S.R. Chen, W. Wright, and M.F. Lopez. United States. Los Alamos National Laboratory. *Constitutive Equations for Annealed Metals Under Compression at High Strain Rates and High Temperatures*. New Mexico: , 1994. Print.

19. P˜odra, P. and S. Anderson. *"Simulating Sliding Wear with Finite Element Method,"* Tribology International, 32(2):71–81, February 1999.

20. Rajagopalan, S., M. A. Irfan, and V. Prakash. *"Novel Experimental Techniques for Investigating Time Resolved High Speed Friction,"* Wear,225-229(Part 2):1222–1237, April 1999.

21. Wolfson, M. R. Wear*, Solid Lubrication, and Bearing Material Investigation for High-Speed Track Applications*. Technical Report AFMDC-TR-60-7, Test Track Division, Air Force Missile Development Center, Holloman AFB, New Mexico, March 1960.

22. Gerstle, F.P., P.S. Follansbee, et al. "Thermoplastic Shear and Fracture of Steel During High-Velocity Sliding." *Wear*. 24. (1973): 97-106. Print.

23. Hooser, M., and A. Schwing. "Validation of Dynamic Simulation Techniques at Holloman High Speed Test Track." 38th Aerospace Sciences Meeting and Exhibit. 10-13 January 2000. Reno: AIAA, 2000. Print.

24. Laird, D.J. The investigation of Hypervelocity Gouging. Ph. D. thesis, Graduate School of Engineering, Air Force Institute of Technology (AETC), March 2002. AFIT/DS/ENY/02-01

25. Szmerekovsky, A. G. *The Physical Understanding of the Use of Coatings to Mitigate Hypervelocity Gouging Considering Real-Test Sled Dimensions* AFIT/DS/ENY/04-06. Ph.D. Dissertation, Air Force Institute of Technology, Wright-Patterson AFB, OH, 2004.

26. Cameron, G. J. *An Evaluation of High Velocity Wear*, AFIT/GAE/ENY/07M06. Master's Thesis, Air Force Institute of Technology, Wright-Patterson AFB, OH, 2007.

27. Chmiel, A. J. *Finite Element Simulation Methods for Dry Sliding Wear*, AFIT/GAE/ENY/08-M03. Master's thesis, Air Force Institute of Technology, Wright Patterson AFB, OH, 2008.

28. Meador, Stephen P. *Consideration of Wear at High Velocities*, AFIT/GAE/ENY/10-M16. Master's thesis, Air Force Institute of Technology, Wright Patterson AFB, OH, 2010.

29. Huber, D. A., *The Use of Various Failure Criteria As Applied To High Speed Wear* AFIT/DS/ENY/11-D01. Thesis, Air Force Institute of Technology, Wright-Patterson AFB, OH, December 2011.

30. Bhushan, B. *Introduction to Tribology*. John Wiley & Sons, New York, 2002.

31. Lee, J.K. Analysis of Multilayered Materials Under High Velocity Impact Using CTH, , March 2008

32. Zukas, J. A., *High Velocity Impact Dynamics,* John Wiley and Sons, Inc., New York, 1990.

33. Palazotto, A. Proposal, November 2012.

34. Meyers, M. A. *Dynamic Behavior of Materials*. John Wiley & Sons, New York, 1994.

35. Lyon, S.P., and J.D. Johnson. United States. Los Alamos National Alamos Laboratory. *SESAME: The Los Alamos National Laboratory Equation of State Database*. 1992. Web. <http://t1web.lanl.gov/doc/SESAME_3Ddatabase_1992.html>.

36. Anderson, C.E. "An Overview of the Theory of Hydrocodes." *International Journal of Impact Engineering*. 5. (1987): 33-59. Print.

37. Cinnamon, J. D., A. N. Palazotto, and Z. Keenan. “Material Characterization and Development of a Constitutive Relationship for Hypervelocity Impact of1080 Steel and VascoMax 300,” International Journal of Impact Engineering, 33(112):180–189, December 2006.

38. Buentello, R., *3D Finite Element Modeling of Sliding Wear* AFIT/DS/ENY/10-13. Prospectus, Air Force Institute of Technology, Wright Patterson AFB, OH , April 2012.

39. Crawford, D. A. and R. L. Bell. CTH User’s Manual and Input Instructions Version 10.1. Technical report, CTH Development Project Sandia National Laboratories, 2007.

40. "The Split Hopkinson Bar Method in Materials Testing." *HBM*. HBM, Inc.. Web. 20 Nov 2012. <http://www.hbm.com/en/menu/applications/test-measurement/split-hopkinson-bar/?geoip_cn=2>.

41. *Lagrangian and Eulerian Reference Frames*. 2010. SAS IP, Inc.Web. 20 Nov 2012. <https://www.sharcnet.ca/Software/Fluent13/help/wb_sim/exp_dyn_theory_lag_eul_360.html>.

42. Jeffery, Thomas. 1998. Missouri S&T, Missouri. Web. 12 Dec 2012. <42.http://classes.mst.edu/ide110/concepts/13/strain/index.html>.

## Vita

Lauren Wuertemberger graduated from Western High School in Russiaville, Indiana in 2007. She then completed a degree in mechanical engineering at Rose-Hulman Institute of Technology in Terre Haute, Indiana in 2013. During her stint there, she was the reigning racquetball singles and doubles champion. After completing her B.S. degree, Lauren entered AFIT's aeronautical engineering program, and intends on staying on to complete a Ph.D. Lauren is currently active in martial arts and has dreams of becoming a breakdancer, hopefully picking up the skills during her Ph.D. program. Eventually Lauren plans on settling down in a lab and performing destructive testing for a living.

# REPORT DOCUMENTATION PAGE

*Form Approved*
*OMB No. 074-0188*



| 1. REPORT DATE *(DD-MM-YYYY)* | 2. REPORT TYPE | 3. DATES COVERED *(From – To)* |
|---|---|---|
| 28-12-2012 | Master's Thesis | Sept 2011-Dec 2012 |

**4. TITLE AND SUBTITLE**
Predicting the Wear of High Speed Rocket Sleds

**5a. CONTRACT NUMBER**

**5b. GRANT NUMBER**

**5c. PROGRAM ELEMENT NUMBER**

**6. AUTHOR(S)**
Wuertemberger, Lauren B., GS-9 USAF

**5d. PROJECT NUMBER**
N/A

**5e. TASK NUMBER**

**5f. WORK UNIT NUMBER**

**7. PERFORMING ORGANIZATION NAMES(S) AND ADDRESS(S)**
Air Force Institute of Technology
Graduate School of Engineering and Management (AFIT/EN)
2950 Hobson Way, Building 640
WPAFB OH 45433

**8. PERFORMING ORGANIZATION REPORT NUMBER**
AFIT-ENY-12-D-02

**9. SPONSORING/MONITORING AGENCY NAME(S) AND ADDRESS(ES)**

**10. SPONSOR/MONITOR'S ACRONYM(S)**

**11. SPONSOR/MONITOR'S REPORT NUMBER(S)**

**12. DISTRIBUTION/AVAILABILITY STATEMENT**
APPROVED FOR PUBLIC RELEASE; DISTRIBUTION UNLIMITED

**13. SUPPLEMENTARY NOTES**


**14. ABSTRACT**
Holloman Air Force Base houses the 10 mile long Holloman High Speed Test Track (HHSTT) in New Mexico and can run hypersonic experiments at speeds up to 10,000m/s. Tested objects are loaded onto sleds, which are connected to the track by "slippers" that slide along the rails. The payload sled is propelled down the track by a series of rocket sleds. The ability to predict the wear that will occur on the slippers during these experiments is important for slipper design and preventing catastrophic failure. However, high speeds complicate wear prediction as there additional contributing factors, including inconsistent surface contact, fluctuating thermal and friction properties, and additional speed-induced melt wear. The goal of this project is to utilize a hydrocode program – CTH – to predict high speed wear results using a damage criterion that allows damage to occur and be removed. Results will be compared to the wear seen in other plane strain models which did not allow the damaged regions to be removed, 3D ABAQUS simulation, and experimental data derived from a 2008 test run at the HHSTT.

**15. SUBJECT TERMS**
High speed wear, CTH, Holloman High Speed Test Track, Johnson and Cook Failure Criterion, rocket sleds, hypervelocity

| 16. SECURITY CLASSIFICATION OF: | | | 17. LIMITATION OF ABSTRACT | 18. NUMBER OF PAGES | 19a. NAME OF RESPONSIBLE PERSON |
|---|---|---|---|---|---|
| a. REPORT | b. ABSTRACT | c. THIS PAGE | | | Dr. Anthony N. Palazotto, USAF |
| U | U | U | SAR | 147 | 19b. TELEPHONE NUMBER *(Include area code)* (937) 255-3636, x 4599 (Anthony.Palazotto@afit.edu) |